Multipolar interactions in *f*-electron systems: The paradigm of actinide dioxides

Paolo Santini, Stefano Carretta, and Giuseppe Amoretti

Dipartimento di Fisica, Università di Parma, Viale G. P. Usberti 7/A, I-43100 Parma, Italy

Roberto Caciuffo,* Nicola Magnani, and Gerard H. Lander

European Commission, Joint Research Centre, Institute for Transuranium Elements, Postfach 2340, D-76125 Karlsruhe, Germany

(Published 2 June 2009)

This article reviews the physics of multipolar interactions and multipolar order in *f*-electron systems, using the actinide dioxides as a paradigm. In the past few years, these apparently simple cubic compounds have been studied intensively, and many new phenomena have been discovered. Here the experimental results are discussed together with the current theoretical understanding of multipolar interactions.

DOI: 10.1103/RevModPhys.81.807 PACS number(s): 75.10.Dg, 75.40.Cx, 75.40.Gb, 78.70.Ck

CONTENTS

I. INTRODUCTION

Electronic low-temperature properties of solids result from open shells of the constituent atoms. The electrons belonging to these shells may either delocalize and form band states or retain a localized behavior. In particular, whereas the spatially extended *s* and *p* states always assume a band character, *d* and *f* electrons display various degrees of localization in the different compounds, ranging from completely localized to highly itinerant band-like situations. The degree of localization also depends on external parameters such as temperature *T* and pressure *p*. If electrons are localized, charge-transfer processes do not usually need to be explicitly considered and can be perturbatively projected out, yielding inter-ion effective couplings between the degrees of freedom of the open shells (e.g., superexchange). A fundamental difference between *d* and *f* electrons is the much larger sensitivity of the former to the crystal field (CF) produced by charges on neighboring ligands. Together with a weaker spin-orbit coupling in the *d* series as compared to the *f* series, this usually leads to an al-

*roberto.caciuffo@ec.europa.eu

most complete quenching of the orbital degrees of freedom of *d* electrons. As in the case of half-filled shells (*S* ions), the charge-density distribution is almost rigid, but its shape is in general not spherical, having the symmetry of the local CF. The low-energy, low-temperature physics is mostly determined by spin degrees of freedom and the leading ion-ion couplings are Heisenberg-type.

Conversely, the interplay of spin and unquenched orbital degrees of freedom of *f* shells leads to a rich variety of observed phenomena. In fact, together with dipoles, higher-rank multipoles may play an important active role. A growing number of phenomena involves multipoles: in particular, exotic phase transitions driven by hidden (nondipolar) order parameters (OPs) have great fundamental interest. For instance, we mention quadrupole order in CeB_6, UPd_3, PrO_2, TmTe, DyB_2C, $PrPb_3$, CeAg, HoB_2C_2, and $PrCu_2$. Moreover, primary OPs involving high-rank magnetic multipoles are very likely to exist in NpO_2 (Sec. IV.B) and La-doped CeB_6. For several compounds, the nature of the hidden OP is still a matter of debate, as in the striking case of URu_2Si_2, where in spite of more than two decades of intense experimental and theoretical investigations no ultimate conclusion has been drawn (Wiebe *et al.*, 2007).

Of course, not all the physics can be addressed by considering localized 5*f* electrons, as in this article. In fact, the majority of metallic actinide materials do not have fully localized electrons. Hybridization between 5*f* and conduction-electron states may result in a variety of different phenomena: damping of the local-moment dynamics, Kondo effect, reduced-moment magnetic phases, valence fluctuations, Mott transitions of 5*f* electrons driven by pressure, temperature, or magnetic field, heavy-Fermi-liquid behavior, unconventional superconductivity, or itinerant magnetic phases. These phenomena have been discussed in detail in articles such as *Los Alamos Science* (Cooper, 2000), and review articles, for example, those by Stewart (1984, 2001), and in many other places. It is not our intention to cover these fields, but it is not always easy to tell *a priori* which is the best framework for discussing actinide materials, as in most cases there are no measurements that indicate in a clear-cut way on which side of the Mott transition 5*f* electrons have to be located.[1] Progress in understanding the nature of the electronic ground state of actinide metals has been reviewed by Moore and van der Laan (2009), who also discussed in detail state-of-the-art *ab initio* methods for electronic structure calculations.

Important issues involving multipoles include quadrupole-fluctuation-mediated superconductivity (Kotegawa *et al.*, 2003), quadrupolar Kondo effects leading to the emergence of novel heavy-fermion states (Cox, 1987; Yatskar *et al.*, 1996; Cox and Zawadowski, 1998), and phenomena associated with the coupling of electric multipoles of the *f* shell to the lattice such as the single-ion dynamical Jahn-Teller (JT) effect, effective two-ion electric-multipole interactions mediated by phonons, and bound states between CF excitations and phonons (Dolling and Cowley, 1966; Allen, 1968a, 1968b; Cowley and Dolling, 1968; Thalmeier and Fulde, 1982; Morin and Schmitt, 1990). Orbital degrees of freedom are also often important in actinide compounds whose 5*f* electrons are itinerant. Indeed, the orbital contribution to the total magnetic moment may be large, unlike the situation for *d* electrons (Brooks and Kelly, 1983a; Wulff *et al.*, 1988, 1989; Hiess *et al.*, 2001).

Thus, multipolar degrees of freedom are now recognized as a central issue in magnetism, and an important subject in condensed-matter physics. Addressing this topic is, however, a formidable task, as multipolar interactions are but one of the pieces of the puzzle (Santini *et al.*, 1999): CF and magnetoelastic (ME) interactions also play a leading role in determining the statics and dynamics of multipolar degrees of freedom. In metallic compounds, a further difficulty lies in the role of the hybridization between *f* orbitals and conduction (*c*) states. If it is not too strong, this hybridization and its associated charge fluctuations in the *f* shell can be perturbatively eliminated, yielding an effective two-body *c*-*f* coupling between conduction electrons and magnetic and electric multipoles of the *f* electrons (Hirst, 1978; Fulde and Löwenhaupt, 1986). Hence, the Hamiltonian may contain many terms (and parameters) having *a priori* comparable strengths, and this makes it difficult to find a simple minimal microscopic model containing the essential physics. In this framework, actinide dioxides (together with the closely related compound PrO_2) provide model systems where the delicate balance of the various interactions can be thoroughly studied. In fact, due to their simple crystallographic structure and their insulating character, they are among the compounds described by the simplest Hamiltonians. In addition, the high (cubic) symmetry of the paramagnetic phase is ideal for maximizing the number of independent multipolar degrees of freedom (see Sec. II). Finally, the existence of a family of isostructural compounds allows the building of a reliable model for the single-ion wave functions working for different *f*-shell configurations involved. Fundamental questions concerning the nature of the 5*f* electrons and their degree of localization and covalency have been explored in numerous experimental investigations.

During the past few years, most effort on dioxides has been focused on the problems connected with multipolar interactions in NpO_2, UO_2, and PrO_2. NpO_2 has recently attracted much attention because it displays a phase transition at about 25 K, which has been proposed as the first example of ordering driven by a magnetic-multipole (MMP) primary OP (Santini and Amoretti, 2000, 2002; Paixao *et al.*, 2002; Caciuffo *et al.*, 2003; Kiss and Fazekas, 2003; Lovesey *et al.*, 2003; Nikolaev and Michel, 2003; Kubo and Hotta, 2005a, 2005b; Magnani, Santini, Amoretti, and Caciuffo, 2005; Nagao and Iga-

[1] URu_2Si_2 is a good example. Many approaches consider it as an itinerant system, but there has also been an effort to understand its properties in terms of multipolar ordering in a localized *f*-electron framework.

rashi, 2005; Sakai *et al.*, 2005; Tokunaga *et al.*, 2005a; Santini *et al.*, 2006; Tokunaga, Aoki, Homma, *et al.*, 2006). Clear evidence for a second-order phase transition was given more than 50 years ago by specific-heat measurements, but no experimental indication of magnetic dipole order has ever been found. Only recently, resonant x-ray scattering (RXS) experiments (Paixao *et al.*, 2002; Caciuffo *et al.*, 2003) and ^{17}O nuclear magnetic resonance (NMR) measurements (Tokunaga *et al.*, 2005a; Tokunaga, Aoki, Homma, *et al.*, 2006) demonstrated the occurrence of longitudinal type-I 3-**k** ordering of electric quadrupoles, which have been interpreted as secondary OPs induced by a longitudinal type-I 3-**k** ordering of MMPs. The analysis of existing experimental data points to rank-5 triakontadipoles as driving OPs (Santini *et al.*, 2006).

ME coupling of 5*f* electric quadrupoles to the lattice permeates the low-temperature behavior of UO_2. For instance, impressing evidence of the role played by quadrupolar interactions is provided by large magnon-phonon anticrossings characterizing the dynamics. Magnetic and quadrupolar OPs jointly drive a phase transition toward a 3-**k** phase at about 31 K. Direct evidence of the quadrupolar order has been provided by recent RXS experiments (Wilkins *et al.*, 2006).

ME interactions also play a key role in determining the low-temperature properties of PrO_2 (Boothroyd *et al.*, 2001; Gardiner, Boothroyd, McKelvy, *et al.*, 2004; Gardiner, Boothroyd, Pattison, *et al.*, 2004; Jensen, 2007; Webster *et al.*, 2007). Rare-earth atoms are usually trivalent, and only dioxides of Ce (with $4f^0$ configuration), Pr ($4f^1$), and Tb ($4f^7$) exist. PrO_2 is the only compound that can display multipolar effects as Ce^{4+} is nonmagnetic and Tb^{4+} has a half-filled 4*f* shell with $L=0$, i.e., orbital degrees of freedom are quenched because of Hund's second rule. PrO_2 exhibits a quadrupolar phase transition at a temperature as high as 120 K with a large static Jahn-Teller (JT) distortion. At 13.5 K, the compound displays a second phase transition toward a complex antiferromagnetic (AF) state. Features indicating a strong dynamic JT effect are seen in the low-temperature dynamics, and hints exist of an active role played by multipolar two-ion couplings in the magnetic transition.

In this review, we first describe the theoretical framework used to address multipolar interactions in condensed matter. After a brief introduction to the physical meaning of multipoles, the possible interaction mechanisms are described in both *LS* and *j-j* coupling, with particular emphasis on symmetry properties. Then important experimental techniques used to observe multipole order phenomena are presented, and selected examples of significant experimental results are reviewed. Finally, the physics of actinide dioxides, archetypes of systems dominated by multipolar effects, is discussed with reference to the experimental and theoretical developments of the past few years. A summary concludes the review.

II. FUNDAMENTAL INTERACTIONS IN *f*-ELECTRON SYSTEMS: THEORETICAL TOOLS

A. Multipoles and their symmetry

1. Electromagnetic multipoles

Multipole expansions are a traditional method of classical electromagnetism, very powerful in describing the electromagnetic interaction between spatially extended sources, and for the study of atomic and nuclear transitions. An exhaustive review of the formal and physical aspects of the multipole expansion in electrodynamics has been given by Dubovik and Tugushev (1990). Multipole moments (including magnetic toroidal ones) can be used to parametrize an arbitrary distribution of charges $\rho_e(\mathbf{r},t)$ and currents $\mathbf{j}_e(\mathbf{r},t)$. Outside the region where such sources are located, the electric and magnetic fields **E** and **H** can be expressed as power series (quasistationary case)

$$\mathbf{E}(\mathbf{r},t) = -\sum_{k=0}^{\infty}\sum_{q=-k}^{k}\frac{4\pi}{2k+1}Q_{kq}(t)\,\boldsymbol{\nabla}\frac{Y_{kq}(\hat{\mathbf{r}})}{r^{k+1}}, \tag{1}$$

$$\mathbf{H}(\mathbf{r},t) = -\sum_{k=1}^{\infty}\sum_{q=-k}^{k}\frac{4\pi}{2k+1}M_{kq}(t)\,\boldsymbol{\nabla}\frac{Y_{kq}(\hat{\mathbf{r}})}{r^{k+1}}, \tag{2}$$

where Q_{kq} and M_{kq} are the qth components of the electric and (poloidal) magnetic multipole moments of order k,

$$Q_{kq}(t) = \int d\mathbf{r}' r'^k Y^*_{kq}(\hat{\mathbf{r}}')\rho_e(\hat{\mathbf{r}}',t), \tag{3}$$

$$M_{kq}(t) = \frac{-1}{c(k+1)}\int d\mathbf{r}' r'^k Y^*_{kq}(\hat{\mathbf{r}}')\,\boldsymbol{\nabla}\cdot[\mathbf{r}'\times\mathbf{j}_e(\mathbf{r}',t)]. \tag{4}$$

In the context of *d*- and *f*-electron magnetism, multipoles are introduced both as an abstract mathematical tool to express the state and the Hamiltonian of the open-shell electrons and for the physical role played by the associated electromagnetic quantities (3) and (4).[2] In

[2]In the present context, Eqs. (3) and (4) must be interpreted as quantum operators acting on the open-shell electrons, with $\rho_e(\mathbf{r},t)$ and $\mathbf{j}_e(\mathbf{r},t)$ given by

$$\rho_e(\mathbf{r},t) = -e\sum_{\sigma=\uparrow,\downarrow}\Psi^\dagger_\sigma(\mathbf{r},t)\Psi_\sigma(\mathbf{r},t), \tag{5}$$

$$\mathbf{j}_e(\mathbf{r},t) = \frac{-e\hbar}{2mi}\sum_{\sigma=\uparrow,\downarrow}[\Psi^\dagger_\sigma(\mathbf{r},t)(\boldsymbol{\nabla}\Psi_\sigma(\mathbf{r},t)) - (\boldsymbol{\nabla}\Psi^\dagger_\sigma(\mathbf{r},t))\Psi_\sigma(\mathbf{r},t)] - \frac{e\hbar}{2m}\boldsymbol{\nabla}\times[\boldsymbol{\Psi}^\dagger(\mathbf{r},t)\underline{\underline{\boldsymbol{\sigma}}}\boldsymbol{\Psi}(\mathbf{r},t)]. \tag{6}$$

Here $\boldsymbol{\Psi}^\dagger(\mathbf{r},t)\equiv[\Psi^\dagger_\uparrow(\mathbf{r},t),\Psi^\dagger_\downarrow(\mathbf{r},t)]$ are two-component electron field operators and $\underline{\underline{\boldsymbol{\sigma}}}$ is a vector formed with the three Pauli matrices. In the presence of an external magnetic field described by a vector potential $\mathbf{A}(\mathbf{r},t)$, the diamagnetic contribution to $\mathbf{j}_e(\mathbf{r},t)$ should be included too, $\mathbf{j}_{\mathrm{dia}}(\mathbf{r},t) = e\mathbf{A}(\mathbf{r},t)\rho_e(\mathbf{r},t)/mc$. Multipole moments can be defined as average values over the quantum state of the system.

particular, electric-multipole (EMP) moments are induced in the open-shell electrons by their coupling to the electric field produced by the environment. The CF yields static moments (e.g., in cubic symmetry the lowest-order nonvanishing static EMP moments are hexadecapoles), whereas dynamic (JT-type) effects are produced by the time-varying electric field accompanying lattice vibrations. These may also transmit effective two-ion EMP-EMP interactions, whereas the electric field (1) generated on neighboring ions by an EMP polarization of the open shell is usually too small to yield sizable direct couplings. As far as MMP moments are concerned, the magnetic field (2) they produce outside the open shell is usually irrelevant to the physical behavior. Yet, this field is extremely important for experimental investigations of the electrons' state, as it can be probed in real space by local techniques such as muon spin rotation or NMR, and especially in reciprocal space by magnetic neutron scattering. Even if dipolar ($k=1$) fields are the easiest to detect, the weaker higher-order fields may be measurable, for instance through their contribution to the neutron cross section at large wave-vector transfer.

2. Multipolar tensor operators

Besides producing and responding to electromagnetic fields, multipoles may be used to parametrize the state and the observables of the open-shell electrons. The usefulness of multipole representations stems from angular-momentum conservation, and the ensuing possibility to map (within a manifold of states) a generic set of observables A_{kq}, transforming under rotations as the representation $D^{(k)}$ of the rotation group, onto simple irreducible tensor operators of rank k, T_{kq} (by the Wigner-Eckart theorem) (Sakurai, 1993). The latter can also be named "multipole operators," in the sense that, by identifying A_{kq} with Q_{kq} (3) or M_{kq} (4), the above-mentioned mapping allows us to attach a physical meaning to T_{kq} as an operator equivalent for an electromagnetic multipole.

The definition of unit multipole (tensor) operators can be found in many textbooks [see, e.g., Sakurai (1993) and Blum (1996)],

$$T_{KQ}(J) = \sum_{MM'} (-1)^{J-M}(2K+1)^{1/2} \times \begin{pmatrix} J & J & K \\ M' & -M & Q \end{pmatrix} |JM\rangle\langle JM'|. \tag{7}$$

The wave function of the system is assumed to belong to the space $\mathcal{H}_J$ spanned by $2J+1$ states $|JM\rangle$ having angular momentum J (see Sec. II.B). The operators (7) transform under rotations like spherical harmonics $Y_{KQ}(\mathbf{r})$, i.e., they provide a basis for the irreducible representation (irrep) $D^{(K)}$ of the rotation group. The set of $(2J+1)^2$ operators $T_{KQ}(J)$ with $K=0,\ldots,2J$, $Q=-K,\ldots,K$ is orthogonal and complete with respect to the trace inner product, and any operator A in $\mathcal{H}_J$ can be expressed as a linear superposition of the $T_{KQ}(J)$,

$$A = \sum_{KQ}\sum_{MM'} \langle M|A|M'\rangle(-1)^{J-M}(2K+1)^{1/2} \times \begin{pmatrix} J & J & K \\ M' & -M & Q \end{pmatrix} T_{KQ}(J). \tag{8}$$

Thus, any observable can be decomposed in multipole operator components. Interestingly, Eq. (8) can be exploited to parametrize any state of the system by multipole moments. In fact, the most general quantum state in $\mathcal{H}_J$ is defined by a density operator ρ. If ρ is decomposed into multipole components according to Eq. (8), one obtains (Blum, 1996)

$$\rho = \sum_{KQ} \langle T_{KQ}(J)^\dagger\rangle T_{KQ}(J), \tag{9}$$

with $\langle T_{KQ}(J)^\dagger\rangle = \mathrm{tr}[\rho T_{KQ}(J)^\dagger]$. Thus, the state can be equivalently identified by the density matrix (if this represents a pure state, by its $2J+1$ coefficients on a given basis), or by the set of nonvanishing multipole moments (also called "state multipoles") $\langle T_{KQ}(J)^\dagger\rangle$. It should be noted that $T_{KQ}(J)$ do not represent observables since they are not self-adjoint for $Q\neq 0$, $T_{KQ}(J)^\dagger = (-1)^Q T_{KQ}(J)$. An equivalent set of observable quantities can be easily built by superposing $T_{KQ}(J)$ and $T_{K-Q}(J)$ (with $Q>0$) in much the same way as real-valued (tesseral) harmonics are built out of spherical harmonics,

$$O_K^Q(J) = \frac{1}{\sqrt{2}}[(-1)^Q T_{KQ}(J) + T_{K-Q}(J)],$$

$$O_K^{-Q}(J) = \frac{i}{\sqrt{2}}[T_{KQ}(J) - (-1)^Q T_{K-Q}(J)]. \tag{10}$$

3. One-body tensor operators

By identifying the $|JM\rangle$ states with the $|lm\rangle$ orbitals ($l=2$ for d electrons and $l=3$ for f electrons) or with the $|\frac{1}{2}m_s\rangle$ spinors, the corresponding $T_{\Lambda\mu}(l)$ $(\Lambda=0,\ldots,2l)$ and $T_{\Sigma\nu}(s)$ $(\Sigma=0,1)$ spherical tensors and the associated double tensors $T_{\Lambda\Sigma\mu\nu}(l,s)=T_{\Lambda\mu}(l)\otimes T_{\Sigma\nu}(s)$ allow a generic one-electron observable $A(\mathbf{x},\mathbf{p},\mathbf{s})$ to be expanded in a set of multipolar components of rank Λ in real space and rank Σ in spin space. This decomposition of one-electron observables in terms of multipolar components can be used in a many-electron configuration d^n or f^n to decompose in the same way one-body observables $\Sigma_i A(\mathbf{x}_i,\mathbf{p}_i,\mathbf{s}_i)$ on one-body tensor operators $\tilde{T}_{\Lambda\Sigma\mu\nu}$, with[3]

[3] $T_{\Lambda\Sigma\mu\nu}(l,s)$ are one-electron operators acting in the corresponding one-electron Hilbert space, whereas $\tilde{T}_{\Lambda\Sigma\mu\nu}$ are one-body many-electron operators acting in the corresponding many-electron Hilbert space.

$$\tilde{T}_{\Lambda\Sigma\mu\nu} = \sum_{mm'\sigma\sigma'} (-1)^{l-m}(2\Lambda+1)^{1/2}\begin{pmatrix} l & l & \Lambda \\ m' & -m & \mu \end{pmatrix} \times(-1)^{1/2-\sigma}(2\Sigma+1)^{1/2}\begin{pmatrix} 1/2 & 1/2 & \Sigma \\ \sigma' & -\sigma & \nu \end{pmatrix} \times a^{\dagger}_{m\sigma}a_{m'\sigma'}, \quad (11)$$

where $a_{m\sigma}$ annihilates an electron with spin σ in orbital m. For instance, the charge density (5) is a one-body observable of orbital type and can be expressed as a superposition of the $2l+1$ multipolar components $\tilde{T}_{\Lambda 0\mu 0}$, whereas the current operator (6) is of mixed orbital and spin type, and in general all components $\tilde{T}_{\Lambda\Sigma\mu\nu}$ contribute. Multipolar components having a well-defined overall (spin+orbital) rank K can be obtained by expanding on the set of tensor products[4]

$$\tilde{T}_{\Lambda\Sigma KQ} = \sum_{\mu\nu} (-1)^{\Lambda-\Sigma+Q}(2K+1)^{1/2} \times \begin{pmatrix} \Lambda & \Sigma & K \\ \mu & \nu & -Q \end{pmatrix}\tilde{T}_{\Lambda\Sigma\mu\nu} \quad (12)$$

with $K=|\Lambda-\Sigma|\cdots\Lambda+\Sigma$. Hence K cannot exceed $2l+1$. Electromagnetic multipoles (3) and (4) are proportional to multipolar operators with rank $K=k$ and component $Q=q$. Thus, an l^n shell cannot produce charge or current densities leading to EMP moments (3) of rank larger than $2l$ and MMP moments of overall rank larger than $2l+1$. Another restriction on allowed moments comes from the fact that, if the state of the system has definite parity, $\langle\rho_e(\mathbf{r})\rangle=\langle\rho_e(-\mathbf{r})\rangle$ and $\langle\mathbf{j}_e(\mathbf{r})\rangle=-\langle\mathbf{j}_e(-\mathbf{r})\rangle$. This implies that only even-k electric and odd-k MMPs may be different from zero. Most compounds whose d or f open-shell electrons are localized are characterized by negligible configuration mixing, i.e., the number n of d or f electrons is fixed. The wave function of these electrons has then definite parity $(-1)^{ln}$, and the above-stated restriction on allowed multipole moments holds (e.g., electrons cannot produce an electric dipole or a magnetic quadrupole).

4. Tensor operators in *L*, *S*, and *J* subspaces

A major advantage of expanding observables in multipole components is that it is straightforward to find the corresponding representation on a subspace of states irreducible under rotation. In particular, for $3d$ electrons the relevant low-energy subspace is usually set by the intra-atomic electron repulsion through the first and second Hund rules. These yield a manifold of states (a spectroscopic term) of fixed total angular (**L**) and spin (**S**) momentum. Within this manifold, the double tensor operators $T_{\Lambda\Sigma\mu\nu}(L,S)=T_{\Lambda\mu}(L)\otimes T_{\Sigma\nu}(S)$ allow a generic (one- or many-body) observable to be expanded in a set of multipolar components of rank Λ in real space and rank Σ in spin space. An operator $T_{\Lambda\Sigma KQ}(L,S)$ with well-defined overall rank K can be obtained by taking linear combinations of the $T_{\Lambda\Sigma\mu\nu}(L,S)$ as in Eq. (12). In particular, one-body observables $\tilde{T}_{\Lambda\Sigma\mu\nu}$ within a spectroscopic term are proportional to $T_{\Lambda\Sigma\mu\nu}(L,S)$. For instance, the CF (Sec. II.B.2) is a one-body orbital-type observable and can be expanded as a sum of $\tilde{T}_{\Lambda 0\mu 0}$ operators, which in turn maps onto a sum of $T_{\Lambda 0\mu 0}(L,S)$ operators. Since only EMP moments are coupled to the CF, Λ is even. The interaction with an external magnetic field is accounted for by the orbital and spin Zeeman terms which are proportional to the $\tilde{T}_{10\mu 0}$ and $\tilde{T}_{010\nu}$ operators, respectively, which in turn map onto $T_{10\mu 0}(L,S)$ and $T_{010\nu}(L,S)$.

For $4f$ and $5f$ electrons, the spin-orbit interaction is strong. It is of the form (12) with $\Lambda=1$, $\Sigma=1$, $K=0$, $Q=0$, and within an (L,S) term it maps onto the rank-0 (scalar) operator $T_{\Lambda\Sigma 00}(L,S)$ (or $\mathbf{L}\cdot\mathbf{S}$). This splits the term into several multiplets with fixed total angular momentum J, with the lowest lying determining low-temperature properties. By exploiting the Wigner-Eckart theorem, an operator $T_{\Lambda\Sigma KQ}(L,S)$ maps onto $T_{KQ}(J)$ within a J subspace. To get an operator basis in the J manifold all $K\leqslant 2J$ are needed, but not all K values necessarily describe one-body operators [Eq. (12)]; in fact, for these operators the upper limit is $K_{\max}=2l+1$. Thus, multipole operators $T_{KQ}(J)$ with $K>K_{\max}$ do not correspond to electromagnetic multipoles (3) or (4).

It is often useful to build linear combinations of multipole operators of the same rank K belonging to a given irrep Γ of the symmetry group of the system,

$$O^K_{\Gamma\gamma}(J) = \sum_Q c(\Gamma,\gamma,K,Q)T_{KQ}(J), \quad (13)$$

where γ labels the different components of Γ and $c(\Gamma,\gamma,K,Q)$ are projection coefficients. For instance, in UO_2 the cubic Γ_5 triplet of quadrupoles plays an important role and is given by

$$O^2_{\Gamma_5 1}(J) = i[T_{22}(J) - T_{2-2}(J)]/\sqrt{2},$$

$$O^2_{\Gamma_5 2}(J) = i[T_{21}(J) + T_{2-1}(J)]/\sqrt{2},$$

$$O^2_{\Gamma_5 3}(J) = [-T_{21}(J) + T_{2-1}(J)]/\sqrt{2}. \quad (14)$$

$T_{KQ}(J)$, as well as $O^K_{\Gamma\gamma}(J)$, can also be expressed as polynomials in J_x, J_y, J_z (Smith and Thornley, 1966; Rudowicz and Chung, 2004). For example, the operators representing the 15 multipoles active within a Γ_8 quartet are listed in Table I; the three operators in Eq. (14) are proportional to O_{xy}, O_{yz}, and O_{zx}, respectively.

[4]Within a manifold of states of fixed total angular momentum J, operators (12) are proportional to those in Eq. (7), where the proportionality constant is

$$(2J+1)\sqrt{2\Lambda+1}\sqrt{2\Sigma+1}\begin{Bmatrix} Q & J & J \\ \Lambda & l & l \\ \Sigma & 1/2 & 1/2 \end{Bmatrix}.$$

TABLE I. Operator equivalents describing active multipoles within a cubic Γ_8 quartet. Bars over symbols indicate the sum with respect to all the possible permutations of the indices, e.g., $\overline{J_xJ_y^2}=J_xJ_y^2+J_yJ_xJ_y+J_y^2J_x$. The five $\hat{O}_2^Q$ are the usual Stevens' operator equivalents (see below). Adapted from Shiina *et al.* (1998).

Moment	Symmetry	Operator
Dipoles	Γ_4	J_x
		J_y
		J_z
Quadrupoles	Γ_3	$O_{3z^2-r^2}=3J_z^2-J(J+1)\equiv\hat{O}_2^0$
		$O_{x^2-y^2}=J_x^2-J_y^2\equiv\hat{O}_2^2$
	Γ_5	$O_{xy}=\overline{J_xJ_y}/2\equiv\hat{O}_2^{-2}$
		$O_{yz}=\overline{J_yJ_z}/2\equiv\hat{O}_2^{-1}$
		$O_{zx}=\overline{J_zJ_x}/2\equiv\hat{O}_2^{1}$
Octupoles	Γ_2	$T_{xyz}=(\sqrt{15}/6)\overline{J_xJ_yJ_z}$
	Γ_4	$T_x^\alpha=J_x^3-(\overline{J_xJ_y^2}+\overline{J_z^2J_x})/2$
		$T_y^\alpha=J_y^3-(\overline{J_yJ_z^2}+\overline{J_x^2J_y})/2$
		$T_z^\alpha=J_z^3-(\overline{J_zJ_x^2}+\overline{J_y^2J_z})/2$
	Γ_5	$T_x^\beta=\sqrt{15}(\overline{J_xJ_y^2}-\overline{J_z^2J_x})/6$
		$T_y^\beta=\sqrt{15}(\overline{J_yJ_z^2}-\overline{J_x^2J_y})/6$
		$T_z^\beta=\sqrt{15}(\overline{J_zJ_x^2}-\overline{J_y^2J_z})/6$

B. The single-ion model

The Hamiltonian describing the quantum state of a single rare-earth ($4f^n$ configuration) or actinide ($5f^n$ configuration) ion in a crystal contains three main contributions: the electronic Coulomb repulsion H_C, the spin-orbit coupling H_{SO}, and the CF potential H_{CF}.

1. The free-ion spectra

For well-localized *f* electrons, the Coulomb repulsion

$$H_C=\sum_{i>j=1}^{n}\frac{e^2}{r_{ij}} \tag{15}$$

is in general the dominant interaction. Since H_C is rotationally invariant, both the total angular momentum operator $\mathbf{L}=\Sigma_i\boldsymbol{l}_i$ and the total spin $\mathbf{S}=\Sigma_i\mathbf{s}_i$ (where $\boldsymbol{l}_i$ and $\mathbf{s}_i$ label the angular and spin momentum of the *i*th electron in the unfilled *f* shell) commute with H_C; therefore, the spectrum is composed of several multiplets labeled by allowed values of *L* and *S*. The lowest-energy multiplet can be determined by following Hund's rules (the value of *S* should be maximized; the value of *L* should be as large as possible, keeping into account the former rule). In the *LS*-coupling approximation, states are restricted to those of this multiplet.

The spin-orbit interaction can be expressed as

$$H_{SO}=\sum_i\zeta(r_i)\mathbf{s}_i\cdot\boldsymbol{l}_i \tag{16}$$

and is diagonal on the basis composed of the eigenvectors of the total angular momentum $\mathbf{J}=\mathbf{L}+\mathbf{S}$. As mentioned in Sec. II.A, within an *LS* multiplet Eq. (16) can be rewritten in the more convenient form

$$H'_{SO}=\Lambda\mathbf{L}\cdot\mathbf{S}. \tag{17}$$

The lowest-energy multiplet is that with $J=|L-S|$ if $n<7$ or that with $J=L+S$ if $n>7$ (for $n=7$, $L=0$). The Russell-Saunders (RS) approximation consists in restricting the calculations to the states belonging to this ${}^{2S+1}L_J$ multiplet. If the spin-orbit interaction is much larger than the Coulomb interaction, the *LS* coupling is not the optimal choice of approximation. In this case, the effect of H_{SO} should be considered before introducing H_C as a perturbation. This leads to the so-called *j-j* coupling: Eq. (16) shows that, by itself, H_{SO} tends to align the spin and orbital moment of each *f* electron, forming single-particle states labeled by $\mathbf{j}_i=\boldsymbol{l}_i+\mathbf{s}_i$. Since $l=3$, the spectrum is composed of a $j=5/2$ sextet (always lower in energy) and a $j=7/2$ octet. How the *n* electrons are accommodated into these states depends on the effect of H_C.

In real systems, of course, neither the *LS* nor the *j-j* coupling provide a 100% correct description of the ground multiplet, which requires a diagonalization of the matrix $H_{SO}+H_C$ with the full f^n configuration. *J* is still a good quantum number, and the ground-state composition depends on ζ and the strength of the effective Coulomb interactions [which is in general expressed by the values of the Slater radial integrals F^k, $k=0,2,4,6$; see Newman and Ng (2000) for discussions on the calculation procedure]. This scheme is referred to as intermediate coupling (IC).

The overall situation is depicted in Fig. 1, where a schematic view of the calculated free-ion energy levels for the f^3 configuration is given. On the left side of the panel, the Coulomb interaction dominates, and ${}^{2S+1}L$ terms are formed; on the right side, the spin-orbit interaction is dominant and *j-j* coupling is appropriate. While trivalent rare earths are well described by the *LS* approximation, the situation for actinides is more complex: for example, for tetravalent neptunium the IC states must be used to obtain a very accurate overall description. On the other hand, if only properties of the ground free-ion manifold are of interest, both the *LS* and *j-j* coupling provide satisfactory approximations: the superposition between the true IC state and the ground state in the *LS* approximation is about 82%, and nearly the same value is obtained for the *j-j* ground state. This has been attributed to the fact that the two schemes are continuously connected, as no level crossing occurs to change the symmetry of the ground state (Kubo and Hotta, 2005a, 2005b, 2005c).

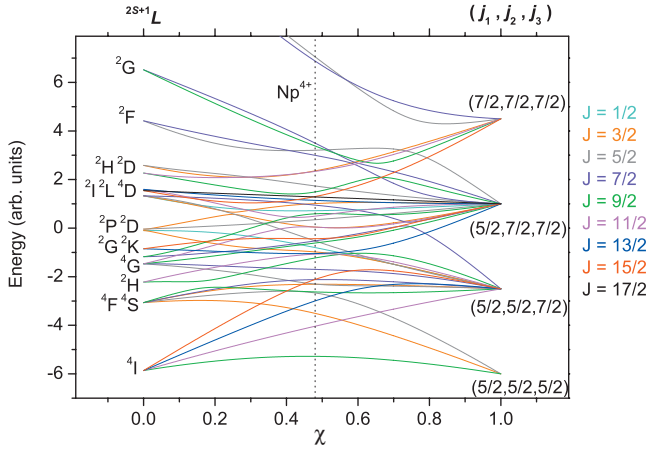

FIG. 1. (Color) Schematic view of the free-ion energy levels for the f^3 electronic configuration. The total Hamiltonian is the sum of H_{SO} multiplied by a factor χ and H_C multiplied by a factor proportional to $1-\chi$. On the left side of the panel, the Coulomb interaction dominates, and ^{2S+1}L terms are formed; on the right side, the spin-orbit interaction is dominant and *j-j* coupling is appropriate. The dashed vertical lines indicate the approximate position of Np^{4+} in the diagram. Arbitrary units are used on the vertical scale.

2. The crystal field

The CF potential experienced by the *f*-electron ions depends on the compound into which they are embedded, and in particular on the local symmetry of the crystallographic site they occupy. As anticipated in Sec. II.A, the CF Hamiltonian can be expressed as

$$H_{\mathrm{CF}} = \sum_{\Lambda=2,4,6} \sum_{\mu=-\Lambda}^{\Lambda} b_{\Lambda\mu} \tilde{T}_{\Lambda 0 \mu 0}. \tag{18}$$

In general, not all $b_{\Lambda\mu}$ coefficients are independent, and symmetry considerations restrict many to zero. If the ground *J* manifold is well isolated (i.e., the CF splitting is significantly smaller than the separation from the lowest excited free-ion manifold; see Sec. II.B.1), one can restrict the CF Hamiltonian to the corresponding $(2J+1)$-state subspace ($|JM\rangle$, $-J \leqslant M \leqslant J$). In this case, it is customary to use the $\hat{O}_K^Q$ operator equivalents defined by Stevens (1952), which are proportional to the O_K^Q defined in Eq. (10). As a typical example, for cubic crystal structures belonging to the O_h group, the CF Hamiltonian is

$$H_{\mathrm{CF}}^{(J)} = A_4\langle r^4\rangle \beta[\hat{O}_4^0(J) + 5\hat{O}_4^4(J)] + A_6\langle r^6\rangle \gamma[\hat{O}_6^0(J) - 21\hat{O}_6^4(J)] \equiv W\left(x\frac{\hat{O}_4(J)}{F(4)} + (1-|x|)\frac{\hat{O}_6(J)}{F(6)}\right), \tag{19}$$

where the (J) argument indicates that the Hamiltonian is restricted to the lowest *J*-manifold subspace, β and γ are the fourth- and sixth-order Stevens factors, $\langle r^n\rangle$ are the expectation values of the r^n operator over the appropriate *f*-electron wave function, and A_K are the CF parameters (Hutchings, 1964). It is also customary to define $B_K = A_K N_K \langle r^K\rangle$ ($N_4=8$, $N_6=16$). The last form in Eq. (19) corresponds to another common parametrization of the same Hamiltonian (Lea *et al.*, 1962).

If different free-ion multiplets cannot be considered isolated from one another, *J* is no longer a good quantum number. A textbook case is the Sm^{3+} ion, and important *J*-mixing effects are known to be present within the actinide series because CF splittings are generally larger for 5*f* than for 4*f* orbitals due to their wider spatial extension. To keep *J* mixing into account correctly, one should diagonalize the full Hamiltonian $H = H_C + H_{SO} + H_{CF}$; although this is a relatively easy task with today's computers, due to the large number of states involved in the process it can be difficult to obtain a full physical comprehension of the role played by each parameter in the model. This is especially difficult when the aim is to include additional cumbersome effects like multipolar interactions, since in this case the representation by Eq. (7) becomes useless. To overcome this problem, a perturbational procedure has recently been developed (Liviotti *et al.*, 2002). It consists in performing a unitary transformation on *H*, such that the off-diagonal blocks (with respect to *J*) of the transformed Hamiltonian H' are zero up to second order in the CF. H' can then be projected on the ground multiplet, thus recovering an effective Stevens-like Hamiltonian which keeps *J*-mixing effects into account. For cubic symmetry, the projected Hamiltonian has the form

$$H_{\mathrm{CF}}'^{(J)} = H_{\mathrm{CF}}^{(J)} + \nu_4[\hat{O}_4^0(J) + 5\hat{O}_4^4(J)] + \nu_6[\hat{O}_6^0(J) - 21\hat{O}_6^4(J)] + \nu_8[\hat{O}_8^0(J) + 28\hat{O}_8^4(J) + 65\hat{O}_8^8(J)] + \cdots. \tag{20}$$

We note that operators of rank higher than 6 appear; however, for all light actinides (which display a $J \leqslant 9/2$ free-ion ground state), those with rank larger than 8 are dropped since $\langle JM|\hat{O}_K^Q|JM'\rangle = 0$ for $K > 2J$. The coefficients appearing in Eq. (20) are dependent on *J* and have been tabulated by Magnani, Santini, Amoretti, and Caciuffo (2005). This formalism has been applied to study the paramagnetic phase of actinide dioxides, and it has been found that this method can quantitatively reproduce the correct ground-manifold CF splittings with an accuracy close to 100%.

The most effective way to determine the CF parameters of a given compound is to directly probe the *f*-shell energy levels with spectroscopic techniques. Inelastic neutron scattering is the method of choice as optical spectroscopy is limited to transparent materials and its cross section is difficult to calculate reliably. Dipolar transitions between CF levels give rise to peaks in the neutron spectra, whose energies and intensities provide information on the eigenvalues and eigenfunctions of the CF Hamiltonian. The cross section for neutron-induced dipolar transitions between CF levels in localized electron systems has been discussed by Fulde and

Löwenhaupt (1986), Lovesey (1987), and Stirling and McEwen (1987).

3. *LS* versus *j-j* couplings

A description based on one-electron states ($\mathbf{j}=\mathbf{s}+\boldsymbol{l}$, $m=-j,-j+1,\ldots,j$) is possible if H_C can be considered negligible and a pure *j-j* coupling scheme is used. The ground $j=5/2$ sextet favored by the spin-orbit coupling is split by the CF term, forming a Γ_8 quartet and a Γ_7 doublet in the case of cubic symmetry, and the $5f^n$ wave functions can be formed by accommodating n electrons in these single-particle states. The Coulomb interaction and CF Hamiltonians can be written as

$$H_{\mathrm{int}} = \frac{1}{2} \sum_{\mu,\nu,\mu',\nu'} I(\mu,\nu;\nu',\mu') a_{\mu}^{\dagger} a_{\nu}^{\dagger} a_{\nu'} a_{\mu'} \tag{21}$$

and

$$H_{\mathrm{CF}} = \sum_{\mu,\nu} B_{\mu\nu} a_{\mu}^{\dagger} a_{\nu}, \tag{22}$$

respectively, with a_μ the annihilation operator of a $5f$ electron in the one-particle state labeled by μ (which coincides with the value of m for the states belonging to the $j=5/2$ sextet). The matrix elements for the Coulomb interaction $I(\mu,\nu;\nu',\mu')$ can be expressed in terms of the Slater parameters F^k (Hotta and Ueda, 2003); within the $j=5/2$ sextet and for cubic symmetry, the one-electron CF coefficients appearing in Eq. (22) can be related to those in Eq. (19) by $B_{\mu\nu}=\langle\mu|H_{\mathrm{CF}}^{(5/2)}|\nu\rangle$.

A *j-j* model based on single-particle states may be convenient to describe compounds in which electron correlation effects are not too strong, as proposed for some intermetallic systems with itinerant f electrons (Hotta, 2006). However, this is a good approximation only immediately close to the *j-j* limit; for well-localized f electrons better results are obtained with a coupling scheme based on *LS* many-electron states. For example, both models satisfactorily approximate the ground state of the Np^{4+} free ion (Sec. II.B.1), but care should be taken in the presence of a CF potential. In particular, in the approximation scheme used for NpO_2 by Kubo and Hotta (2005b), the cubic Γ_7 pair of single-particle states which result from the CF splitting of the $j=5/2$ sextet are neglected in addition to the $j=7/2$ states. Even if for the f^3 configuration this greatly simplifies calculations, the resulting Γ_8 ground state has only a 40% superposition with the actual Γ_8 quartet. As is evident from Fig. 1, a very large admixture of states with different J is expected in the CF ground state calculated in both the $H_C\to 0$ ($\chi\to 1$, *j-j*) and $H_{\mathrm{SO}}\to 0$ ($\chi\to 0$, *LS*) limits; none of these situations is realistic, since the IC free-ion spectrum features a $J=9/2$ ground multiplet relatively well isolated from the subsequent $J=11/2$ manifold. Indeed, *LS* states are firmly constructed in a multielectron way, and the effect of the spin-orbit interaction in selecting the full lowest-energy J manifold can easily be kept into account before truncating the basis and adding the CF (RS coupling). On the contrary, to maintain the single-particle character of the *j-j* CF states for f^3, a truncation of the $j=5/2$ manifold must be performed before considering the effect of H_C, which explains why the approximate *j-j* Γ_8 state is quite different from the exact one. One consequence is that, whereas the total angular momentum of the CF ground state of NpO_2 is a good quantum number in the RS approximation $[\langle\Gamma_8|\mathbf{J}\cdot\mathbf{J}|\Gamma_8\rangle_{\mathrm{RS}} = J(J+1)=(9/2)\times(11/2)=24.75]$ and nearly so for the true ground state ($\langle\Gamma_8|\mathbf{J}\cdot\mathbf{J}|\Gamma_8\rangle=24.8$, due to small admixture with $^4I_{11/2}$ states), this is markedly not the case for the approximate *j-j* quartet ($\langle\Gamma_8|\mathbf{J}\cdot\mathbf{J}|\Gamma_8\rangle_{j\text{-}j}=15.4$). Attempts to correct this situation are under way (Hotta and Harima, 2006), but the simplicity of the original *j-j* model would obviously not be retained.

When valid, the *j-j* model would account more easily for a certain degree of *f*-electron delocalization, which could be important in studying multipolar effects in *5f*-based intermetallic compounds. However, even in this case the localized picture is qualitatively correct for most of the known multipolar ordered phases. Delocalization effects might exist in the disordered phases of $PrFe_4P_{12}$ and URu_2Si_2, where broad excitations are found in the energy spectra; however, these turn into sharply defined peaks below the ordering temperature (Broholm *et al.*, 1987; Park *et al.*, 2005).

C. Multipolar interactions in *LS* coupling

In most cases, the single-site (intra-ion and CF) interactions strongly reduce the ionic degrees of freedom relevant at low temperature without, however, completely quenching them. This means that the distribution of charge and magnetic moment of the ion is not frozen. In terms of spectral properties, the low-energy part of the single-ion spectrum does not reduce to an isolated singlet. In this situation, the low-T and ground-state static properties, as well as the low-energy dynamics, are eventually determined by ion-ion interactions. The low-T ground state will usually be an *ordered* state, in that the internal degrees of freedom will freeze in the configuration optimizing these ion-ion interactions. The lowest-energy excitations will be small deformations of this ordered state, propagating over the lattice.

One remarkable success of the early theory of magnetism was the application of the simple Heisenberg-Dirac exchange Hamiltonian to model ion-ion interactions (Anderson, 1963; Herring, 1966). The two-ion coupling is assumed to be

$$H_{\mathrm{exch}} = J\mathbf{S}_1\cdot\mathbf{S}_2, \tag{23}$$

where $\mathbf{S}_1$ and $\mathbf{S}_2$ are the spins of the two ions. This Hamiltonian was successfully used for various $3d$ compounds. The effective spin coupling arises either from the exchange part of the ion-ion Coulomb interaction or from superexchange (SE) processes mediated by intervening ligand ions.

The reason why the simple coupling H_{exch} works so well in many $3d$ compounds is that very often the spin-orbit coupling is small compared with CF splittings. In

this case, the CF perturbation is applied first on the $|LSM_LM_S\rangle$ states of the lowest $(2S+1)(2L+1)$-degenerate multiplet. It is clear that the CF, affecting the electric-charge-multipole degrees of freedom of the ion [represented by their equivalent operators $T_{KQ}(L)$], acts only on the orbital $|M_L\rangle$ part of the state, without removing the spin degeneracy. If the CF is such as to give an orbital singlet ground manifold (of the form $|0\rangle=|LS\Gamma M_S\rangle$, where Γ is a nondegenerate representation of the point symmetry group), it is easy to prove that $\langle 0|L_i|0\rangle=0$, with $i=x,y,z$. This implies that the spin-orbit interaction is not active to first order, but only couples the ground with excited eigenspaces, so that it can be neglected if the CF is strong enough. In this case, the low-energy degrees of freedom are pure spin degrees of freedom, and the orbital moment is said to be quenched. The inter-ion Hamiltonian will couple pure spins, as in Eq. (23). If, however, the orbital moment is not quenched, the Heisenberg form is not expected to be adequate. Some of the 3*d* compounds fall into this class, but so especially do 4*f* and 5*f* ones. For these systems, the spin exchange may be highly anisotropic, and, in addition, degrees of freedom other than spin are relevant at low T and must be considered in the interaction Hamiltonian.

The most important interactions between ions with unquenched **L** are (i) direct and electron-mediated EMP and MMP exchange interactions, (ii) lattice-mediated EMP interactions, and (iii) direct classical EMP and MMP interactions (usually negligible). All these interactions can be described in terms of effective couplings between operator equivalents for the lowest ionic manifold (Sec. II.A): in the case of an $|L\ S\ M_L\ M_S\rangle$ manifold, spin and orbital degrees of freedom can be separated, and the operators $T_{\Lambda\Sigma\mu\nu}(L,S)=T_{\Lambda\mu}(L)\otimes T_{\Sigma\nu}(S)$ form a complete set in the operator space for the lowest LS manifold, with $\Lambda=0,\ldots,2L$, $\mu=-\Lambda,\ldots,\Lambda$, $\Sigma=0,\ldots,2S$, $\nu=-\Sigma,\ldots,\Sigma$. In the case of rare-earth or actinide ions, spin-orbit coupling prevents a separation of spin and orbital degrees of freedom, and the operators $T_{KQ}(J)$ will be used as a complete operator set for the lowest $|L\ S\ J\ M_J\rangle$ manifold, with $K=0,\ldots,2J$ and $Q=-K,\ldots,K$. Equivalently, the Hermitian multipole operators $O^{\mu}_{\Lambda}(L)\otimes O^{\nu}_{\Sigma}(S)$ or $O^{Q}_{K}(J)$ [Eq. (10)] can be used. For example, the most general interaction between a pair of *f*-electron ions (1 and 2) within their ground J manifolds has the form

$$H_{12}=\sum_{K,K'}\sum_{Q,Q'} I^{QQ'}_{KK'}O^{Q}_{K}(J_1)O^{Q'}_{K'}(J_2), \tag{24}$$

where $K\leqslant 2J_1$, $Q=-K,\ldots,K$, $K'\leqslant 2J_2$, and $Q'=-K',\ldots,K'$. Constraints on the $I^{QQ'}_{KK'}$ coefficients are imposed by symmetry. In particular, since the $O^{Q}_{K}(J)$ have parity $(-1)^K$ under time reversal, only multipoles with the same rank parity are coupled if (as usual) H_{12} has to be time-reversal invariant. If spherical symmetry is imposed, only couplings between multipoles with the same rank K are allowed, whereas in a crystal H_{12} must be invariant under the symmetry operations of the 1-2 bond. By rewriting Eq. (24) in terms of the symmetry-adapted multipoles $O^{K}_{\Gamma\gamma}(J)$ [Eq. (13)], where Γ refers to representations of the bond symmetry group, only Γ-Γ couplings are allowed but ranks need not be equal. Also, if the bond has inversion symmetry, the interaction constant I does not change when ions 1 and 2 are swapped. Finally, if ion 1 is held fixed, H_{12} must rotate as prescribed by the symmetry of the lattice when equivalent ions $2'$ are considered. The form of $H_{12'}$ may be obtained by applying rotation operators to H_{12}. Equivalently, one can directly obtain the total coupling for ion 1 as

$$H_1=\sum_{2} H_{12}=\sum_{K,K'}\sum_{\Gamma,\gamma} A(K,K',\Gamma)O^{K}_{\Gamma\gamma}(J_1)O^{K'}_{\Gamma\gamma}(\{J_2\}). \tag{25}$$

$O^{K}_{\Gamma\gamma}(J_1)$ are symmetry-adapted multipoles for the central ion 1 [Eq. (13)], where Γ refers to representations of the point group of site 1 and $O^{K'}_{\Gamma\gamma}(\{J_2\})$ indicates linear combinations of the form $\Sigma_2\Sigma_Q c(2,Q)O^{Q}_{K'}(J_2)$ spanning the same representation as the $O^{K}_{\Gamma\gamma}(J_1)$ (Sakai *et al.*, 2003). The $c(2,Q)$ are group-theoretical projection coefficients analogous to those used in building symmetry-adapted electron orbitals in molecules.

1. Direct classical electric- and magnetic-multipole interactions

These interactions arise from the effect of the electric and magnetic fields [Eqs. (1) and (2)] produced by a given ion on surrounding ions, and can be written in the form of a series of multipole-multipole couplings (Wolf and Birgeneau, 1968; Birgeneau *et al.*, 1969; Baker, 1971). They are very weak and usually can be safely neglected in theoretical models. The matrix elements of EMP interactions within an LS multiplet of a given configuration coincide with those of the effective Hamiltonian,

$$H_{\mathrm{emi}}=\sum_{\lambda\lambda'(\mathrm{even})}\sum_{\mu\mu'} K^{\mu\mu'}_{\lambda\lambda'}O^{\mu}_{\lambda}(L_1)O^{\mu'}_{\lambda'}(L_2), \tag{26}$$

which involves the pure orbital degrees of freedom. The coefficients K are proportional to $\langle r_1^{\lambda}\rangle\langle r_2^{\lambda'}\rangle R^{-(\lambda+\lambda'+1)}$, with r_1 and r_2 the radial electron coordinates and R the distance between the nuclei of the two ions. The maximum value permitted for λ and λ' is $\min(2L,2l)$ (see Sec. II.A). Within the lowest J multiplet of an f ion, the coupling has the form (24) with K and K' even and not exceeding $\min(2L,2J,2l)$.

Direct MMP interactions also exist, the strongest being the dipole-dipole interaction. In the lowest J multiplet, the MMP operators are proportional to odd-rank $O^{Q}_{K}(J)$ equivalent operators, and the interaction Hamiltonian will be of the form (24), where for f electrons $K,K'=1,3,5,7$, and again the coefficients $I^{QQ'}_{KK'}$ are proportional to $R^{-(K+K'+1)}$.

2. Electric- and magnetic-multipole interactions arising from direct exchange

Several electronic mechanisms provide effective couplings between multipoles belonging to different ions. For instance, the familiar exchange interaction, which leads to ferromagnetic Heisenberg spin-spin couplings in the simplest frameworks, may also produce couplings between multipoles of high ranks (Levy, 1964; Elliott and Thorpe, 1968; Copland and Levy, 1970). The exchange part of the Coulomb interaction couples both the magnetic and electric multipoles of two ions whose wave functions overlap. The two-site (1 and 2) exchange interaction between electrons belonging to a pair of atomic-like inner shells (nl) may be written as (Anderson, 1963; Mattis, 2006)

$$H_{12} = \sum_{\substack{m_1 m_2 \sigma \\ m_1' m_2' \sigma'}} V_{m_1,m_1',m_2,m_2'} a^\dagger_{2m_2'\sigma'} a^\dagger_{1m_1'\sigma} a_{2m_2\sigma} a_{1m_1\sigma'}, \quad (27)$$

where $a_{im_i\sigma_i}$ are annihilation operators for electrons in (m_i,σ_i) spin orbitals of ion i and $V_{m_1,m_1',m_2,m_2'}$ is a Coulomb matrix element. By exploiting Eq. (11), it is possible to reformulate Eq. (27) in terms of ionic multipoles $\tilde{T}_{\Lambda\Sigma\mu\nu}(l,s)$,

$$H_{12} = \sum_{\Lambda\Lambda'\Sigma} \sum_{\mu\mu'\nu} J^{\mu\mu'}_{\Lambda\Lambda'} (-1)^\nu \tilde{T}_{\Lambda\Sigma\mu\nu}(l_1,s_1) \tilde{T}_{\Lambda'\Sigma\mu'-\nu}(l_2,s_2) \quad (28)$$

with $\Lambda,\Lambda' \leqslant 2l$ and $-\Lambda \leqslant \mu \leqslant \Lambda$, $-\Lambda' \leqslant \mu' \leqslant \Lambda'$. Moreover, $\Lambda+\Lambda'$ is even, due to time-reversal invariance. $J^{\mu\mu'}_{\Lambda\Lambda'}$ coefficients are functions of the $V_{m_1,m_1',m_2,m_2'}$. Within a given LS multiplet, the Wigner-Eckart theorem enables a projection from single-electron to ionic operators to be made, $\tilde{T}_{\Lambda\Sigma\mu\nu}(l,s) \propto T^\mu_\Lambda(L) T^\nu_\Sigma(S)$. The spin-independent ($\Sigma=0$) part of Eq. (28) has the same form as Eq. (26), whereas the spin-dependent ($\Sigma=1$) contribution can be written as

$$H_{12} = \sum_{\Lambda\Lambda'} \sum_{\mu\mu'} I^{\mu,\mu'}_{\Lambda,\Lambda'} O^\mu_\Lambda(L_1) O^{\mu'}_{\Lambda'}(L_2) \mathbf{S}_1 \cdot \mathbf{S}_2, \quad (29)$$

where the coefficients $I^{\mu,\mu'}_{\Lambda,\Lambda'}$ are proportional to $J^{\mu,\mu'}_{\Lambda,\Lambda'}$, and $\Lambda,\Lambda' \leqslant \min(2l,2L)$. It is clear that, for a $3d$ ion with quenched orbital angular momentum, the orbital operators will not be active in the $(2S+1)$-degenerate ground manifold, and the usual Heisenberg form for the exchange will be valid. To be more precise, time-reversal invariance demands only odd-rank orbital operators to have zero expectation value if the ground state is orbitally nondegenerate. Even-rank multipoles may have a nonzero average value, but this will be frozen. For a $4f$ or $5f$ ion, Eq. (29) has to be projected onto the lowest $|LSJ\rangle$ multiplet. Spin and orbital processes are no longer separated and only the total angular momentum is meaningful, yielding an effective Hamiltonian of the form (24) with $K,K' \leqslant \min(2l+1,2L+1,2J)$, and $K+K'$ even.

In most cases, indirect coupling mechanisms are more important than direct exchange, whose strength rapidly decreases with increasing ion-ion distance. In particular, in insulators, SE couplings through the orbitals of intervening ligands often dominate among ion-ion interactions. In metals, the leading group of ion-ion interactions are those mediated by conduction electrons [Ruderman-Kittel-Kasuya-Yosida (RKKY)]. Finally, effective two-ion EMP couplings may be transmitted by phonons through the ME coupling.

3. Superexchange electric- and magnetic-multipole interactions

Ligands shared by two magnetic ions can transmit effective interactions through a kinetic exchange mechanism called superexchange (SE) (Anderson, 1959, 1963; Herring, 1966). A microscopic and quantitative description of SE is complex and dependent on the specific type of involved orbitals and the form of the associated Hamiltonian, whose parameters (e.g., hopping integrals or on-site Coulomb matrix elements) need to be assessed. In the classical cluster-based approaches, SE interactions are limited to nearest-neighbor pairs, but actual interactions may involve more distant pairs. These longer-range interactions can be derived by a band-based approach analogous to the RKKY formalism in metals (Khomskii and Sawatzky, 1997; Schwieger and Nolting, 2002). However, because of the Friedel-type response of conduction electrons to a local polarization of the magnetic ion, RKKY couplings decay algebraically with the ion-ion distance R, whereas in insulators the presence of a band gap leads to an exponential decay of SE interactions with R. In the simplest models of SE, ligand orbitals are not explicitly included and effective hopping integrals between the orbitals of nearby magnetic ions are introduced. Although this approach does not include all possible perturbative paths, it is very useful to capture general essential features of SE. The simplest such model is the nondegenerate tight-binding Hubbard Hamiltonian

$$H_{\mathrm{Hub}} = -t \sum_{\langle ij \rangle} \sum_{\sigma=\uparrow,\downarrow} (a^\dagger_{i,\sigma} a_{j,\sigma} + \mathrm{H.c.}) + U \sum_i n_{i\uparrow} n_{i\downarrow}, \quad (30)$$

where $\langle ij \rangle$ are nearest-neighbor sites and a single orbital per site is assumed. t is an inter-atomic (effective) hopping integral and U is the intra-atomic Coulomb repulsion. For half filling (one electron per site) and in the limit $U \gg t$, charge fluctuations may be perturbatively eliminated and the model maps onto the antiferromagnetic isotropic Heisenberg model (23), with exchange constant $J=4t^2/U$ (Fazekas, 2003).

The simplest possible extension of Eq. (30) including orbital degrees of freedom is the two-orbital Hubbard Hamiltonian (Cyrot and Lyon-Caen, 1975; Kugel and Khomskii, 1982; Fazekas, 2003),

$$H_{\mathrm{Hub}}^{(2)} = \sum_{\langle ij\rangle} \sum_{\alpha\beta=1,2} \sum_{\sigma} t_{i,j}^{\alpha\beta} (a_{i,\alpha\sigma}^{\dagger} a_{j,\beta\sigma} + \mathrm{H.c.}) + \sum_{i\alpha} U_{\alpha} n_{i\alpha\uparrow} n_{i\alpha\downarrow} + U_{12} \sum_{i\sigma\sigma'} n_{i1\sigma} n_{i2\sigma'} - 2J \sum_{i} \mathbf{s}_{i,\alpha} \cdot \mathbf{s}_{i,\beta}, \tag{31}$$

where α and β label the two orbitals, $t_{i,j}^{\alpha\beta}$ are hopping integrals between orbitals α on ion i and β on ion j, U_{α} and U_{12} describe the on-site intraorbital and interorbital Coulomb repulsion, and J represents the intra-atomic exchange constant (leading to Hund's first rule). The Hamiltonian (31) is used mainly to model some cubic d-electron compounds (for instance, $KCuF_3$ or $LaMnO_3$) in which the two orbitals are identified with the two components of a Γ_3 (e_g) doublet, $d_{x^2-y^2}$ and $d_{3z^2-r^2}$. Assuming one electron per site and projecting out charge fluctuations, the effective Hamiltonian for the low-energy configurations is much richer than the Heisenberg model and the pair coupling has a structure of the form (28), restricted to the subspace spanned by the two orbitals. In materials with large hopping amplitude and small on-site Coulomb energy, a cyclic four-spin exchange emerging from a t/U expansion of the Hubbard Hamiltonian (Takahashi, 1977) could also be important in determining the dynamics of the system. These multiple-spin ring-exchange processes were found to be relevant to some strongly correlated electron systems such as La_2CuO_4 (Coldea *et al.*, 2001; Katanin and Kampf, 2002).

A spin-Hamiltonian form analogous to Eq. (29) is often introduced by defining orbital pseudospin operators for each site $\tau_{xi}, \tau_{yi}, \tau_{zi}$ which identify (τ_{zi}) or flip (τ_{xi} and τ_{yi}) the orbital state occupied by the electron at the ith site. For instance, $\tau_{zi} = \Sigma_{\sigma\alpha} c_{\alpha} a_{i,\alpha\sigma}^{\dagger} a_{i,\alpha\sigma}$ with $c_{\alpha} = -1/2$ ($c_{\alpha} = 1/2$) if $\alpha = 1$ ($\alpha = 2$). Thus, the four possible states of each ion are mapped onto the four states of a pair of spins 1/2, $\mathbf{S}$ and $\boldsymbol{\tau}$. The resulting spin Hamiltonian is isotropic with respect to real spins (but not so in general with respect to pseudospins) and has the form

$$H_{\mathrm{eff}} = \sum_{\langle ij\rangle} \sum_{\Lambda\Lambda'=0}^{1} \sum_{\mu\mu'} O_{\Lambda}^{\mu}(\tau_i) O_{\Lambda'}^{\mu'}(\tau_j) (I_{\Lambda,\Lambda'}^{\mu,\mu'} + \tilde{I}_{\Lambda,\Lambda'}^{\mu,\mu'} \mathbf{S}_i \cdot \mathbf{S}_j), \tag{32}$$

where $I_{\Lambda,\Lambda'}^{\mu,\mu'}$ and $\tilde{I}_{\Lambda,\Lambda'}^{\mu,\mu'}$ are functions of the parameters in Eq. (31).

In the following, we use a Hubbard-type model to illustrate the importance and the origin of SE multipolar couplings in localized f-electron compounds. We show how such couplings are ubiquitous and do not result from fortuitous, ad hoc combinations of model parameters. Their size is mostly determined by the configuration-specific intra-atomic interactions. As in Elliott and Thorpe (1968), we neglect energy differences between states belonging to charge-transfer configurations in which an f-electron is transferred from an ion i to one of its neighbors j, i.e., $E(f^{n+1}(i)f^{n-1}(j)) - E(f^{n}(i)f^{n}(j)) = U$ independently of the specific charge-transfer state, in order to minimize the number of free parameters. The hopping Hamiltonian

$$H_{\mathrm{hop}} = \sum_{\langle ij\rangle} \sum_{mm'=-3}^{3} \sum_{\sigma} t_{i,j}^{mm'} (a_{i,m\sigma}^{\dagger} a_{j,m'\sigma} + \mathrm{H.c.}) \tag{33}$$

acts on unperturbed states with n f electrons on each ion and produces charge-transfer states of the form $f^{n+1}(i)f^{n-1}(j)$. The latter can be eliminated in second-order perturbation theory, as with the one- and two-orbital Hubbard models discussed above, to yield an effective two-ion coupling of the form

$$H_{f\text{-}f} = \sum_{\langle ij\rangle} \sum_{mm'pp'\sigma\sigma'} \frac{2 t_{i,j}^{mm'} t_{i,j}^{p'p}}{U} a_{i,m\sigma}^{\dagger} a_{i,p\sigma'} a_{j,p'\sigma'}^{\dagger} a_{j,m'\sigma}, \tag{34}$$

having the same operator structure as Eq. (27). Additional one-body terms produced by the perturbation are not included in Eq. (34) because they simply renormalize the CF. The Hamiltonian (34) is projected onto the lowest $|LSJ\rangle$ as outlined above, thus expressing the multipole coupling parameters in terms of the $t_{i,j}^{mm'}$ hopping parameters,

$$H_{ij} = \sum_{K_i,K_j=1,7} \sum_{Q_i,Q_j} C_{K_i,K_j}^{Q_i,Q_j} T_{K_iQ_i}(J_i) T_{K_jQ_j}(J_j), \tag{35}$$

$$C_{K_i,K_j}^{Q_i,Q_j}(i,j) = \sum_{m,m',\sigma,p,p',\sigma'} \frac{2 t_{i,j}^{mm'} t_{i,j}^{p'p}}{U} \sum_{\Lambda_i,\mu_i,\Sigma_i,\nu_i} \sum_{\Lambda_j,\mu_j,\Sigma_j,\nu_j} \Theta(\Lambda_i,\mu_i,3,m,p)\Theta(\Sigma_i,\nu_i,1/2,\sigma,\sigma')\Theta(\Lambda_j,\mu_j,3,p',m') \times \Theta(\Sigma_j,\nu_j,1/2,\sigma',\sigma)\Omega(\Lambda_i,\Sigma_i,\mu_i,\nu_i,K_i,Q_i)\Omega(\Lambda_j,\Sigma_j,\mu_j,\nu_j,K_j,Q_j)\alpha(n_i,\Lambda_i,\Sigma_i)\alpha(n_j,\Lambda_j,\Sigma_j)(2J_i+1)(2J_j+1) \times \begin{Bmatrix} L_i & L_i & \Lambda_i \\ S_i & S_i & \Sigma_i \\ J_i & J_i & K_i \end{Bmatrix} \begin{Bmatrix} L_j & L_j & \Lambda_j \\ S_j & S_j & \Sigma_j \\ J_j & J_j & K_j \end{Bmatrix} \tag{36}$$

TABLE II. Ground-state energy of various dimers of *f*-electron ions coupled with the part of Eq. (35) associated with a specific pair (K_i,K_j). Spherical symmetry ($t_{i,j}^{mm'}=t\delta_{m,m'}$) is assumed. Energy is expressed in units of $2t^2/U$.

	K_i	K_j	f^1	f^2	f^3	f^4	f^5
Spherical							
	1	1	−0.5	−0.89	−1.26	−1.63	−1.86
	2	2	−0.42	−0.23	−0.23	−0.23	−0.16
	3	3	−1.17	−0.32	−0.26	−0.22	−0.15
	4	4	−0.75	−0.44	−0.12	−0.10	−0.11
	5	5	−1.83	−1.09	−1.04	−0.69	−0.08
	6	6		−0.16	−0.24	−0.14	
	7	7		−0.02	−0.05	−0.02	

with

$$\Theta(\Lambda,\mu,l,m,p)=(-1)^{l-m}\sqrt{2\Lambda+1}\begin{pmatrix} l & \Lambda & l \\ -m & \mu & p\end{pmatrix},$$

$$\Omega(\Lambda,\Sigma,\mu,\nu,K,Q)=(-1)^{\Lambda-\Sigma+Q}\begin{pmatrix}\Lambda & \Sigma & K \\ \mu & \nu & -Q\end{pmatrix}\times\sqrt{(2\Lambda+1)(2\Sigma+1)(2K+1)}, \tag{37}$$

and the $\alpha(n,\Lambda,\Sigma)$ coefficients have been tabulated by Hirst (1978). n_i is the number of *f* electrons of ion *i*, $\Lambda_i=0,\ldots,\min(6,2L_i)$, $\Sigma_i=0,1$, $\mu_i=-\Lambda_i,\ldots,\Lambda_i$, and $\nu_i=-\Sigma_i,\ldots,\Sigma_i$. Once the $t_{i,j}^{mm'}$ hopping parameters are fixed, Eq. (36) yields definite values for the interaction coefficients. The simplest possible choice for the $t_{i,j}^{mm'}$ is that of *spherical symmetry* corresponding to $t_{i,j}^{mm'}=t\delta_{m,m'}$. In this case $C_{K_i,K_j}^{Q_i,Q_j}(i,j)=C_S(K_i)(-1)^{Q_i}\delta_{K_i,K_j}\delta_{Q_i,-Q_j}$. In the special case of the f^1 configuration, $C_S(K)=2t^2/U$ independently of *K*, i.e., the coupling constant is rank independent. This shows that the strength of multipole-multipole couplings produced by SE does not generally decrease with the rank *K*. This property is not specific of the spherical symmetry nor of the f^1 configuration. In order to compare the overall strength of the contributions to Eq. (35) associated with a given pair of ranks $(\bar{K}_i,\bar{K}_j)$, we have calculated the ground-state energy of a dimer of ions in their (*LSJ*) RS ground manifolds, interacting only through the $K_i=\bar{K}_i$ and $K_j=\bar{K}_j$ contributions to Eq. (35). Tables II and III show the results obtained for two cases characterized by a single hopping parameter: spherical symmetry (i.e., $t_{i,j}^{mm'}=t\delta_{m,m'}$) and σ bonding (i.e., $t_{i,j}^{mm'}=t\delta_{m,m'}\delta_{m,0}$, where the bond is the quantization axis). For spherical symmetry $K_i=K_j$ and in general couplings with rank larger than 1 appear to be important. For f^1 and f^2, the largest coupling energy is associated with $K=5$ (triakontadipoles). f^3 is similar to f^2, whereas in f^4 the dipole coupling begins to dominate, and it remains the only relevant one in f^5. f^6 and f^7 are not of interest since for the former $J=0$ and for the latter $L=0$; hence only dipole couplings survive.

For σ bonding, couplings with rank larger than 1 are important too, and the lower symmetry yields nonzero couplings for $\bar{K}_i\neq\bar{K}_j$. Again, in the f^5 case the Hamiltonian (35) is nearly purely dipolar. For actinide dioxides, the actual bond symmetry in the paramagnetic phase is C_{2v} and the bond possesses an inversion center. In this symmetry, there are ten independent $t_{i,j}^{mm'}$ integrals that can be identified by building the linear combinations of the *f* orbitals belonging to definite irreps Γ_l of C_{2v}. Thus, $t_{i,j}^{mm'}$ are expressed as a function of ten $t_{i,j}^{\Gamma_l\Gamma_l}$ parameters. In the present model of SE, ligand orbitals have not been explicitly considered and $t_{i,j}^{\Gamma_l\Gamma_l}$ must be interpreted as effective hopping integrals between the orbitals of the magnetic ions. For actinide dioxides, processes involving oxygen *p* orbitals provide an important contribution to $t_{i,j}^{mm'}$ (Mironov *et al.*, 2003; Kubo and Hotta, 2005a), but other processes may be important too (e.g., involving other orbitals of oxygen or the actinide). A reliable *ab initio* calculation of all $t_{i,j}^{\Gamma_l\Gamma_l}$ is difficult and requires knowledge of a large number of parameters. In view of the fact that we have already neglected the splitting of charge-transfer configurations, we chose to assess the weight of nondipolar interactions by varying the ten independent hopping parameters on a (hyper)cubic grid of values, thus producing the histograms in Fig. 2 for PrO_2 and NpO_2. These histograms only depend on the bond symmetry and the ionic configuration, and show how multipolar interactions do not result from choosing specific sets of values for the hopping matrix elements, but are sizable for most choices of $t_{i,j}^{mm'}$. For every set of $t_{i,j}^{\Gamma_l\Gamma_l}$ resulting from the grid, we have calculated the corresponding $C_{K_i,K_j}^{Q_i,Q_j}$ coupling coefficients. The ground-state energy $E(K',K)$ for a dimer of ions coupled with the part of Eq. (35) associated with a specific pair $(K_i=K,K_j=K)$ has been divided by $E(1,1)$ to explore the relative importance of dipolar and nondipolar interactions. The histograms illustrate the range of variation of these ratios when $t_{i,j}^{\Gamma_l\Gamma_l}$ are varied on the grid. It can be seen that for most choices of the $t_{i,j}^{\Gamma_l\Gamma_l}$ parameters, all

TABLE III. Ground-state energy of various dimers of *f*-electron ions coupled with the part of Eq. (35) associated with a specific pair (K_i,K_j). σ bonding is assumed, i.e., $t_{i,j}^{mm'}=t\delta_{m,m'}\delta_{m,0}$. Energy is expressed in units of $2t^2/U$ and has been multiplied by 10.

	K_i	K_j	f^1	f^2	f^3	f^4	f^5
σ-bond							
	1	1	−0.19	−0.47	−0.8	−1.4	−2.12
	2	2	−0.17	−0.16	−0.02	−0.02	−0.09
	3	3	−0.23	−0.16	−0.05	−0.04	−0.07
	4	4	−0.11	−0.09	−0.03	−0.03	−0.02
	5	5	−1.04	−0.27	−0.53	−0.33	−0.03
	6	6		−0.18	−0.27	−0.17	
	7	7		−0.01	−0.02	−0.01	
	1	3	−0.15	−0.09	−0.15	−0.22	−0.37
	1	5	−0.31	−0.25	−0.5	−0.64	−0.18
	1	7		−0.04	−0.1	−0.09	
	3	5	−0.37	−0.16	−0.16	−0.11	−0.03
	3	7		−0.03	−0.03	−0.02	
	5	7		−0.05	−0.11	−0.05	
	2	4	−0.15	−0.16	−0.04	−0.03	−0.05
	2	6		−0.21	−0.1	−0.07	
	4	6		−0.13	−0.1	−0.08	

nondipolar interactions are important in the f^1 case, which is appropriate for PrO_2. The rank-5 interactions (involving magnetic triakontadipole) are on average the largest and dominate over the dipolar interactions. In the f^3 case, which is appropriate for NpO_2, nondipolar interactions are weaker than in the f^1 case but remain substantial. The largest nondipolar couplings again have rank 5 and are typically half the dipolar ones. When two interactions are of the same order of magnitude, like $K=5$ and 1 in the Np case, the CF plays a key role in determining which of them will eventually drive the ordering (see Sec. IV). It is also worth noting that for both f^1 and f^3, even-rank (EMP) interactions are important too and do not decrease with K. Finally, as in the case of σ bonding (Table III), terms with $K_i\neq K_j$ (not reported here) are sizable.

These calculations show that for *f* electrons SE may produce multipolar interactions comparable to or larger than the dipolar ones, and that rank-5 interactions provide in general the largest nondipolar contribution.

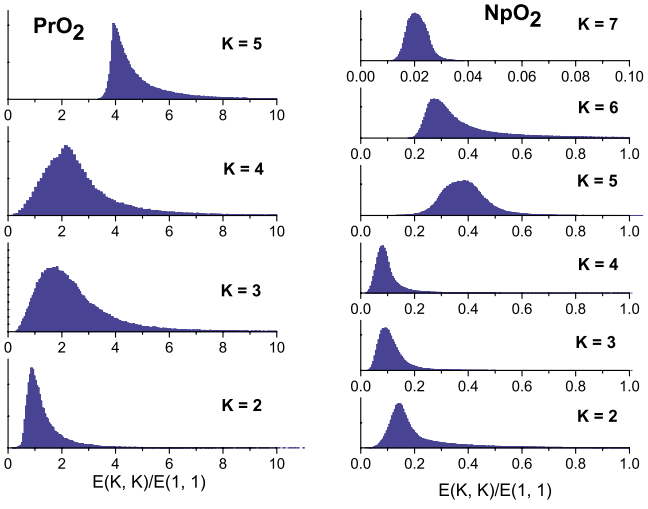

FIG. 2. (Color online) Distribution of the ratio $E(K,K)/E(1,1)$, with $E(K_i,K_j)$ the ground-state energy of a dimer (C_{2v} bond) of Pr^{4+} and Np^{4+} ions coupled with the part of Eq. (35) associated with a specific pair of ranks K_i, K_j. The $t_{i,j}^{\Gamma_l\Gamma_l}$ parameters are varied on a cubic grid.

4. Conduction-electron mediated electric- and magnetic-multipole interactions

In metallic compounds, a very important group of ion-ion interactions are those mediated by conduction electrons. The most studied of these is the pure-spin RKKY coupling, but if the orbital momentum is not quenched, multipole couplings of higher rank may be equally significant. The multipolar degrees of freedom of a given ion produce a polarization of the charge and spin distribution of conduction electrons, which is felt by a second ion and results in effective ion-ion interactions. To simplify the calculations, the electron-mediated coupling is often derived under the assumption of spherical symmetry around each ion (Hirst, 1978). The starting point is the band-ion (*c*-*f*) interaction. In the hypothesis of spherical symmetry, the most general form of this interaction is obtained by exploiting the ionic double-tensor operators $\tilde{T}_{\Lambda\Sigma\mu\nu}$ [Eq. (11)] and analogous quantities defined for conduction electrons, where for the latter one-body operators of the type $c^{\dagger}_{k'l'm'\sigma'}c_{klm\sigma}$ are combined through 3*j* symbols as in Eq. (11) to yield spherical

double tensors for *c*-electrons $C_{\Lambda\Sigma\mu\nu}(k'l'kl)$. They describe a process in which a conduction electron is annihilated in the partial wave (kl) and recreated in the partial wave $(k'l')$. The most general spherically symmetric *c*-*f* interaction is thus written as

$$H_{cf}=\sum_{k'l'kl\Lambda\mu\Sigma\nu} I(k'l'kl\Lambda\Sigma)\tilde{T}^{\dagger}_{\Lambda\Sigma\mu\nu}(l_0,s)C_{\Lambda\Sigma\mu\nu}(k'l'kl), \tag{38}$$

where I (independent of μ and ν) is the *c*-*f* coupling constant and $l_0=3$ for *f* electrons. Parity imposes the requirement that $l-l'$ be even, and Hermiticity demands that $I(k'l'kl\Lambda\Sigma)=I(klk'l'\Lambda\Sigma)$. By projecting the interaction onto the lowest *LS* manifold, and then onto the lowest *J* manifold, orbital and spin flips can no longer be separated for ionic electrons, although such separation continues to exist for *c* electrons. To simplify the form of the final Hamiltonian, one can combine the double tensors $C_{\Lambda\Sigma\mu\nu}(k'l'kl)$ into a single tensor $C_{\Lambda\Sigma KQ}(k'l'kl)$ as in Eq. (12). This gives

$$H_{cf}=\sum_{k'l'kl}\sum_{\Lambda\Sigma KQ} K(k'l'kl\Lambda\Sigma K) \times T^{\dagger}_{KQ}(J)C_{\Lambda\Sigma KQ}(k'l'kl). \tag{39}$$

Having determined the general form of the two-body *c*-*f* coupling, the microscopic interactions that generate it remain to be characterized. There are two main mechanisms providing the *c*-*f* coupling: Coulomb interactions (both direct and exchange) and effective two-body interactions arising from virtual valence fluctuations. These are produced by one-body *c*-*f* processes (hybridization). The *c*-*f* processes from the direct part of the Coulomb coupling represent a classical electrostatic interaction and are characterized by having $\Sigma=0$ and $\Lambda=0,2,\ldots,2l$. They describe the EMP polarization of the band produced by the magnetic ion. There are actually also MMP processes which arise from the classical electrodynamic interaction between ionic and conduction currents, but these relativistic terms are much smaller and are usually neglected. The exchange part of the Coulomb coupling, on the contrary, contains all possible *c*-*f* processes, namely, $\Lambda=0,1,2,\ldots,2l$ and $\Sigma=0,1$. $\Lambda=0$ processes usually dominate, even if in some cases $\Lambda\neq 0$ processes turn out to be important (Fert and Levy, 1977; Fulde and Löwenhaupt, 1986).

A sizable contribution to the *c*-*f* interaction may come from virtual valence fluctuations, i.e., processes in which an electron is transferred between ionic and conduction states. The most important processes are one-body (hybridization) processes described by a Hamiltonian of the form

$$H_{\mathrm{hyb}}=\sum_{km\sigma} V(k)(a^{\dagger}_{l_0m\sigma}c_{kl_0m\sigma}+\mathrm{H.c.}), \tag{40}$$

where $l_0=3$ for *f* electrons (spherical symmetry has been assumed). If the ionic configuration (f^n or d^n) is sufficiently stable, hybridization processes can be eliminated by second-order perturbation theory (Schrieffer and Wolff, 1966), thus obtaining an effective *c*-*f* two-body coupling as in Eq. (39). This interaction will be of order $|V|^2/E$, where $V=V(k_F)$ and E is the energy cost of an electron-transfer process. The condition $\pi|V|^2\rho(E_F)\ll E$ (with ρ the *c*-electron density of states) has to be satisfied in order to remain far from a valence instability, i.e., for a single ionic configuration to predominate. The effective interaction for processes with k,k' near k_F has the form of Eq. (38) (Hirst, 1978) with coupling constants $I(k'l'kl\Lambda\Sigma)=I\delta_{l'l_0}\delta_{ll_0}$ and the usual constraints $\Lambda\leqslant 2l_0$ and $\Sigma=0,1$. The spin Kondo coupling corresponds to $\Lambda=0$, $\Sigma=1$. Next, the interaction can be projected onto the lowest *LS* or *J* manifolds. In the special case of an f^1 configuration (Ce^{3+}), the *J*-projected Hamiltonian can be shown to coincide with the Coqblin-Schrieffer Hamiltonian (Coqblin and Schrieffer, 1969). A characteristic of the effective *c*-*f* interaction produced by virtual mixing is that all conduction and *f* multipoles (either electric and magnetic) are coupled, with a strength that does not usually decrease with the rank (K) of the multipole. For instance, in the Coqblin-Schrieffer Hamiltonian the coupling constant is K independent and antiferromagnetic.

Whether the *c*-*f* interaction arises from Coulomb or virtual mixing processes, it will produce an effective coupling of the multipole moments of different ions when conduction-electron degrees of freedom are eliminated by second-order perturbation theory. The conduction-electron tensor operators at the different sites can be expanded in terms of creation and annihilation operators of Bloch electrons $c^{\dagger}_{\mathbf{k},\sigma}c_{\mathbf{k}',\sigma'}$. The relevant second-order processes are those in which an electron-hole pair is created at site i and annihilated at a different site j, these processes accompanied by a flip of one of the ion's multipoles. An explicit calculation of the resulting coupling requires detailed knowledge of the band structure (Teitelbaum and Levy, 1976). In any case, the *J*-projected effective ion-ion interaction will be of the form of Eq. (24), where both odd and even values of K and K' are allowed, provided $K+K'$ is even. The direct part of the Coulomb *c*-*f* interaction couples only EMPs (even K and K'), whereas its exchange part, as well as the virtual mixing interaction, contribute to all kinds of couplings. Since in the virtual mixing *c*-*f* coupling all multipoles are equally important, the same will hold for the effective ion-ion interaction it produces. The coupling constants $I^{QQ'}_{KK'}$, are of order $F(K)F(K')$, where $F(K)$ is the *c*-*f* coupling constant for multipoles of rank K, and are long range and oscillatory.

5. Lattice-mediated electric-multipole interactions

Indirect interactions between EMPs may also be transmitted by lattice vibrations (Sugihara, 1959; Birgeneau *et al.*, 1969; Gehring and Gehring 1975). To describe this effect, the starting point is the one-ion ME Hamiltonian H_{ME}, usually limited to the first order in the displacements (harmonic approximation). This Hamiltonian describes the coupling between the EMPs

of the magnetic shell and the local deformations of the lattice, and can be considered as the strain derivative of the CF Hamiltonian $H_{\rm CF}$ (MMPs do not couple with the lattice displacements due to time-reversal invariance). Just like $H_{\rm CF}$, $H_{\rm ME}$ contains multipoles with even rank up to $2l$.

The most general ME coupling is obtained by classifying the normal modes of vibration of a cluster formed by the magnetic ion at site i and its ligands according to irreducible representations of the point symmetry group. The cluster Hamiltonian has to transform as the identity representation of the point group. This is achieved by classifying the magnetic-ion degrees of freedom in terms of point-group representations as in Eq. (13). Next, all possible ME invariants are obtained by coupling ionic multipoles of symmetry Γ_s with local normal modes Q having the same symmetry. If the cluster has an inversion center, only even normal modes couple to the ion. The ME coupling for an ion will then be of the type (Gehring and Gehring, 1975; Morin and Schmitt, 1990)

$$H_{\rm ME} = \sum_{K=2,4,6} \sum_{s,t} V_K(\Gamma_s) O^K_{\Gamma_s t}(J) Q(\Gamma_s,t), \tag{41}$$

where $Q(\Gamma_s,t)$ represents the local distortion, t labels the components of the Γ_s representation of the site symmetry group, and V are coupling constants.

The same type of expansion will be made for an ion at a different site j. The effective interaction between sites i and j arises because the normal modes of the two clusters are not independent. In fact, they arise from the normal modes of the crystal as a whole, namely, the phonons. The local normal modes at sites i and j may then be expanded in terms of creation and annihilation operators of lattice phonons of wave vector $\mathbf{k}$ and polarization index p. With second-order perturbation theory one obtains the effective two-ion interaction between EMPs of the form (24). The $I^{QQ'}_{KK'}$ coefficients can be calculated in terms of V_K and the specific phonon spectrum, and are of order $V_K V_{K'} \eta_K \eta_{K'}$ with η_K the proportionality coefficient between the ion's EMP moments of rank K and their corresponding operator equivalents. For instance, $\eta_2 \equiv \alpha$, the second-order Stevens coefficient (Abragam and Bleaney, 1970).

A detailed microscopic calculation of the $I^{QQ'}_{KK'}$ is very difficult, so that the coupling constants are often considered as unknown parameters. In ionic compounds it is possible to estimate the ion-lattice coupling constants with a *point-charge model* approach, in which the magnetic ion and its neighbors are approximated by point charges. For instance, a calculation of this type has been made for the quadrupolar interactions in UO_2 (Allen, 1968a, 1968b). It is clear that a point-charge calculation of the ME couplings has more or less the same degree of accuracy as a point-charge calculation of the CF parameters. It should be noted that, just as the importance of the various CF contributions does not decrease with increasing multipole rank, the size of the coefficients V_K does not decrease with increasing K. If acoustic phonons provide the main transmitting medium, the coupling constants $I^{QQ'}_{KK'}$ are rather long ranged, as may be expected given the long-range character of strain fields in an elastic continuum.

D. Multipolar interactions in *j-j* coupling

Multipolar interactions can be studied by multiorbital Hubbard models in the *j-j* coupling limit (Hotta and Ueda, 2003; Kubo and Hotta, 2005b; Hotta, 2006). Even if for *f*-electron systems it suffers from the limitations mentioned in Sec. II.B.3, this approach may simplify calculations with respect to the *LS* scheme of the previous section. For instance, in the truncated Γ_8 model (Hotta and Ueda, 2003; Kubo and Hotta, 2005b), a hopping term of the form

$$H_{\rm kin} = \sum_{\mathbf{i},\mathbf{a},\mu,\nu} t^{\mathbf{a}}_{\mu\nu} a^\dagger_{\mathbf{i}\mu} a_{\mathbf{i}+\mathbf{a}\nu} \tag{42}$$

is added to $H_{\rm int}$ [Eq. (21)] and $H_{\rm CF}$ [Eq. (22)]. If only σ bonding is assumed to be sizable, the direct hopping amplitude for f electrons along the vector $\mathbf{a}$ is given by (Hotta and Ueda, 2003)

$$t^{\mathbf{a}}_{\mu\nu} = \sum_{\sigma=\pm 1/2} \frac{4\pi}{7} S_{33} C_{\mu\sigma} C_{\nu\sigma} Y^*_{3,\mu-\sigma}(\theta,\phi) Y^*_{3,\nu-\sigma}(\theta,\phi), \tag{43}$$

where $S_{ll'}$ denotes Slater's two-center integral (Slater and Koster, 1954) through a σ bond (for f electrons, $l=l'=3$), $C_{\mu\sigma} = -\sigma(2-8\mu\sigma/7)^{1/2}$, and θ,ϕ are the polar and azimuthal angles defined by $\mathbf{a}$. In the presence of ligand anions, an effective hopping integral can be derived with second-order perturbation theory (Hotta and Ueda, 2003).

We recall that the one-electron CF potential with cubic symmetry splits the $j=5/2$ sextet into a Γ_8 quartet and a Γ_7 doublet; the former is the ground state for $A^0_4 < 0$, a situation that is normally realized when ligand anions are positioned in a fcc or bcc lattice. In the truncated Γ_8 model, the doublet is ignored and four new annihilation operators for the Γ_8 states are defined:

$$f_{\mathbf{i}\alpha\uparrow} = \sqrt{5/6} a_{\mathbf{i}-5/2} + \sqrt{1/6} a_{\mathbf{i}3/2}, \tag{44}$$

$$f_{\mathbf{i}\alpha\downarrow} = \sqrt{5/6} a_{\mathbf{i}5/2} + \sqrt{1/6} a_{\mathbf{i}-3/2}, \tag{45}$$

$$f_{\mathbf{i}\beta\sigma} = a_{\mathbf{i}-\sigma}, \tag{46}$$

where $\sigma = \pm\frac{1}{2}$. The resulting Hamiltonian is

$$\begin{aligned} H_{\Gamma_8} = & \sum_{\mathbf{i},\mathbf{a},\sigma,\tau,\tau'} t^{\mathbf{a}}_{\tau\tau'} f^\dagger_{\mathbf{i}\tau\sigma} f_{\mathbf{i}+\mathbf{a}\tau'\sigma} + \mathcal{U} \sum_{\mathbf{i},\tau} f^\dagger_{\mathbf{i}\tau\uparrow} f_{\mathbf{i}\tau\uparrow} f^\dagger_{\mathbf{i}\tau\downarrow} f_{\mathbf{i}\tau\downarrow} \\ & + \mathcal{U}' \sum_{\mathbf{i},\sigma,\sigma'} f^\dagger_{\mathbf{i}\alpha\sigma} f_{\mathbf{i}\alpha\sigma} f^\dagger_{\mathbf{i}\beta\sigma'} f_{\mathbf{i}\beta\sigma'} \\ & + \mathcal{J} \sum_{\mathbf{i},\sigma,\sigma'} f^\dagger_{\mathbf{i}\alpha\sigma} f^\dagger_{\mathbf{i}\beta\sigma'} f_{\mathbf{i}\alpha\sigma'} f_{\mathbf{i}\beta\sigma} \\ & + \mathcal{J}' \sum_{\mathbf{i},\tau\neq\tau'} f^\dagger_{\mathbf{i}\tau\uparrow} f^\dagger_{\mathbf{i}\tau\downarrow} f_{\mathbf{i}\tau'\downarrow} f_{\mathbf{i}\tau'\uparrow}, \end{aligned} \tag{47}$$

where $\mathcal{U}$, $\mathcal{U}'$, $\mathcal{J}$, and $\mathcal{J}'$ are the intraorbital, interorbital, exchange, and pair-hopping contributions to the Coulomb interaction term (these four coefficients can be expressed as a linear combination of Slater radial integrals; note that $\mathcal{U}=\mathcal{U}'+\mathcal{J}+\mathcal{J}'$).

Considering an occupancy of one electron (hole) per site within the Γ_8 quartet (applicable to the f^1 and f^3 configurations) and applying second-order perturbation theory on the hopping term, one can determine an effective Hamiltonian for the exchange interaction,

$$H_{\rm ex} = -\sum_{\langle \mathbf{i},\mathbf{i}'\rangle} \sum_{\tau_1,\tau_2,\tau_3,\tau_4} \sum_{\sigma_1,\sigma_2,\sigma_3,\sigma_4} \mathcal{I}^{\mathbf{i}-\mathbf{i}'}_{\tau_3\sigma_3,\tau_4\sigma_4;\tau_1\sigma_1,\tau_2\sigma_2} \times f^{\dagger}_{\mathbf{i}\tau_3\sigma_3} f_{\mathbf{i}\tau_1\sigma_1} f^{\dagger}_{\mathbf{i}'\tau_4\sigma_4} f_{\mathbf{i}'\tau_2\sigma_2}, \quad (48)$$

where $\langle \mathbf{i},\mathbf{i}'\rangle$ denotes a pair of nearest neighbors and the generalized exchange interaction $\mathcal{I}$ can be calculated by evaluating the matrix elements between ground and excited states and is of the order $t^2/(\mathcal{U}'-\mathcal{J})$.

Depending on the lattice structure, the explicit form of each multipolar interaction term can be evaluated and, within a mean-field approximation, it is possible to verify the nature of the occurring ordered phase. For example, in the case of a simple-cubic lattice, an antiferromagnetic ordering of Γ_3 quadrupoles is found, whereas for a bcc lattice, Γ_2 octupoles first order antiferromagnetically; in both cases, a transition to a ferromagnetic state follows at lower temperature (Kubo and Hotta, 2005c). We discuss in more detail the fcc lattice case, as it is the relevant one for dioxides. The correlation function

$$\chi_{\mathbf{q}} = \frac{1}{N}\sum_{\mathbf{r},\mathbf{r}'} \exp[i\mathbf{q}\cdot(\mathbf{r}-\mathbf{r}')]\langle X_{\mathbf{r}} X_{\mathbf{r}'}\rangle \quad (49)$$

has been evaluated for each of the 15 multipole operators X active in the Γ_8 quartet (listed in Table I) for different wave vectors $\mathbf{q}$, by exact diagonalization performed on an eight-site cluster (Kubo and Hotta, 2005b). The correlation function [Fig. 3(a)] is clearly enhanced for O_{xy}, T^{α}_z, and T^{β}_z multipoles at $\mathbf{q}=(0,0,1)$. The fact that no term in the effective model stabilizes O_{xy}-type order at this wave vector indicates that the enhancement of the corresponding correlation function is due to the presence of induced quadrupolar moments resulting from one of the two octupoles. Mean-field theory predicts that the T^{β}_z octupole ordered state has the lowest energy, and the anisotropy of the Γ_5 moments in the Γ_8 subspace (which has an easy axis along [1 1 1] and equivalent directions) indicates the occurrence of longitudinal 3-**k** multipolar order. Specific heat and magnetic susceptibility calculated within this model [Figs. 3(b) and 3(c)] are qualitatively compatible with experimental values: quantitative agreement is not to be expected, mainly because of the limitations in assessing the correct CF ground state within a pure *j*-*j* model (as discussed in Sec. II.B.3).

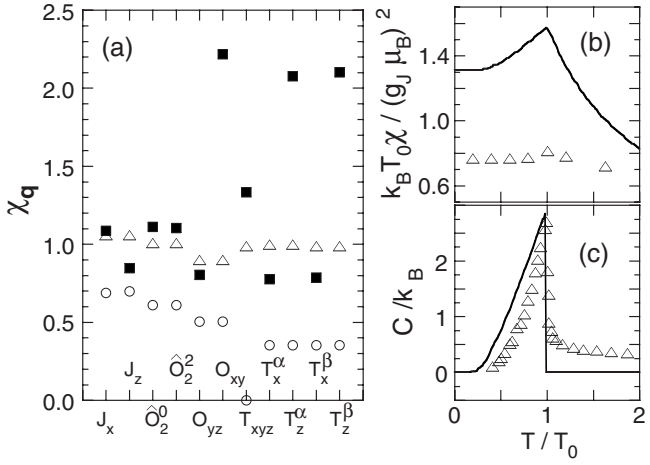

FIG. 3. Results of the multipolar model in *j*-*j* coupling proposed for NpO_2 by Kubo and Hotta (2005b). (a) Correlation functions for multipolar operators on a fcc lattice, calculated by exact diagonalization on an eight-site cluster, for $\mathbf{q}=(0,0,0)$ (circles), $\mathbf{q}=(0,0,1)$ (squares), and $\mathbf{q}=(1/2,1/2,1/2)$ (triangles). The $T^{\alpha,\beta}_x$ and $T^{\alpha,\beta}_y$ operators have the same correlation function as O_{yz} and O_{zx}. (b) Magnetic susceptibility and (c) specific heat calculated (lines) for NpO_2 in mean-field approximation, compared with experimental data (triangles).

E. Group theory considerations

The two-ion Hamiltonians H_{ij} of the previous sections may drive phase transitions toward dipole-or multipole-ordered phases. Whether an ordered phase exists and which is the OP is determined by the joint action of H_{ij} and single-ion terms.

In most practical cases, the phase diagram is calculated by performing a mean-field (MF) decoupling in H_{ij}, thus producing a Hamiltonian describing a single ion or a few ions in an effective molecular field of dipole or multipole character. Of course, its effect depends crucially on the response of each ion to it. Part of the multipolar degrees of freedom of the free ion may be quenched by the CF, i.e., the corresponding multipolar susceptibility does not diverge at low T, and saturates to a small value (i.e., it has a Van Vleck-type response associated with second-order mixing of excited CF states). The opposite is possible too, i.e., some multipolar susceptibilities may be enhanced by the CF with respect to their free-ion values.

The CF also leads to equivalences between multipolar OPs of different ranks: multipoles will be labeled as in Eq. (13) by the point-group irreps which are subdued by the full orthogonal group irrep of rank-K multipoles. For example, magnetic dipoles belong to the $D^{(1+)}$ irrep of $O(3)$ and will be labeled as Γ^+_4 in O_h. Such an irrep also appears in the decomposition of the magnetic-octupole irrep $D^{(3+)}$. This implies that in O_h three out of seven octupoles are equivalent to dipoles from the point of view of symmetry. Even if they represent physically distinct observables, an ordering of dipoles will be accompanied by an ordering of Γ_4 octupoles, and vice versa. Thus, the CF greatly reduces the number of pos-

sible inequivalent ordered phases. For instance, the Hamiltonian (32) may lead to phase transitions characterized by spin ($\langle \mathbf{S}_j \rangle \neq 0$) or orbital ($\langle \tau_j \rangle \neq 0$) ordering. Since the cubic Γ_3 orbital doublet described by the pseudospin τ does not carry any magnetic dipole moment (the reduction of $\Gamma_3 \times \Gamma_3$ does not contain the magnetic moment Γ_4 irrep), pure orbital ordering will be of multipolar type. In particular, τ_{xi} and τ_{zi} describe the order of Γ_3 electric quadrupoles (Kugel and Khomskii, 1982) (i.e., the symmetry of the charge-density distribution of d electrons becomes lower than cubic), whereas τ_{yi} describes the order of the Γ_2 magnetic octupole, which represents an orbital current distribution of tetrahedral symmetry with no associated magnetic-dipole moment and no charge distortion (Takahashi and Shiba, 2000; van den Brink and Khomskii, 2001). In this context, as far as symmetry is concerned, an order of Γ_3 electric hexadecapoles would be equivalent to the above-mentioned quadrupole ordering. In fact, these high-rank quantities are locked to the low-rank ones by the CF potential.

In the case of *f*-electron ions, active multipole degrees of freedom are set by the symmetry of the lowest-lying CF states $|J\Gamma_g l\rangle$, where Γ_g is a point-group irrep and l labels its components. The multipoles $O^K_{\Gamma\gamma}(J)$ [Eq. (13)] carried by the ground-state $|J\Gamma_g l\rangle$ can be identified by the irreps appearing in the decomposition of the symmetric and antisymmetric components in $\Gamma_g \times \Gamma_g$: if the multipole is time even (time odd), Γ must be contained in $[\Gamma_g \times \Gamma_g]_S$ for an even (odd) number of electrons, and in $[\Gamma_g \times \Gamma_g]_A$ for an odd (even) number of electrons (Abragam and Bleaney, 1970). For instance, the cubic Γ_5-triplet ground state of U ions in UO_2 satisfies $[\Gamma_5 \times \Gamma_5]_S = \Gamma_1 + \Gamma_3 + \Gamma_5$ and $[\Gamma_5 \times \Gamma_5]_A = \Gamma_4$. Considering that the number of electrons is even, Γ_5 carries (i) a triplet of Γ_4 time-odd degrees of freedom, whose lowest-rank component represents the magnetic dipole; (ii) a triplet of Γ_5 time-even degrees of freedom, whose lowest-rank component represents electric quadrupoles (transforming as xy, xz, yz); and (iii) a doublet of Γ_3 time-even degrees of freedom, whose lowest-rank component represents the two remaining electric quadrupoles (transforming as $3z^2 - r^2$ and $x^2 - y^2$). There is also a single totally symmetric time-even multipole, whose lowest-rank component represents the electric hexadecapoles coupled to the CF. Of course, the latter are frozen to a finite value within the ground state, and cannot induce a phase transition (the associated susceptibility does not diverge as $T \to 0$).

Another important case occurring in both PrO_2 and NpO_2 is that of a Γ_8-quartet CF ground state. Since $[\Gamma_8 \times \Gamma_8]_S = \Gamma_2 + 2\Gamma_4 + \Gamma_5$ and $[\Gamma_8 \times \Gamma_8]_A = \Gamma_1 + \Gamma_3 + \Gamma_5$, and since the number of electrons is odd, this state carries the same time-even multipoles (Γ_1, Γ_3, Γ_5) as the Γ_5 triplet, but a larger number of time-odd ones: in addition to two independent sets of time-odd degrees of freedom with Γ_4 symmetry (whose lowest-rank component represents magnetic dipoles), time-odd multipoles transforming as Γ_2 and Γ_5 are also present (Table I). Their lowest-rank components are octupoles, since both these irreps appear in the decomposition of the octupole irrep $D^{(3+)}$ in O_h.

The way a phase transition affects the multipole moments of an ion can be established by explicitly performing a MF calculation for a given ordered structure. If a single-site MF model is appropriate, the corresponding effective Hamiltonian will be of the form

$$H = H_{\mathrm{CF}} + \sum_{KQK'Q'} J^{QQ'}_{KK'} O^Q_K(J) \langle O^{Q'}_{K'}(J) \rangle_T + C, \tag{50}$$

where $\langle \cdots \rangle_T$ is a self-consistent thermal average and C is a T-dependent energy shift.

Qualitative information can also be gathered by inspecting the corresponding Landau free energy $\mathcal{F}$ without performing an explicit calculation by Eq. (50). The OP of the phase transition coincides locally with a given set of multipole moments of the ion belonging to some irrep Γ_0 of the ion's point group. The symmetry-allowed low-order terms in the expansion of the MF free energy allow us to determine the order of the phase transition and also which additional multipole moments can be induced as secondary (local) OPs by the primary OP. If the phase transition is second order, a typical minimal expansion near the transition temperature T_c has the form

$$\mathcal{F} = \mathcal{F}_0 + a(T - T_c) \sum_i \psi_i^2 + f_4(\{\psi_i\}) + \alpha \sum_j \eta_j^2 + h_{mn}(\{\psi_i\}, \{\eta_j\}), \tag{51}$$

where $\mathcal{F}_0$ is a smooth contribution, $a > 0$, $\alpha > 0$, and ψ_i are the primary OP components spanning the Γ_0 irrep, whereas η_j are the components of a secondary OP and span irrep Γ_{sec}. f_4 is a polynomial of order 4 in ψ_i and h_{mn} is a mixed polynomial of order m in ψ_i and n in η_j. These polynomials make $\mathcal{F}$ invariant under the point-group operations and their structure is fixed by the Clebsch-Gordan coupling coefficients which single out the totally symmetric irrep Γ_1 in the direct product irreps $[\Gamma_0]^4$ and $[\Gamma_0]^m \times [\Gamma_{\mathrm{sec}}]^n$.

For $T < T_c$, the primary OP $\psi \neq 0$, and the secondary OP η can be induced by ψ only if $n = 1$ (Toledano and Toledano, 1987). This implies that, independently of the specific system and symmetries involved, a primary OP of EMP type cannot induce a secondary OP of MMP type since h_{m1} would not be invariant under the operation of time reversal. Of course, the opposite is not true and a primary MMP OP can (and, usually, does) induce secondary OPs of both electric and magnetic type. In particular, let ψ_i be identified with the rank-K quantities $\langle O^K_{\Gamma_0 i}(J) \rangle$ [Eq. (13)]. If below T_c $\mathcal{F}$ is minimized by some linear combination of ψ_i, the same linear combination of the $\langle O^{K'}_{\Gamma_0 i}(J) \rangle$ is induced for all K' (with the same T dependence). For instance, standard dipole order in dioxides corresponds to $\psi_i \equiv \langle O^1_{\Gamma_4 i}(J) \rangle$ since the three dipoles span a Γ_4 irrep of the O_h point group. An ordering of all $\eta_j \equiv \langle O^{K'=3,5,\ldots,2J-1}_{\Gamma_4 j}(J) \rangle$ multipoles is induced by the coupling $h_{11} \propto \Sigma_i \psi_i \eta_i$, resulting in $\eta_i(T) \propto \psi_i(T)$ (η_i represent

electromagnetic multipoles for $K' \leqslant 7$ only). Other secondary OPs are associated with mixed invariants h_{m1} with $m>1$. In particular, since $\Gamma_4 \times \Gamma_4 = \Gamma_1 + \Gamma_3 + \Gamma_4 + \Gamma_5$, there are h_{21} terms where η_j is a set of Γ_3, Γ_4, or Γ_5 EMPs, which can be induced quadratically as secondary OPs. Which of the possible η_j are actually induced depends on the specific linear combination of ψ_i minimizing $\mathcal{F}$. For instance, the type-I 1-**k** AF order initially proposed for UO_2 (see Sec. IV.A) corresponds to a local dipole moment along one of the cubic axes, i.e., $\psi_1 = \langle J_\alpha \rangle$, $\psi_2 = \psi_3 = 0$ with $\alpha = x$ or y or z depending on which domain is selected. In this case, out of the five Γ_3 and Γ_5 electric quadrupoles, only the axial combination η^α transforming as $3\alpha^2 - r^2$ is induced, $\eta^\alpha \propto (\psi_1)^2$ to leading order. Thus, the *f*-electron charge distribution would become prolate (or oblate) along the α axis with a critical exponent β twice that of the dipole OP.

Even if the point-group framework is suitable for studying some aspects of the ordering process in the MF approximation, the appropriate mathematical context for a full and rigorous symmetry analysis of a phase transition is of course that of the space group G. The set of all multipole moments or operators on all magnetic ions provides a basis for a tensor representation of the space group (Evarestov and Smirnov, 1997), which can be reduced into $\Gamma_\nu(\{\mathbf{k}\})$ irreps labeled by a wave-vector star $\{\mathbf{k}\}$ and a little-group irrep index ν (Bradley and Cracknell, 1972). This corresponds to Fourier transforming at $\mathbf{k}$ the ionic multipole operators

$$O_K^Q(\mathbf{k},d) = \frac{1}{\sqrt{N}} \sum_i O_K^Q(\mathbf{R}_{id}) e^{i\mathbf{k}\cdot\mathbf{R}_i}, \tag{52}$$

where i labels cells and d labels ions in the basis ($d=1$ in dioxides), and to build linear combinations of the $O_K^Q(\mathbf{k},d)$ which transform as a specific small irrep Γ_ν of the little group of wave vector $\mathbf{k}$, $G_\mathbf{k}$. For instance, for the $Fm\bar{3}m$ space group of dioxides and $\mathbf{k} = X_z \equiv (0,0,2\pi/a)$ (in the reference frame of the conventional cell), the star of $\mathbf{k}$ is made of the three arms $\mathbf{k}_1 = (0,0,2\pi/a)$, $\mathbf{k}_2 = (0,2\pi/a,0)$, and $\mathbf{k}_3 = (2\pi/a,0,0)$. Since the space-group is symmorphic, the small irreps of $G_\mathbf{k}$ are those of the little cogroup of X_z, which is D_{4h}. If $K=1$ we have dipole irreps with $\Gamma_\nu \equiv \Gamma_2^{(+)}$ (one dimensional) or $\Gamma_\nu \equiv \Gamma_5^{(+)}$ (two dimensional). Since there are three star arms, the corresponding space-group irreps have dimensions 3 and 6, respectively. A phase transition where the active irrep is $\Gamma_2^{(+)}$ ($\Gamma_5^{(+)}$) corresponds to longitudinal (transverse) type-I AF order. The transverse case is realized in UO_2, the longitudinal one in USb.

The direction of the OP within the representation subspace determines the type of order (1-**k** or multi-**k**), and equivalent directions distinguish the possible domains. In the phenomenological Landau-theory framework, the actual direction depends on the form of the Landau free energy $\mathcal{F}$ for T close to T_c. For instance, for the longitudinal $\Gamma_2^{(+)}$ OP ($\psi_{\mathbf{k}_1}$, $\psi_{\mathbf{k}_2}$, $\psi_{\mathbf{k}_3}$),

$$\mathcal{F} = \mathcal{F}_0 + a(T-T_c) \sum_{i=1,3} \psi_{\mathbf{k}_i}^2 + a_4 \sum_{i=1,3} \psi_{\mathbf{k}_i}^4 + b_4 \sum_{i \neq j} \psi_{\mathbf{k}_i}^2 \psi_{\mathbf{k}_j}^2 + a_6 \sum_{i=1,3} \psi_{\mathbf{k}_i}^6 + b_6 \sum_{i \neq j} \psi_{\mathbf{k}_i}^4 \psi_{\mathbf{k}_j}^2 + c_6 \psi_{\mathbf{k}_1}^2 \psi_{\mathbf{k}_2}^2 \psi_{\mathbf{k}_3}^2 + \cdots . \tag{53}$$

It is clear that, up to second order, the OP components on the different star arms are decoupled, i.e., 1- and multi-**k** structures have the same free energy. This degeneracy is removed only by fourth- or sixth-order terms, which can originate from CF or multipolar interactions. For instance, if sixth-order terms are neglected, the structure will be 1-**k** if $b_4>0$ and 3-**k** if $b_4<0$. A 2-**k** structure is always unfavorable, but it can be stabilized by large enough sixth-order terms. The importance of multipolar interactions in the stabilization of multi-**k** structures explains why the latter are fairly common in Ce and actinide compounds, and much less in *d*-electron systems.

Type-I AF order of quadrupoles, $K=2$, corresponds to the small irreps $\Gamma_\nu \equiv \Gamma_3^{(+)}$ (one dimensional), $\Gamma_4^{(+)}$ (one dimensional), or $\Gamma_5^{(+)}$ (two dimensional). In particular, $\Gamma_4^{(+)}$ describes a symmetry lowering to the tetragonal space groups $P4_2/mmc$ and $P4_2/nnm$ for 1- and 2-**k** orderings, respectively, and to the cubic group $Pn\bar{3}m$ for 3-**k** ordering. The latter describes the quadrupole structure of NpO_2. A $\Gamma_5^{(+)}$ OP describes a symmetry lowering to several different space groups depending on the direction of the OP in the six-dimensional irreducible subspace. We explicitly mention the 3-**k** case which is relevant to UO_2 where the structure is described by the cubic $Pa\bar{3}$ group. For both the $\Gamma_4^{(+)}$ and $\Gamma_5^{(+)}$ quadrupolar structures, the quadrupole contribution to the Landau free energy $\mathcal{F}_Q$ qualitatively differs from Eq. (53) for the presence of third-order invariants, which are forbidden if the OP is odd under time reversal. For instance, in the $\Gamma_4^{(+)}$ case,

$$\mathcal{F}_Q = a_2 \sum_{i=1,3} \psi_{\mathbf{k}_i}^2 + a_3 \psi_{\mathbf{k}_1} \psi_{\mathbf{k}_2} \psi_{\mathbf{k}_3} + \cdots . \tag{54}$$

This implies that the Landau condition for a second-order phase transition is not satisfied, and a transition to type-I antiferroquadrupolar order in which the primary OP is a $\Gamma_5^{(+)}$ or $\Gamma_4^{(+)}$ quadrupole cannot be of second order. However, it must be observed that neither in UO_2 nor in NpO_2 is the quadrupole a primary OP, since it is induced as a secondary OP by an underlying magnetic order. Thus, a_2 remains positive across the transition and there is no quadrupolar instability. Indeed, the transition is second order in NpO_2, and the first-order character of the UO_2 transition is not due to the breakdown of the Landau condition (see Sec. IV.A).

Secondary OPs are important quantities in a multipolar phase transition since they may be easier to detect than the primary OP, thus providing an indirect way to extract information on the ordering. For instance, quadrupolar secondary OPs are likely to occur and may be probed by RXS or NMR (Sec. III). Since ionic quadrupoles are linearly coupled with appropriately symme-

trized displacements of the ion's ligands, lattice distortions may occur as secondary OPs too, and can usually be detected by diffraction techniques. Also, if a magnetic field is applied (thus breaking the time-reversal invariance), an antiferroquadrupolar primary OP may induce an antiferromagnetic secondary OP which can be probed by magnetic neutron diffraction (Effantin *et al.*, 1985; Link *et al.*, 1998).

The T dependence of a secondary OP η is typically different from that of the primary OP ψ, and in the Landau framework for $(T_c-T)/T_c \ll 1$ it depends on the power n appearing in the lowest-order invariant $\eta\psi^n$, which results in $\eta \propto \psi^n \propto (T_c-T)^{n/2}$. For instance, for the dipolar primary OP of UO_2, since the space group irrep $\Gamma_5^{(+)}(\{\mathbf{k}\})$ for the star of X satisfies $\Gamma_5^{(+)}(\{\mathbf{k}\}) \times \Gamma_5^{(+)}(\{\mathbf{k}\}) \supset \Gamma_5^{(+)}(\{\mathbf{k}\})$ there are third-order invariants involving two components of the primary dipolar OP and one component of a secondary quadrupolar OP having the same spatial symmetry properties. This leads to $n=2$, i.e., a type-I AF quadrupole moment and a nonuniform lattice distortion proportional to the square of the ordered moment to lowest order. In addition, since $\Gamma_5^{(+)}(\{\mathbf{k}\}) \times \Gamma_5^{(+)}(\{\mathbf{k}\}) \supset \Gamma_3^{(+)}(\mathbf{k}=\mathbf{0}) + \Gamma_5^{(+)}(\mathbf{k}=\mathbf{0})$ (the Γ-point irrep label are those of the O_h point group), macroscopic distortions of the crystal associated with a ferroquadrupolar secondary OP may be induced by a type-I dipole OP. However, the actual presence and the type of such distortions depends on the OP direction in the $\Gamma_5^{(+)}(\{\mathbf{k}_i\})$ subspace. For instance, 1-**k** ordering leads to a macroscopic tetragonal distortion associated with the $\Gamma_3^{(+)}(\mathbf{k}=\mathbf{0})$ quadrupoles, whereas 3-**k** ordering has no associated macroscopic distortion since, in this case, all mixed invariants linear in the quadrupoles vanish.

The presence or absence of distortions for a specific ordered structure can be easily established by looking at the way the Wyckoff positions occupied by atoms of the crystal split in the lower-symmetry group. For instance, in UO_2, U atoms occupy 4*a* positions and oxygen atoms occupy 8*c* positions of $Fm\bar{3}m$. In the $Pa\bar{3}$ group describing the 3-**k** phase, these positions are still labeled as 4*a* and 8*c*, but while the former are fixed by symmetry, the latter are not and depend on a free parameter x. Thus, a distortion of the oxygen cages is expected in the ordered phase and has indeed been observed experimentally (see Sec. IV.A).

III. MULTIPOLAR ORDERING IN SOLIDS: EXPERIMENTAL TOOLS

A. Indirect techniques

Historically, the existence of multipolar order was suggested by a combination of measurement techniques which, by themselves, are not able to probe directly the nature of the ordered phase. For example, in the presence of antiferroquadrupolar (AFQ) order, bulk measurements such as specific heat, magnetic susceptibility, and the temperature derivative of the electrical resistivity may display sizable Néel-type anomalies, indicating

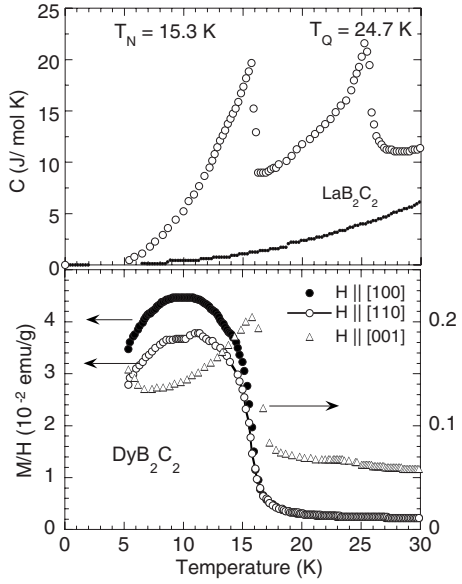

FIG. 4. Specific heat (upper panel) and magnetic susceptibility (lower panel) of DyB_2C_2. Data from Yamauchi *et al.*, 1999.

that a phase transition is taking place at a given temperature T_0 without a ferromagnetic dipolar component; on the other hand, attempts to detect the order by dipolar-sensitive probes such as neutron scattering or Mössbauer spectroscopy would invariably fail. This was the case, for instance, encountered in the study of the magnetic properties of DyB_2C_2. For this compound, the specific-heat curve shows two large λ-type anomalies, one at $T_N=15.3$ K and the other at $T_Q=24.7$ K. The magnetic entropy variation associated with each transition is very close to $R \ln 2$, suggesting a pseudoquartet ground state in the paramagnetic phase, which is split into two well-separated doublets at T_Q, and into four singlets below T_N. Such an energy level scheme was later confirmed by neutron scattering measurements (Nakamura *et al.*, 2003; Staub *et al.*, 2005). However, only at T_N is an anomaly clearly visible in the susceptibility curves (Fig. 4). Neutron powder diffraction studies show magnetic reflections only below T_N, where the system is antiferromagnetic.

To explain this behavior, the presence of AFQ order was suggested for $T_N<T<T_Q$ (Yamauchi *et al.*, 1999) as the entropy release revealed by the specific heat is in line with the presence of two quasidegenerate Kramers doublets. The occurrence of AFQ order was later confirmed by resonant x-ray scattering and neutron diffraction studies (Tanaka *et al.*, 1999; Hirota *et al.*, 2000; Tanaka, Inami, Lovesey, *et al.*, 2004; Zaharko *et al.*, 2004; Matsumura *et al.*, 2005; Mulders *et al.*, 2006)

Similar situations have often been described as manifestations of a "hidden order," and indicate that it is usually difficult to prove the existence of a nondipolar OP. For instance, URu_2Si_2 displays a second-order phase transition marked by a large anomaly in the heat capacity at $T_0=17.5$ K (Palstra *et al.*, 1985) The magnetic ordered moment revealed by neutron scattering (μ_0

$=0.03\mu_B$) is much too small to account for this anomaly (Broholm *et al.*, 1987, 1991), and a number of speculations about the primary order parameter have been advanced, from electric quadrupoles (Santini and Amoretti, 1994; Santini, 1998; Ohkawa and Shimizu, 1999; Santini *et al.*, 2000) to magnetic octupoles (Fazekas *et al.*, 2005; Kiss and Fazekas, 2005; Hanzawa, 2007), orbital currents (Chandra *et al.*, 2002), and condensation of heavy fermion quasiparticles (Wiebe *et al.*, 2007).

For a transition to a quadrupolar ordered state, ME interactions can couple electric quadrupole degrees of freedom with lattice distortions of the same symmetry; this can be useful to study the ordered phase, as demonstrated for several insulating and intermetallic rare-earth compounds where the ME coupling and the quadrupolar pair interactions responsible for the quadrupolar ordering have been determined by elastic constants, nonlinear susceptibility, and parastriction measurements (Aléonard and Morin, 1979; Levy *et al.*, 1979; Morin and Schmitt, 1990; Morin and Rouchy, 1993).

An instructive example is the study of the phase transition to a ferroquadrupole ordered state associated with an orthorhombic γ-symmetry-lowering mode in the tetragonal intermetallic compound $TmAg_2$. Morin and Rouchy (1993) analyzed this phenomenon using the mean-field approximation to describe the two-ion quadrupolar term H_Q, and expressing the equilibrium strains appearing in the ME Hamiltonian H_{ME} as a function of the expectation values of quadrupole operators,

$$H_Q + H_{ME} = -G^{\alpha}\langle\hat{O}_2^0\rangle\hat{O}_2^0 - G^{\gamma}\langle\hat{O}_2^2\rangle\hat{O}_2^2 - G^{\delta}\langle\hat{O}_2^{-2}\rangle\hat{O}_2^{-2} - G^{\epsilon}[\langle\hat{O}_2^1\rangle\hat{O}_2^1 + \langle\hat{O}_2^{-1}\rangle\hat{O}_2^{-1}], \quad (55)$$

where the coefficients G^{μ} are determined by the ME coefficients B^{μ}, the symmetrized background elastic constants C_0^{μ}, and the two-ion quadrupolar interaction coefficients K^{μ}. The total Hamiltonian is obtained by adding the CF term, the Zeeman, and the bilinear exchange contributions to Eq. (55). Perturbation theory can then be applied to the disordered phase to analyze each of the possible symmetry lowering modes and to determine magnetic, strain, and quadrupolar susceptibilities. The relevant coefficients can be determined experimentally from measurements of macroscopic quantities. For instance, the total quadrupolar coefficients G^{μ} can be obtained from the third-order magnetic susceptibility $\chi_M^{(3)}$ (Morin *et al.*, 1988; Morin and Rouchy, 1993),

$$\chi_M^{(3)} = \frac{1}{(1-n\chi_0)^4}\left(\chi_0^{(3)} + \frac{2G^{\alpha}(\chi_{\alpha}^{(2)})^2}{1-G^{\alpha}\chi_{\alpha}} + \frac{2G^{\mu}(\chi_{\mu}^{(2)})^2}{1-G^{\mu}\chi_{\mu}}\right), \quad (56)$$

which is determined by four single-ion susceptibilities involving matrix elements between CF eigenstates of J_z and of $\hat{O}_2^{\mu}$ quadrupole operators appearing in Eq. (55), selected by the field direction. The parameter n is the bilinear exchange coefficient, χ_0 and $\chi_0^{(3)}$ are the single-ion linear and third-order magnetic susceptibility, $\chi_{\mu} = \partial\langle\hat{O}_2^{\mu}\rangle/\partial\epsilon^{\mu}$ is the strain susceptibility, and $\chi_{\mu}^{(2)} = \partial\langle\hat{O}_2^{\mu}\rangle/\partial H^2$ is a quadrupolar field susceptibility giving the response of the quadrupolar components to the associated strain in the presence of a magnetic field. In general terms, the strain susceptibilities χ_{μ} which appear in Eq. (56) are associated with quadrupolar degrees of freedom and, therefore, they can selectively probe the quadrupolar character of the CF ground state. If a given χ_{μ} saturates to a constant value at low temperatures, this is an indication that the associated quadrupole $\hat{O}_2^{\mu}$ has a zero intrinsic moment within the ground state. On the other hand, quadrupolar active modes will give rise to a divergence in the temperature dependence of χ_{μ}. This is often the case when a second-order transition involving $\hat{O}_2^{\mu}$ as primary OP is present.

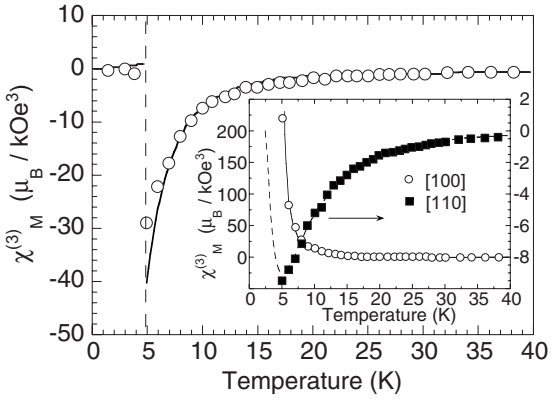

FIG. 5. Temperature variation of the third-order magnetic susceptibility along the [0 0 1] crystallographic direction of $TmAg_2$. Data for the [1 0 0], and [1 1 0] directions are shown in the inset. The nonmagnetic transition at $T_0=4.74$ K is analyzed assuming ferroquadrupolar order within the orthorhombic Γ_3 symmetry-lowering mode ($G^{\alpha}=0$; $G^{\gamma}=17$ mK). Data from Morin and Rouchy, 1993.

Figure 5 shows the values of $\chi_M^{(3)}$ measured as a function of temperature along different directions of a $TmAg_2$ crystal. The occurrence of a phase transition at about 5 K is clearly revealed. The solid lines are calculations by Morin and Rouchy, assuming CF parameters determined by inelastic neutron scattering, $G^{\alpha}=0$, and $G^{\gamma}=17$ mK. The excellent agreement between experiment and theory strongly supports the hypothesis of ferroquadrupolar ordering involving the $\hat{O}_2^2$ quadrupole component (Morin and Rouchy, 1993). The ME and two-ion quadrupolar coefficients can be extracted separately from the temperature dependence of the elastic constants C^{μ}, which in turn can be obtained from ultrasonic velocity measurements. For instance, in the case of a γ mode,

$$C^{\gamma} = C_{11} - C_{12} = C_0^{\gamma} - (B^{\gamma})^2\frac{\chi_{\gamma}}{1-K^{\gamma}\chi_{\gamma}}. \quad (57)$$

The data obtained for $TmAg_2$ are shown in Fig. 6; the softening of C_{γ} indicates that the corresponding strain susceptibility χ_{γ} is diverging as a result of the ordering of the $\hat{O}_2^2$ quadrupole. Fitting the experimental curve to

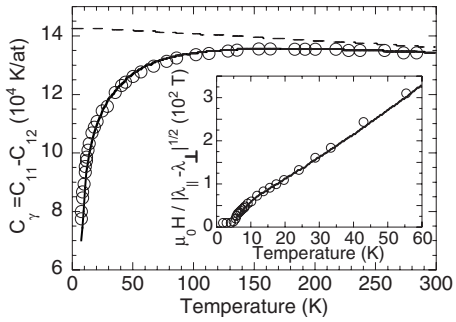

FIG. 6. Temperature dependence of the C_γ elastic constant in $TmAg_2$. The dashed line indicates the value of C_γ^0 measured for the nonmagnetic isostructural compound YAg_2. The solid line is a fit to Eq. (57) with $K^\gamma=10$ mK and $|B^\gamma|=32$ K. Inset: Temperature dependence of the parastriction for an external magnetic field applied along the [1 0 0] direction. Relative length changes are measured along [1 0 0] and [0 1 0]. The solid line is a fit leading to the determination of ME and total quadrupolar coefficients. Data from Morin and Rouchy, 1993.

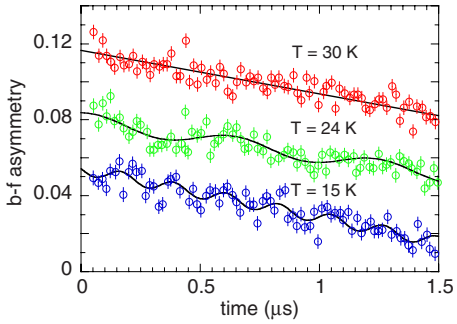

FIG. 7. (Color online) Time dependence of the zero-field backward-forward positron count rate asymmetry for NpO_2 at different temperatures. A vertical offset has been applied to the different data sets. Data from Kopmann *et al.*, 1998.

Eq. (57) gives $K^\gamma=10$ mK and $|B^\gamma|=32$ K.

A third experimental probe of the quadrupolar field susceptibility is provided by parastriction measurements, i.e., measurements in the paramagnetic phase of the relative change of length, $\lambda=\delta\ell/\ell$, induced by the application of a magnetic field along a given direction. Parastriction measures the quadrupolar moment induced by the applied field through the anisotropic deformation of the lattice (Morin *et al.*, 1980). Experiments are performed by measuring λ along high-symmetry directions, parallel and perpendicular to the magnetic field H, using a capacitance dilatometer or a strain gauge. By plotting $H/|\lambda_\parallel-\lambda_\perp|^{1/2}$ vs T, a linear dependence is expected at high temperature, with a slope determined by B^μ. Parastriction data obtained for $TmAg_2$, with a field applied along the [100] axis, are shown in Fig. 6. In this case,

$$\frac{H}{|\lambda_{100}-\lambda_{010}|^{1/2}}=\left(\frac{C_0^\gamma}{\sqrt{2}|B^\gamma|}\right)^{1/2}\left(\frac{1-G^\gamma\chi_\gamma}{\chi_\gamma^{(2)}}\right)^{1/2}(1-n\chi_0). \tag{58}$$

Fitting the experimental data to this equation gives $B^\gamma=-31$ K and $G^\gamma=18$ mK, in excellent agreement with other techniques; parastriction is also sensitive to the sign of B^γ, which is the same as the sign of $\lambda_{100}-\lambda_{010}$. Mean-field calculations performed with these parameters predict a spontaneous strain at 5 K, in agreement with the experimentally determined quadrupolar transition temperature (Morin and Rouchy, 1993). A similar analysis has been used to study quadrupolar ordering in the isostructural compound $TmAu_2$ (Kosaka *et al.*, 1998). It should be noted that since the above-mentioned macroscopic techniques probe uniform quadrupolar susceptibilities, they are less useful if the order is antiferroquadrupolar.

Electric quadrupole related effects in metallic compounds can also be probed by muon spin rotation (μSR) techniques measuring the anisotropy and T dependence of the Fermi contact hyperfine coupling to the conduction electrons $A_i^{\rm con}$. This quantity can be extracted from the Knight shift of positive muons and, in the presence of *s-f* exchange and spin-orbit coupling, is sensitive to multipolar degrees of freedom (Schenck and Solt, 2004).

The μSR technique can also give indirect information on the ordered quadrupolar state by monitoring the evolution of the local internal magnetic field as a function of an external parameter. This has been exploited in a study of the magnetic ordering in $PrCu_2$, where a temperature- and orientation dependent $A_i^{\rm con}$ has been observed (Schenck *et al.*, 2003).

Anomalies in the muon spin relaxation rate can be detected if the fluctuation of the dipolar magnetic moments is influenced by the order of electric quadrupoles. This effect has been observed in $DyPd_3S_4$, and was used together with inelastic neutron scattering and neutron diffraction to characterize the AFQ phase appearing in this compound below 3.4 K (Keller *et al.*, 2004).

Notice that μSR measurements are sensitive probes of the local static magnetic field at the implanted muon site. Parity violation in weak interactions causes a sizable backward-forward asymmetry for the emitted positrons along the direction of the muon spin at the moment of muon decay. If the muon senses a magnetic field, for example, from surrounding ordered dipoles, its spin performs a precessional motion which is detected as a sinusoidal modulation in the time dependence of the backward-forward asymmetry. In favorable cases where the dipole contribution is absent, the observation of a muon spin precession signal would indicate the presence of ordered MMPs of higher rank. For instance, the appearance of a spontaneous muon spin precession signal in NpO_2 below $T_0=25$ K (Fig. 7) indicates the occurrence of a phase transition associated with a magnetic order parameter, i.e., breaking time-reversal symmetry (Kopmann *et al.*, 1998). The nature of this phase transition will be discussed in Sec. IV.B.

B. Resonant x-ray scattering

1. Introduction

Indirect methods for investigating multipolar order in solids, such as those discussed above, may track out

phase boundaries, but the nature of the intrinsic order remains obscure. For an unambiguous identification of the order parameter, microscopic probes that couple directly to the multipole degrees of freedom are required. RXS is a powerful technique that fulfills this requirement.

RXS occurs when a linearly polarized photon is virtually absorbed by exciting a core electron to empty states, and subsequently reemitted when the excited electron and the core hole recombine (Blume, 1985; Blume and Gibbs, 1988; Hannon *et al.*, 1988; Luo *et al.*, 1993; Hill and McMorrow, 1996; Lovesey, 1996; Lovesey and Balcar, 1996). This process introduces anisotropic contributions to the x-ray susceptibility tensor (Ovchinnikova and Dmitrienko, 2000), whose amplitude dramatically increases as the photon energy is tuned to an atomic absorption edge. In the presence of long-range order of magnetic moments, electronic orbitals occupancy, or spatially anisotropic valence-electron clouds, the interference of the anomalous anisotropic scattering amplitudes leads to the excitation of Bragg peaks at positions forbidden by the crystallographic space group. RXS can therefore probe long-range order of magnetic moments and anisotropic charge distributions. In the latter case, it is the asphericity of the atomic electron density that generates the anomalous tensor component in the atomic scattering factor. If the electron clouds on different sublattices have different orientations, superlattice reflections occur due to the reduced translational symmetry. This is the so-called Templeton scattering (Templeton and Templeton, 1982, 1985; Dmitrienko, 1983) and is observed, for instance, in the case of antiferromagnetic electric order of the quadrupole moments. Comprehensive reviews of RXS theory and applications can be found (Lovesey and Collins, 1996; Lovesey *et al.*, 2005; Collins *et al.*, 2007).

A typical diffractometer for RXS experiments at a synchrotron radiation source (Paolasini *et al.*, 2007) uses the linearly polarized beam delivered by undulator insertion devices. A system consisting of total reflection mirrors and single-crystal monochromators allows one to focus the beam at the sample position and to select its energy over a wide range, with high resolution. For instance, at the ID20 beamline of the ESRF in Grenoble, the incident photon energy can be chosen between 3.4 and 25 keV, with a resolution of the order of 10^{-4}. This energy range includes most of the absorption edges explored in hard-x-ray resonant scattering studies (K edges of transition metals, L edges of rare earths, L and M edges of actinides).

A schematic of the experimental setup is shown in Fig. 8. The incident photon beam is defined by the wave vector $\mathbf{k}_0$ and the polarization vector $\boldsymbol{\epsilon}_0$; the diffracted beam propagates along the wave vector $\mathbf{k}_f$ with polarization $\boldsymbol{\epsilon}_f$; $\mathbf{k}_0$ and $\mathbf{k}_f$ define the scattering plane Π. A beam with polarization perpendicular to Π is said to have σ polarization, whereas a beam has π polarization if $\boldsymbol{\epsilon}$ is parallel to Π. The sample is mounted at the center of a four-circle cradle. An extra circle allows one to perform azimuth scans, where the intensity of the diffracted beam is recorded while rotating the sample around the scattering vector $\mathbf{Q}=\mathbf{k}_0-\mathbf{k}_f$. To analyze the polarization of the scattered beam, one makes use of a mosaic crystal positioned between sample and detector, and continuously rotatable by an angle η around $\mathbf{k}_f$. If the Bragg angle of the analyzer is close to $\pi/4$, and the scattering planes Π_S and Π_A of the sample and the analyzer are parallel ($\eta=0$), only photons with σ polarization are diffracted by the analyzer and detected. On the other hand, if $\eta=\pi/2$ (Π_A perpendicular to Π_S), only photons with π polarization are selected.

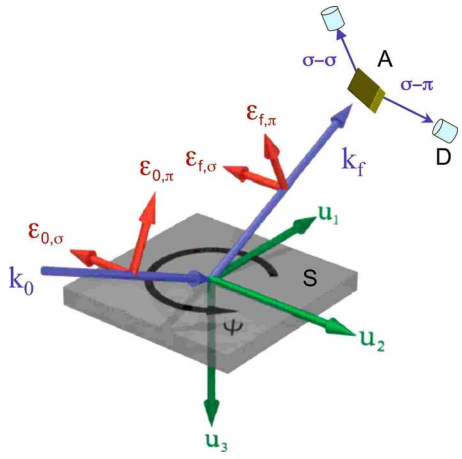

FIG. 8. (Color online) Schematic of the experimental setup for RXS studies. A photon beam polarized perpendicular to the scattering plane impinges on the sample S and is scattered toward the analyzer crystal A. The scattered beam components with polarization parallel (π) or perpendicular (σ) to the scattering plane can be selected by an appropriate orientation of the analyzer. D is a standard scintillation detector. Integrated intensities of Bragg peaks are measured as a function of photon energy for different values of the azimuth angle Ψ, defining the crystal orientation about the scattering vector. The unit vectors $\mathbf{u}_i$ define the reference frame.

2. Theoretical background

The cross section for elastic x-ray scattering can be written as (Blume, 1994)

$$\frac{d\sigma}{d\Omega} \propto \left| \sum_j [f_{0j} + f_j'(\omega) + if_j''(\omega)] e^{i\mathbf{Q}\cdot\mathbf{R}_j} \right|^2, \tag{59}$$

where the sum includes the atoms in the crystallographic unit cell, $\mathbf{R}_j$ is the relative position in the cell of the jth atom, $\hbar\omega$ is the photon energy, f_0 is the Thompson scattering factor, and

$$f_j'(\omega) + if_j''(\omega) = \frac{m_e}{\hbar^2}\frac{1}{\hbar\omega} \times \sum_n \frac{(E_n - E_g)^3 \langle \psi_g^{(j)} | \hat{O}_f^\dagger | \psi_n^{(j)} \rangle \langle \psi_n^{(j)} | \hat{O}_0 | \psi_g^{(j)} \rangle}{\hbar\omega - (E_n - E_g) - i\Gamma_n/2} \tag{60}$$

is the anomalous atomic scattering factor (Blume, 1994).

In Eq. (60), m_e is the electron mass, $|\psi_g^{(j)}\rangle$ and $|\psi_n^{(j)}\rangle$ are the initial and photoexcited states of atom j, E_g and E_n are their respective energies, and Γ_n is the inverse lifetime of the core-hole excited state. Determining the valence excited states is a crucial part of evaluating the RXS amplitude that can be addressed in the framework of the multiple scattering theory or using the finite-difference method, as discussed by Joly *et al.* (2004). To calculate the matrix elements in Eq. (60), the radiation-matter interaction operator for incident ($\hat{O}_0$) and final ($\hat{O}_f$) photons can be expanded in multipole terms. Only the electric dipole ($E1$) and electric quadrupole ($E2$) contributions need to be retained (Blume, 1994), as the radial integrals for higher multipoles are negligible,

$$\langle \psi_g^{(j)}|\hat{O}_{0(f)}|\psi_n^{(j)}\rangle = \langle \psi_g^{(j)}|\boldsymbol{\epsilon}_{0(f)}\cdot\mathbf{r}(1-\tfrac{1}{2}i\mathbf{k}_{0(f)}\cdot\mathbf{r})|\psi_n^{(j)}\rangle, \quad (61)$$

with $\mathbf{r}$ the electron position from the nucleus of the absorbing ion. With this approximation, the amplitude of the RXS signal, Eq. (60), is a linear combination of complex Cartesian tensors of rank 2, 3, and 4 (Dmitrienko and Ovchinnikova, 2001; Joly *et al.*, 2004),

$$\begin{aligned}\sum_n \langle \psi_g^{(j)}|\hat{O}_f^\dagger|\psi_n^{(j)}\rangle\langle\psi_n^{(j)}|\hat{O}_0|\psi_g^{(j)}\rangle &= \sum_{\alpha,\beta}\epsilon_{f\alpha}^*\epsilon_{0\beta}D_{\alpha\beta} \\ &- \frac{i}{2}\sum_{\alpha,\beta\gamma}\epsilon_{f\alpha}^*\epsilon_{0\beta}(k_{0\gamma}I_{\alpha;\beta\gamma}-k_{f\gamma}I_{\beta;\alpha\gamma}^*) \\ &+ \frac{1}{4}\sum_{\alpha,\beta,\gamma,\delta}\epsilon_{f\alpha}^*\epsilon_{0\beta}k_{f\gamma}k_{0\delta}Q_{\alpha\gamma\beta\delta}, \end{aligned} \quad (62)$$

where the sums over α, β, γ, and δ run over the Cartesian coordinates x, y, and z, and

$$D_{\alpha\beta} = \sum_n \langle \psi_g^{(j)}|r_\alpha|\psi_n^{(j)}\rangle\langle\psi_n^{(j)}|r_\beta|\psi_g^{(j)}\rangle, \quad (63)$$

$$I_{\alpha;\beta\gamma} = \sum_n \langle \psi_g^{(j)}|r_\alpha|\psi_n^{(j)}\rangle\langle\psi_n^{(j)}|r_\beta r_\gamma|\psi_g^{(j)}\rangle, \quad (64)$$

$$Q_{\alpha\beta\gamma\delta} = \sum_n \langle \psi_g^{(j)}|r_\alpha r_\beta|\psi_n^{(j)}\rangle\langle\psi_n^{(j)}|r_\gamma r_\delta|\psi_g^{(j)}\rangle. \quad (65)$$

The first term in Eq. (62) is associated with the $E1$-$E1$ contribution to the RXS signal, whereas the second and third terms give the $E1$-$E2$ and $E2$-$E2$ amplitudes, respectively. It is evident that the rank-2 and rank-4 tensors are parity even, and can therefore be associated with order parameters invariant under space inversion. On the other hand, the rank-3 $E1$-$E2$ tensor gives access to the observation of parity odd multipoles.

Equation (62) can be conveniently written in terms of scalar products of irreducible tensor operators (ITOs) as discussed in Sec. II.A (Carra and Thole, 1994; Di Matteo *et al.*, 2003). In particular, the $E1$-$E1$ channel can be decomposed into the scalar products of rank $p=0$, 1, and 2 ITOs,

$$E1-E1 = \sum_{p=0}^{2}\sum_{q=-p}^{p}(-1)^{p+q}T_q^{(p)}F_{-q}^{(p)}. \quad (66)$$

In the above equation, the tensors $T^{(p)}$ are defined by the radiation parameters $\boldsymbol{\epsilon}$ and $\mathbf{k}$; the $F(j,\omega)^{(p)}$ operators describe the properties of the absorbing atom. The three $F^{(p)}$ tensors are parity even, and their components are linear combinations of the Cartesian components $D_{\alpha\beta}$. The tensors with rank even, $p=0$ and 2, are invariant also under time reversal, whereas the $p=1$ tensor is time odd. Writing the $F_q^{(p)}$ components explicitly using the definition given by Eq. (63), it is easy to realize that $F^{(1)}$ is related to the magnetic dipole moment, and $F^{(0)}$ and $F^{(2)}$ to the charge and the electric quadrupole, respectively (Di Matteo and Natoli, 2002).

The $E1$-$E2$ channel can be written as a function of parity-odd ITOs of rank $p=1$, 2, and 3 (Carra *et al.*, 1993, 2003; Di Matteo and Natoli, 2002; Marri and Carra, 2004),

$$E1-E2 = \sum_{p=1}^{3}\sum_{q=-p}^{p}(-1)^{p+q}(T_q^{(p)}F_{-q}^{(p)}+\tilde{T}_q^{(p)}\tilde{F}_{-q}^{(p)}). \quad (67)$$

In this case, the tensors $F(j,\omega)^{(p)}$ and $\tilde{F}(j,\omega)^{(p)}$ correspond to the Cartesian tensor $I_{\alpha;\beta\gamma}$ and $I_{\alpha;\beta\gamma}^*$ given by Eq. (64), and contain both time-even and time-odd operators, independent of the parity of the rank. The time-even components are proportional to the electric dipole ($p=1$), the polar (G) toroid quadrupole ($p=2$), and the electric octupole ($p=3$). Time-odd ITOs are proportional to the polar toroid dipole ($p=1$), the magnetic quadrupole ($p=2$), and the polar toroid octupole ($p=3$) (Di Matteo *et al.*, 2005).

Finally, parity-even ITOs of rank $p=0$, 1, 2, 3, and 4 appear in the expansion of the $E2$-$E2$ channel, with $F(j,\omega)^{(p)}$ operators constructed from the Cartesian tensors $Q_{\alpha\beta\gamma\delta}$ of Eq. (65). Only those of rank $p=3$ and 4 are related to new order parameters, namely, the time-odd magnetic octupole ($p=3$) and the time-even electric hexadecapole ($p=4$).

For absorbing atoms belonging to the transition-metal series, RXS experiments are usually performed at the K edge, as the energy of other absorption edges is usually below the cutoff for Bragg diffraction. The intermediate states involved are the $4p$ (electric-dipole $E1$ transitions) and the $3d$ (electric-quadrupole $E2$ transitions). The sensitivity of the experiment to magnetic order at the quadrupole, $1s$-$3d$, threshold energy has its origin in the spin polarization of the $3d$ states, whereas at the $1s$-$4p$ dipole transition energy the resonant enhancement for magnetic reflections is due to the $4p$-$3d$ intra-atomic Coulomb interaction and mixing of the $4p$ with the $3d$ states of neighboring atoms (Igarashi and Takahashi, 2001). Following pioneering studies in $LaMnO_3$ (Murakami, Hill, Gibbs, *et al.*, 1998; Murakami, Kawada, Kawata, *et al.*, 1998), a number of RXS experiments have been performed at the K edge of transition-metal (TM) compounds, giving contributions to unravel the physics of

several systems, such as V_2O_3 (Paolasini *et al.*, 1999) $KCuF_3$ (Caciuffo *et al.*, 2002; Paolasini *et al.*, 2002). Experiments performed with soft x rays at the L edges of TM atoms directly probe the $3d$ states through the virtual $E1$ transition (Castleton and Altarelli, 2000). Resonant soft-x-ray diffraction at the Mn L edges was first reported by Wilkins, Hatton, Roper, *et al.* (2003) and used to characterize the orbital ordering in $La_{0.5}Sr_{1.5}MnO_4$ (Wilkins, Spencer, Hatton, *et al.*, 2003; Wilkins *et al.*, 2005). For atoms belonging to the actinide series, both L and M edges are of practical use, as their energies are large enough for Bragg diffraction to be allowed in most actinide compounds. Most of the experiments reviewed here have been performed at the M_5 and M_4 U and Np edges, involving, $3d_{5/2}\rightarrow 5f$ and $3d_{3/2}\rightarrow 5f$ $E1$ virtual excitations, respectively. The relevant part of the scattering amplitude is given by Eq. (66). The rank-0 tensor describes the nonresonant charge scattering and is not discussed further. The rank-1 contribution is

$$[f_j'(\omega)+if_j''(\omega)]_m \propto \alpha_{1j}(\omega)\boldsymbol{\epsilon}_f\cdot\begin{pmatrix} 0 & \mu_z & -\mu_y \\ -\mu_z & 0 & \mu_x \\ \mu_y & -\mu_x & 0 \end{pmatrix}_j\cdot\boldsymbol{\epsilon}_0 = \alpha_{1j}(\omega)(\boldsymbol{\epsilon}_0\times\boldsymbol{\epsilon}_f)\cdot\boldsymbol{\mu}_j, \tag{68}$$

where $\boldsymbol{\mu}_j$ is the magnetic moment of the atom j. This term, therefore, probes the magnetic dipole order in a crystal. It is different from zero provided that the polarization of the scattered beam is rotated with respect to the incident polarization and that the vector product $\boldsymbol{\epsilon}_0\times\boldsymbol{\epsilon}_f$ has a nonvanishing component along the magnetic moment direction. In an experiment with σ incident polarization, the magnetic contribution is zero if the diffracted beam also has σ polarization, whereas it has a maximum if the diffracted beam has π polarization. The prefactor $\alpha_1(\omega)$ gives the energy dependence of the scattering amplitude and requires a net spin polarization of the $5f$ states, or a difference between overlap integrals, resonant energy, and lifetime for spin-up and spin-down channels (Blume, 1985; Blume and Gibbs, 1988; Hill and McMorrow, 1996).

The scattering amplitude, on the other hand, arising from the second-rank tensor in the $E1$-$E1$ term, even under time reversal, is proportional to the electric quadrupole operator that, in turn, is proportional to the matrix,

$$M_{\alpha\beta}^{[2]}=\hat{\mu}_\alpha\hat{\mu}_\beta-\tfrac{1}{3}\delta_{\alpha\beta}\sum_\gamma\hat{\mu}_\gamma\hat{\mu}_\gamma, \tag{69}$$

with $\hat{\mu}=\boldsymbol{\mu}/\mu$.

$$[f_j'(\omega)+if_j''(\omega)]_{eq}\propto\alpha_{2j}(\omega)\boldsymbol{\epsilon}_f\cdot\vec{M}_j^{[2]}\cdot\boldsymbol{\epsilon}_0. \tag{70}$$

In this case, with an incident beam with σ polarization, contributions are expected to diffracted beams with both σ and π polarization.

An expression of the energy profiles $\alpha_1(\omega)$ and $\alpha_2(\omega)$, going beyond the fast-collision approximation and suitable to describe the scattering from localized f-electron atoms, has been derived by Nagao and Igarashi (2005, 2006) assuming a CF split ground state but intermediate states with spherical symmetry. This is a reasonable assumption, as CF and intersite interactions are usually much smaller than the spin-orbit and intra-atomic Coulomb interactions giving rise to the multiplet structure. By writing the ground-state wave function of a generic site as a linear combination of the eigenfunctions of the angular momentum operator, $\psi_g^{(j)}=\Sigma_M c_{JM}|JM\rangle$, and describing the intermediate state by means of the magnitude J' and the magnetic quantum number M' of a total angular momentum including the core-hole contribution, one obtains

$$\alpha_1(\omega)=-(2J-1)F_{J-1}(\omega)-F_J(\omega)+(2J+3)F_{J+1}(\omega), \tag{71}$$

$$\alpha_2(\omega)=\tfrac{4}{3}[-F_{J-1}(\omega)+F_J(\omega)-F_{J+1}(\omega)], \tag{72}$$

where

$$F_{J'}(\omega)=2^{1-|J-J'|}\sqrt{(2J+1)(2J'+1)}\times\frac{(J+J'-1)!}{(J+J'+2)!}|(J\|V_1\|J')|^2\sum_{s=1}^{N_{J'}}E_i(\omega,J'). \tag{73}$$

In Eq. (73), $J'=J$, $J\pm1$, $(J\|V_1\|J')$ is the reduced matrix element of the set of irreducible tensor operators of the first rank. The sum includes all multiplets with the same J' but different energy $E_{sJ'}$, and $E_s(\omega,J')=1/[\hbar\omega-(E_{sJ'}-E_g)+i\Gamma]$. When the multiplet splitting of the intermediate state can be neglected, an average energy value can be used in the denominator of the RXS amplitude, Eq. (60), and the resonant factor can be replaced by a Lorentzian-shaped energy profile.

The RXS scattering amplitude from localized f-electron systems at the $E2$-$E2$ channel can be written in terms of expectation values of rank-ν multipole operator components as

$$[f_j'(\omega)+if_j''(\omega)]_{E2E2}=\frac{1}{9}\sum_{\nu=0}^{4}\alpha_{E2,j}^{\nu}(\omega)\times\sum_{\lambda=1}^{2\nu+1}P_\lambda^{(\nu)}(\boldsymbol{\epsilon}_0,\boldsymbol{\epsilon}_f,\mathbf{k}_0,\mathbf{k}_f)\times\langle\psi_g|z_{\lambda,j}^{(\nu)}|\psi_g\rangle. \tag{74}$$

Explicit expressions for the energy profile functions $\alpha_{E2,j}^{\nu}$, the geometrical factors $P_\lambda^{(\nu)}(\boldsymbol{\epsilon}_0,\boldsymbol{\epsilon}_f,\mathbf{k}_0,\mathbf{k}_f)$, and the components of the multipole operators, $z_{\lambda,j}^{(\nu)}$ have been given by Nagao and Igarashi (2006).

The expressions given above allow one to perform a quantitative analysis of RXS experiments and, in favorable cases, to disentangle the contributions to the scattering intensity given by different multipole order parameters. To achieve this result, the energy profile and the azimuth angle dependence of resonant superlattice

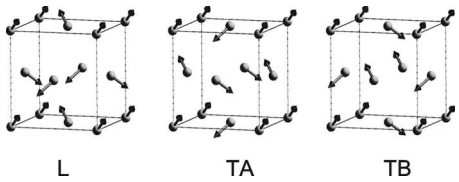

FIG. 9. Type I, 3-**k** magnetic structure in an fcc lattice. The dipole magnetic moment direction is shown as an arrow; $R_1=000$, $R_2=\frac{1}{2}\frac{1}{2}0$, $R_3=\frac{1}{2}0\frac{1}{2}$, $R_4=0\frac{1}{2}\frac{1}{2}$. Left, the longitudinal (L) structure with $\boldsymbol{\mu}_1=\mu_0(1,1,1)/\sqrt{3}$, $\boldsymbol{\mu}_2=\mu_0(\bar{1},\bar{1},1)/\sqrt{3}$, $\boldsymbol{\mu}_3=\mu_0(\bar{1},1,\bar{1})/\sqrt{3}$, $\boldsymbol{\mu}_4=\mu_0(1,\bar{1},\bar{1})/\sqrt{3}$; middle, TA transverse *S*-domain, with $\boldsymbol{\mu}_1=\mu_0(1,1,1)\sqrt{3}$, $\boldsymbol{\mu}_2=\mu_0(1,\bar{1},\bar{1})/\sqrt{3}$, $\boldsymbol{\mu}_3=\mu_0(\bar{1},\bar{1},1)/\sqrt{3}$, $\boldsymbol{\mu}_4=\mu_0(\bar{1},1,\bar{1})/\sqrt{3}$; right, TB transverse *S*-domain, with $\boldsymbol{\mu}_1=\mu_0(1,1,1)/\sqrt{3}$, $\boldsymbol{\mu}_2=\mu_0(\bar{1},1,\bar{1})/\sqrt{3}$, $\boldsymbol{\mu}_3=\mu_0(1,\bar{1},\bar{1})/\sqrt{3}$, $\boldsymbol{\mu}_4=\mu_0(\bar{1},\bar{1},1)/\sqrt{3}$.

reflections must be measured, and the degrees of freedom related to the incident and the final beam polarization must be exploited.

3. RXS from 3-k fcc structures

We describe in some detail the resonant scattering of x rays from type I, 3-**k** ordered, face-centered-cubic (fcc) structures, that is the kind of order observed at low temperatures in AO_2. The propagation vector is $\mathbf{k}=(0,0,1)$, and all three members of its star enter in the Fourier sum describing the order in the lattice (Rossat-Mignod, 1987). In the case of magnetic dipole order, the magnetic moment at the generic site j, located at the position $\mathbf{R}_j$ within the cubic unit cell, is given by $\boldsymbol{\mu}_j=(\mu_o/\sqrt{3})\Sigma_{n=1}^{3}\mathbf{m}_{k_n}\exp(i\mathbf{k}_n\cdot\mathbf{R}_j)$, where μ_o is the amplitude of the ordered moment. The symmetry remains cubic and the magnetic moments point along the [1 1 1] directions of the cubic unit cell. In this kind of structure there is only one **k** domain. However, several orientations of the Fourier components of the magnetic moment $\mathbf{m}_{k_n}$ relative to the corresponding wave vector $\mathbf{k}_n$ are possible (Sec. II.E). One *longitudinal* structure is obtained if $\mathbf{m}_{k_n}$ is parallel to $\mathbf{k}_n$, whereas two crystallographically equivalent but distinct *S* domains are possible in the case of a *transverse* structure, that is, if $\mathbf{m}_{k_n}$ is orthogonal to $\mathbf{k}_n$ ($\mathbf{m}_{k_1}\|\mathbf{k}_2$, etc. or $\mathbf{m}_{k_1}\|\mathbf{k}_3$, etc.). The representation of the three structures is given in Fig. 9. The lattice becomes simple cubic with four atoms in the base.

The RXS from the magnetic order is described by the traceless and antisymmetric matrix $M_j^{[1]}$ appearing in Eq. (68), which can be constructed from the components of the magnetic moment of the atom at position $\mathbf{R}_j$. The structure factor corresponding to a Bragg vector $\mathbf{Q}=(h,k,l)$ can then be calculated as $\overleftrightarrow{F}^{[1]}=\Sigma_j M_j^{[1]}\exp(i\mathbf{Q}\cdot\mathbf{R}_j)$, where the summation is over all inequivalent atoms in the unit cell. For instance, for longitudinal order and a reflection with Miller index $h+k$ even and $h+l$ odd,

$$\overleftrightarrow{F}_L^{[1]}=\frac{4\mu_o}{\sqrt{3}}\begin{pmatrix}0 & 1 & 0\\ \bar{1} & 0 & 0\\ 0 & 0 & 0\end{pmatrix}. \tag{75}$$

A similar procedure can be used to evaluate the RXS signal in the case of 3-**k** electric quadrupole order, Eq. (70). The matrix $M_j^{[2]}$ in the anisotropic scattering amplitude is symmetric and traceless, as for all of the above structures $\hat{\mu}_\alpha^2=1,\forall\ \alpha$. For Γ_5 quadrupoles, this leads to the general form (Wilkins *et al.*, 2004)

$$M^{[2]}=\begin{pmatrix}0 & \hat{\mu}_x\hat{\mu}_y & \hat{\mu}_x\hat{\mu}_z\\ \hat{\mu}_x\hat{\mu}_y & 0 & \hat{\mu}_y\hat{\mu}_z\\ \hat{\mu}_x\hat{\mu}_z & \hat{\mu}_y\hat{\mu}_z & 0\end{pmatrix}. \tag{76}$$

The structure factor $\overleftrightarrow{F}^{[2]}=\Sigma_j M_j^{[2]}\exp(i\mathbf{Q}\cdot\mathbf{R}_j)$ can then be easily calculated.

To evaluate the azimuth dependence of the scattered intensity (Wilkins *et al.*, 2004), we consider a coordinate system with base vectors $\hat{c}_3=-\mathbf{Q}/Q$, $\hat{c}_2=\hat{c}_3\times\hat{k}_{\rm ref}$, and $\hat{c}_1=\hat{c}_2\times\hat{c}_3$, with $\hat{k}_{\rm ref}$ along an arbitrary reference direction in the scattering plane. We then do a rotation around $\hat{c}_3$ to transform into the coordinate system of Blume and Gibbs (1988). We therefore obtain three new unit vectors of the form $\hat{u}_3=\hat{c}_3$, $\hat{u}_2=\hat{c}_1\sin\Psi+\hat{c}_2\cos\Psi$, and $\hat{u}_1=\hat{c}_1\cos\Psi-\hat{c}_2\sin\Psi$. We can then define the polarization vectors for the incident and exit beams in the new coordinate system. For σ polarization and vertical scattering plane, $\hat{\epsilon}_{0\sigma}$ and $\hat{\epsilon}_{f\sigma}$ are both parallel to the unit vector $\hat{u}_2$ (Fig. 8). For π polarization, the Bragg angle of the reflection has to be included, giving $\hat{\epsilon}_{0\pi}=\hat{u}_1\sin\theta_B-\hat{u}_3\cos\theta_B$ and $\hat{\epsilon}_{f\pi}=-\hat{u}_1\sin\theta_B-\hat{u}_3\cos\theta_B$.

The azimuth dependence can then be calculated from Eqs. (68) and (70) as $\hat{\epsilon}_f\cdot\overleftrightarrow{F}^{[l]}\cdot\hat{\epsilon}_0$ to give the amplitude of the scattered radiation as a function of the azimuth angle Ψ. For instance, in a (0 0 1) face crystal, the intensity in the σ-σ channel for a specular quadrupolar reflection such as $\mathbf{Q}=(0,0,3)$ would be proportional to $\sin^2 2\Psi$ if the structure is longitudinal, whereas it would be absent if the structure is transverse. In the σ-π channel, the intensity would be proportional to $\sin^2\theta_B\cos^2 2\Psi$ in the longitudinal case, to $\cos^2\theta_B\cos^2\Psi$ for a transverse *A* domain, and to $\cos^2\theta_B\sin^2\Psi$ for a transverse *B* domain. The latter intensities would have exactly the same azimuth dependence as the magnetic dipole contribution, and it would not be possible to observe separately the two order parameters. On the other hand, for a nonspecular reflection such as $\mathbf{Q}=(1,1,2)$, quadrupolar intensity from a transverse structure would also be different from zero in the σ-σ channel, with an azimuth dependence proportional to $\sin^2 2\Psi$ or $\cos^4\Psi$ for an *A* or *B* domain, respectively.

C. Nonresonant x-ray diffraction

As RXS involves excited electronic states, a quantitative treatment of the results is often cumbersome. In

some cases, conventional x-ray diffraction at intermediate angles can bring information on the magnitude and the orientation of the aspherical charge distribution that is easier to understand, as first demonstrated in a seminal study of holmium (Keating, 1969). The experimental difficulty in exploiting Thompson scattering for probing periodical aspherical electronic densities is linked to the extremely weak intensity of the associated Bragg reflections. With the advent of high-brilliance third-generation synchrotron x-ray sources, this technique can, however, become effective.

Using an expansion in spherical harmonics, the Thompson x-ray atomic scattering amplitude for *f*-electron shells can be written as the sum of four terms $f_{2k}(\mathbf{Q})$, representing even-rank electric multipolar contributions (Amara and Morin, 1998; Amara *et al.*, 2001),

$$f = \left\langle \psi_g \left| \sum_j \exp(i\mathbf{Q}\cdot\mathbf{r}_j) \right| \psi_g \right\rangle = f_0(\mathbf{Q}) + \sum_{k=1}^{3} f_{2k}(\mathbf{Q}), \tag{77}$$

where ψ_g is the ground state, $\mathbf{r}_j$ is the position vector of the jth f electron, and $f_0(\mathbf{Q})$ is the usual scattering amplitude of a spherical shell. The additional terms will produce superlattice Bragg reflections in the presence of periodically arranged aspherical charge densities. When only the spherical and quadrupole terms are relevant, the scattering factor becomes

$$f(\mathbf{Q}) = n_f\langle j_0\rangle - \frac{5}{2}\alpha_J\langle j_2\rangle\left[\frac{1}{2}\left(3\frac{Q_z^2}{Q^2}-1\right)\langle O_{3z^2-r^2}\rangle + \frac{3}{2}\left(\frac{Q_x^2-Q_y^2}{Q^2}\right)\langle O_{x^2-y^2}\rangle + 6\left(\frac{Q_xQ_y}{Q^2}\langle O_{xy}\rangle + \frac{Q_yQ_z}{Q^2}\langle O_{yz}\rangle + \frac{Q_zQ_x}{Q^2}\langle O_{zx}\rangle\right)\right], \tag{78}$$

where n_f is the number of f electrons, $\langle j_k\rangle$ are radial integrals of the kth-order spherical Bessel function, α_j is the second-order Stevens factor, and Q_μ are components of the scattering vector $\mathbf{Q}$ along the lattice coordinate system.

Nonresonant x-ray diffraction has been successfully used to study the order of electric quadrupoles in DyB_2C_2 (Adachi *et al.*, 2002) and to investigate the simultaneous ordering of quadrupoles and hexadecapoles in CeB_6 (Tanaka, Staub, Katsumata, *et al.*, 2004).

D. Neutron diffraction and nuclear magnetic resonance

X-ray diffraction is particularly powerful for characterizing electric quadrupole motifs, which can also be studied by neutron diffraction in applied fields where induced magnetic dipole moments reveal the periodicity and symmetry of the underlying quadrupolar order. For instance, neutron diffraction on the cubic compound $PrPb_3$ in a [0 0 1] magnetic field provided evidence for a non-square-modulated quadrupolar phase through the observation of magnetic superlattice reflections (Onimaru *et al.*, 2005) appearing below T_Q=0.4 K (Sakakibara *et al.*, 2003). On the other hand, neutron diffraction is a more direct technique for studying MMP order. Although the large majority of magnetic neutron diffraction experiments have been performed to study dipolar order, neutrons can in principle be used for measuring any spatial distribution of the magnetization density.

For localized f electrons, the coherent elastic cross section for unpolarized neutrons has been given by Squires (1978) and Lovesey (1987),

$$\frac{d\sigma}{d\Omega} \propto \sum_{\mathbf{G}} \delta(\mathbf{Q}-\mathbf{G})|\mathbf{F}_M(\mathbf{Q})|^2, \tag{79}$$

where $\mathbf{G}$ is a vector of the reciprocal lattice of the ordered phase and $\mathbf{F}_M$ is the magnetic structure factor,

$$\mathbf{F}_M(\mathbf{Q}) = \frac{1}{Q^2}\left[\mathbf{Q}\times\left(\sum_d \exp(i\mathbf{Q}\cdot\mathbf{r}_d)\mathbf{F}_d(\mathbf{Q})\times\mathbf{Q}\right)\right], \tag{80}$$

where the label d runs over the atoms in the unit cell and

$$\mathbf{F}_d(\mathbf{Q}) = -\frac{1}{2\mu_B}\int \exp(i\mathbf{Q}\cdot\mathbf{r})\langle\hat{\mathbf{M}}_d(\mathbf{r})\rangle d\mathbf{r}. \tag{81}$$

The operator $\hat{\mathbf{M}}_d$ represents the sum of the spin and orbital contributions to the atomic magnetization density. The vector products in Eq. (80) imply that $\mathbf{F}_M$ is only sensitive to the magnetization component perpendicular to the scattering vector $\mathbf{Q}$.

For localized f-electron compounds, the Cartesian components of the atomic vector form factor $\mathbf{F}_d(\mathbf{Q})$ can be written as a linear combination of multipole moments of odd rank (Lovesey, 1987; Santini and Amoretti, 2002; Shiina *et al.*, 2007),

$$F_{d,\alpha}(\mathbf{Q}) = \frac{g_L}{2}f(Q)\left[\langle J_{d,\alpha}\rangle + \sum_{KQ} C_{KQ}^{\alpha}(\mathbf{Q})\langle T_{KQ}(d)\rangle\right], \tag{82}$$

where g_L is the Landé factor, $f(Q)$ is the dipolar form factor, and d labels inequivalent atoms. The coefficients C_{KQ} can be calculated as described by Lovesey (1987). In the dipole approximation, only the first term is present in Eq. (82). In this case, the $\mathbf{Q}$ dependence of the scattering amplitude is determined by $f(Q)$, which falls rapidly to zero at large Q. On the other hand, the multipolar contributions have maxima at $Q>0$ and are strongly anisotropic, which makes possible the observation of ordered MMPs from measurements (at high Q and along appropriate directions) of structural forbidden reflections with no superimposed dipolar scattering. The most accurate experimental method would involve using a beam of polarized neutrons (Nathans *et al.*, 1959; Brown *et al.*, 1980), but unpolarized neutron diffraction can also be employed in favorable cases.

The possibility to detect the asphericity of the magnetization distribution by neutron diffraction was demonstrated in a study of the spiral magnetic structure of Ho

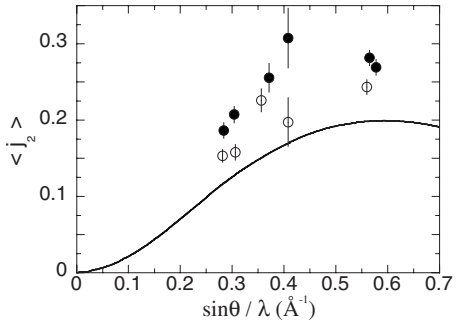

FIG. 10. Bessel transform of the magnetization distribution for Ho (open circles) and $Ho_{0.9}Sc_{0.1}$ (full circles), derived from the intensity of third-order neutron diffraction satellites in the magnetic spiral phase. The solid line is the theoretical prediction for a single ion model. Data from Felcher *et al.*, 1976.

and $Ho_{0.9}Sc_{0.1}$ (Felcher *et al.*, 1976). This experiment consisted in measuring the Q dependence of a set of coherent third-order diffraction satellites occurring at $\mathbf{Q}=\mathbf{G}_{hk\ell}\pm 3\tau$ positions, with $\mathbf{G}_{hk\ell}$ a reciprocal-lattice vector and τ the propagation vector of the spiral. Only the aspherical term in the magnetization density contributes to these satellites, which have zero intensity if the magnetization distribution around each atom is spherically symmetric. The results obtained by Felcher *et al.* (1976), shown in Fig. 10, demonstrate the asphericity of the local $4f$ magnetization distribution in the investigated compounds.

Short-wavelength neutron diffraction has the potential of becoming a useful technique for the study of MMP order, provided that large enough single crystals are available in order to overcome the intrinsic weakness of the signal. Experimental determinations of $\mathbf{F}_d(\mathbf{Q})$ can be used to calculate the magnetization density $\langle\hat{\mathbf{M}}_d(\mathbf{r})\rangle$ and the interstitial magnetic field set up by a single ordered ion,

$$\mathbf{H}(\mathbf{r}) = -\frac{\mu_B}{\pi^2}\int \exp(-i\mathbf{Q}\cdot\mathbf{r})\frac{\mathbf{Q}\times[\mathbf{F}_d(\mathbf{Q})\times\mathbf{Q}]}{Q^2}d\mathbf{Q}. \tag{83}$$

As discussed in Sec. III.A, the interstitial field $\mathbf{H}$ in a lattice of ordered MMPs can also be sensed by μSR experiments.

A further microscopic probe of MMP order is provided by NMR experiments, which are sensitive to the magnetic field at the ligand site through the hyperfine (HF) interaction with the nuclear spins. For instance, ^{11}B NMR has been used to study field-induced dipole and octupolar Ce moments in the AFQ ordered phase (phase II) of CeB_6 (Sakai *et al.*, 1997; Shiina *et al.*, 1998). These experiments demonstrated the possibility of identifying MMP order parameters through measurements of the NMR line splitting Δ for different directions of an applied magnetic field. ^{17}O NMR experiments have been used to study U and Np dioxides (Ikushima *et al.*, 2001; Sakai *et al.*, 2005; Tokunaga *et al.*, 2005b; Tokunaga, Aoki, Homma *et al.*, 2006, 2007; Tokunaga, Homma, Kambe, *et al.*, 2006; Tokunaga, Sakai, Fujimoto, *et al.*, 2007; Tokunaga, Walstedt, Homma, *et al.*, 2007; Walstedt *et al.*, 2007). The NMR effort dedicated to the observation of multipolar moments on actinide dioxides will be discussed in Sec. IV. In these compounds, NMR experiments were able to characterize not only field-induced dipolar and octupolar magnetic moments from the field orientation dependence of the hyperfine splitting at the oxygen nuclei, but also the electric quadrupole order from the oscillatory spin-echo decay resulting from the electric field gradient (Tokunaga, Aoki, Homma, *et al.*, 2006).

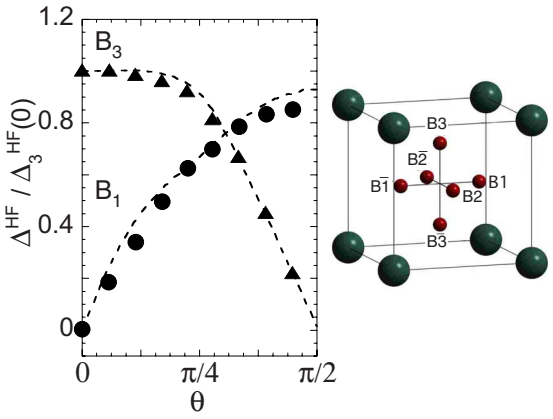

FIG. 11. (Color online) Splitting of the ^{11}B NMR resonance lines observed in the phase II of CeB_6 at $T=2.78$ K and 10.7 MHz, as a function of the angle θ between the direction of the applied magnetic field and the [1 0 0] axis. Triangles (circles) refer to B sites with axial symmetry along [0 0 1] (B_3) and [1 0 0] (B_1), respectively. Dashed lines are theoretical calculations including magnetic dipole and octupole contributions (Shiina *et al.*, 1998). The crystallographic structure of CeB_6 is shown in the right panel.

E. Evidence of multipolar order: Selected examples

1. $Ce_{1-x}La_xB_6$

CeB_6 and $Ce_{1-x}La_xB_6$ are dense Kondo systems with fascinating physical properties and a rich phase diagram strongly influenced by the interaction between high-rank multipoles of f electrons.[5] These compounds have the simple-cubic crystal structure (space group $Pm\bar{3}m$) shown in Fig. 11, where a B_6 molecule forms an octahe-

[5]See Hanzawa and Kasuya, 1984; Effantin *et al.*, 1985; Erkelens *et al.*, 1987; Regnault *et al.*, 1988; Hiroi, Kobayashi, Sera, *et al.*, 1997; Shiina *et al.*, 1997, 1998, 2003, 2007; Tayama *et al.*, 1997; Thalmeier *et al.*, 1998; Sakai *et al.*, 1999; Sera and Kobayashi, 1999; Shiba *et al.*, 1999; Hall *et al.*, 2000; Hanzawa, 2000a, 2000b; Kusunose and Kuramoto, 2001, 2005; Nakao *et al.*, 2001; Sera *et al.*, 2001; Lovesey, 2002; Schenck *et al.*, 2002, 2004; Givord *et al.*, 2003; Kubo and Kuramoto, 2003; Zaharko *et al.*, 2003; Tanaka, Staub, Katsumata, *et al.*, 2004; Fischer *et al.*, 2005; Kishimoto *et al.*, 2005; Kiss and Fazekas, 2005; Mannix *et al.*, 2005; Staub *et al.*, 2006; Tanaka *et al.*, 2006; Kondo *et al.*, 2007; and Kuwohara *et al.*, 2007.

dron around the body center of the simple-cubic lattice of Ce ions. The B sites have uniaxial symmetry along directions parallel to [1 0 0], [0 1 0], and [0 0 1] (sites $i=1$, 2, and 3). The CF of cubic symmetry splits the Ce^{3+} multiplet ($4f^1$, $j=5/2$) and gives a Γ_8 quartet ground state well isolated from an excited Γ_7 doublet. The active moments in the Γ_8 state are 15 independent multipoles, namely, three dipoles, five quadrupoles, and seven octupoles (Table I).

In CeB_6, two phase transitions are observed with decreasing temperature in zero field, the first at $T_Q=3.3$ K from the paramagnetic (phase I) to a AFQ state with ordering vector $\mathbf{k}_Q=(1/2,1/2,1/2)$ (phase II) and the second at $T_N=2.3$ K into an AF 2-**k** commensurate structure of wave vector $\mathbf{k}_M=(1/4,1/4,1/2)$ (phase III) (Effantin *et al.*, 1985). When an external field is applied, T_N drops rapidly to zero, while T_Q displays an amazing increase, reaching 10 K in a field of 30 T (Hall *et al.*, 2000; Goodrich *et al.*, 2004). This increase cannot be simply due to a quenching of Kondo fluctuations by the field. The Kondo energy scale is too small, and fluctuations of ionic multipoles should be largely suppressed already with an applied field of a few tesla. Instead, the behavior of T_Q can be understood by considering that in the presence of a field magnetic-multipole OPs switch on together with the AFQ order. The two-ion couplings involving octupoles stabilize the ordered phase, thus leading to an increase of T_Q (Shiina *et al.*, 1998; Sera and Kobayashi, 1999; Shiba *et al.*, 1999).

Detailed information on the multipolar order has been provided by NMR studies. In the paramagnetic phase (phase I), both the electric field gradient and the HF coupling tensor have the same uniaxial symmetry. The Hamiltonian of the B nuclear spin at site i is the sum of the Zeeman and quadrupolar nuclear terms, and can be written as

$$H_i^{\mathrm{HF}} = -\gamma \mathbf{I}_i \cdot \mathbf{H} + q[3I_{iz}^2 - I_i(I_i+1)]. \tag{84}$$

Experiments in phase I, where the three B sites are equivalent, give a ^{11}B NMR spectrum consisting of three lines, as expected for $q \neq 0$ ($I=3/2$). In phase II and in the presence of an external magnetic field **H**, neutron diffraction indicates AF order of a simple G type, with propagation vector $\mathbf{q}=(1/2,1/2,1/2)$ (Effantin *et al.*, 1985). On the other hand, in the NMR spectra, for each B site the three lines split into two components (Takigawa *et al.*, 1983). When the magnetic field is rotated in the $(1\ \bar{1}\ 0)$ plane, sites 1 and 2 are equivalent, so that the splittings Δ_1^{HF} and Δ_2^{HF} are equal but different from Δ_3^{HF}. A total of 12 lines is then observed. Δ_i^{HF} shows a marked dependence on the field strength and angle between the symmetry axis of each B site and the direction of **H**.

Assuming a zero-field AFQ order of Γ_5-type moments, and an ordered admixture of MMPs with propagation vector $\mathbf{q}=(1/2,1/2,1/2)$, the HF Hamiltonian of the B nuclear spin becomes (Shiina *et al.*, 1998)

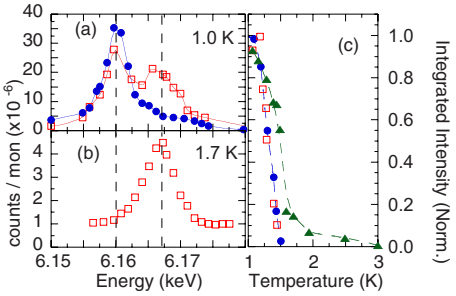

FIG. 12. (Color online) Energy dependence of the (3/2 3/2 3/2) superlattice reflection in $Ce_{0.7}La_{0.3}B_6$, around the Ce L_2 absorption edge, at (a) $T=1.0$ K and (b) $T=1.7$ K. Squares represent the intensity in the σ-π channel and circles refer to σ-σ polarization. The $E1$-$E1$ and $E2$-$E2$ energy thresholds are shown by vertical dashed lines. (c) Temperature dependence of the intensity for (triangles) $E1$-$E1$ σ-π intensity, (squares) $E2$-$E2$ σ-π, and (circles) $E2$-$E2$ σ-σ signals. Data from Mannix *et al.*, 2005.

$$H_3^{\mathrm{HF}} = aI_z\tilde{T}_{xyz}(\mathbf{q}) - b[I_x\tilde{J}_y(\mathbf{q}) + I_y\tilde{J}_x(\mathbf{q})] - c[I_x\tilde{T}_y^{\alpha}(\mathbf{q}) + I_y\tilde{T}_x^{\alpha}(\mathbf{q})], \tag{85}$$

$$H_{1,2}^{\mathrm{HF}} = aI_x\tilde{T}_{xyz}(\mathbf{q}) - b[I_y\tilde{J}_z(\mathbf{q}) + I_z\tilde{J}_y(\mathbf{q})] - c[I_y\tilde{T}_z^{\alpha}(\mathbf{q}) + I_z\tilde{T}_y^{\alpha}(\mathbf{q})], \tag{86}$$

where a, b, and c are coupling parameters, and $\tilde{\mathbf{J}}$ and $\tilde{T}$ are scaled magnetic dipole and octupole operators (T_{xyz} of Γ_2 symmetry, T_μ^α of Γ_4 symmetry). Moreover, considering the AF arrangement of Ce multipoles, $H_i^{\mathrm{HF}} = -H_{\bar{i}}^{\mathrm{HF}}$, where $\bar{i}$ refers to B ions obtained by ion i through inversion of the octahedron. The interaction terms (85) and (86) thus produce the splitting of the resonance lines (Shiina *et al.*, 1998). A comparison with experimental data is shown in Fig. 11. The agreement is good provided that the contribution of the octupoles is taken into account. These results, therefore, provide convincing evidence of the presence of an ordered field-induced magnetic octupole in the phase II of CeB_6.

Lanthanum doping at the Ce site results in the appearance of a new phase below a temperature T_{IV} depending on the La content ($T_{\mathrm{IV}}=1.5$ K for $x=0.3$). This phase IV condenses out of the paramagnetic state and shows ordering of T^β magnetic octupoles with Γ_5 symmetry (Hiroi, Sera, Kobayashi, *et al.*, 1997; Tayama *et al.*, 1997; Morie *et al.*, 2004; Suzuki *et al.*, 2005). The phase transition is revealed by a large anomaly in the specific heat (Furuno *et al.*, 1985), a cusp in the magnetic susceptibility (Tayama *et al.*, 1997), a large anomaly of the C_{44} elastic constant (Suzuki *et al.*, 1998), and a $\Delta L/L=10^{-6}$ contraction of the cube body diagonal (Akatsu *et al.*, 2003).

RXS experiments at the Ce L_2 absorption edge have been performed in $Ce_{0.7}La_{0.3}B_6$ by Mannix *et al.* (2005). Their main results are summarized in Fig. 12, where the integrated intensity of the (3/2 3/2 3/2) superlattice reflection is shown as a function of the incident photon energy. With the sample kept at 1 K, the intensity in the

σ-π polarization channel shows resonant enhancements at both the $E1$-$E1$ and $E2$-$E2$ energy values (6.167 and 6.160 keV, respectively). The first resonance probes the itinerant $5d$ states, the second gives access to the $4f$ states. On the other hand, no σ-σ resonance is observed at 6.167 keV. This suggests AF order of the $5d$ electrons as the origin of the $E1$-$E1$ σ-π resonant enhancement, whereas the resonance at lower energy in both polarization channels must be due to some kind of multipole order. AFQ order seems to be excluded by this experiment, as no σ-σ intensity is observed at the dipole edge, 6.167 keV. Further information is given by the azimuth angle dependence of the resonant intensities. This is flat for the $E1$-$E1$ σ-π signal, while the $E2$-$E2$ intensity exhibits sixfold symmetry in the σ-σ channel and a threefold periodicity in σ-π. Good agreement with the experimental results is obtained if an antiferro-octupolar order of $4f$ moments with Γ_5 symmetry is assumed (Mannix *et al.*, 2005). This order would coexist below 1.5 K with AF order having the same propagation vector and appearing at about 3 K. In fact, increasing the temperature to 1.7 K, the intensity at 6.160 keV vanishes in both polarization channels, and only the σ-π enhancement at 6.167 keV survives. The temperature dependence of the intensities is shown in Fig. 12. The $E2$-$E2$ intensities decrease rapidly with T and disappear at T_{IV}, whereas the σ-π intensity at the dipole edge continues into the nominal paramagnetic state up to 3 K.

The conclusions of Mannix *et al.* (2005) were challenged by Nagao and Igarashi (2006), who argued that the relative intensity between the two polarization channels depends strongly on the domain distribution and showed that the energy and azimuth dependence of the RXS intensities can also be reproduced by assuming AFQ order in conjunction with an induced hexadecapole contribution. On the other hand, the ordering of a Γ_5 magnetic octupole is supported by a recent neutron diffraction experiment (Kuwahara *et al.*, 2007). Weak superlattice reflections, with vanishing intensity above T_{IV}, have been observed at scattering vectors $\mathbf{Q}=(h/2,h/2,\ell/2)$ with h and ℓ odd (Fig. 13). The largest intensity is observed along [1 1 1], and increases with Q as expected for nondipolar order. Comparison with theoretical predictions (Shiina *et al.*, 2007) confirms the Γ_5 magnetic octupole as the order parameter. In fact, a Γ_2 octupole would give zero intensity along [1 1 1], whereas a Γ_4 octupole would induce the order of magnetic dipoles with the same symmetry, which is excluded by the experiment.

A broadening of NMR lines in phase IV has been interpreted as evidence for broken time-reversal symmetry (Magishi *et al.*, 2002). Detailed calculations of the HF splitting have been discussed by Sakai *et al.* (2005), together with the invariant form of the HF interaction. In this work, it was also predicted that in the presence of Γ_5 antiferro-octupolar ordering, the HF splitting of the B atom pair at $\frac{1}{2}\frac{1}{2}\pm z$ sites crosses zero on the $(1\ \bar{1}\ 0)$ plane when the magnetic field is rotated around the [0 0 1] axis.

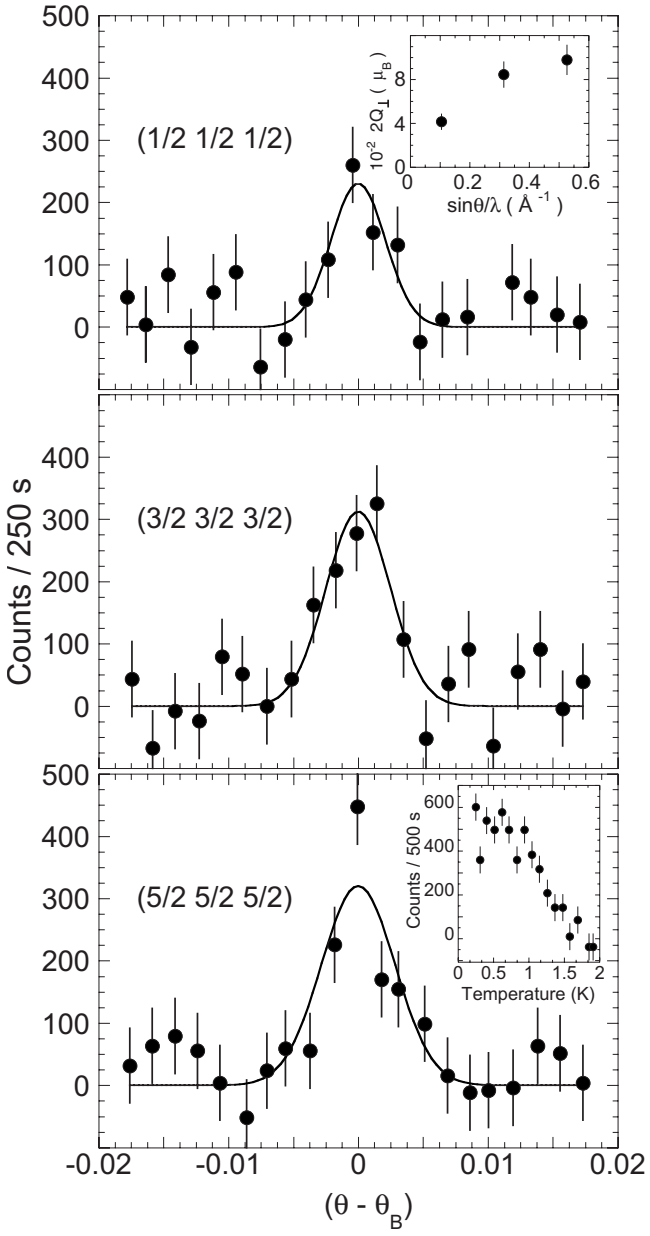

FIG. 13. Difference between neutron diffraction rocking curves measured at $T=0.25$ and 2 K at several $(h/2,h/2,h/2)$ positions in $Ce_{0.7}La_{0.3}B_6$. The temperature dependence of the integrated intensity and the Q dependence of the magnetic structure factor are shown in the insets. Data from Kuwahara *et al.*, 2007.

2. RB_2C_2

Ordering of EMPs has been well studied in the isostructural RB_2C_2 family (R=Dy,Ho,Tb). At room temperature these compounds crystallize in the tetragonal $P4/mbm$ space group (van Duijn *et al.*, 2000; Ohoyama *et al.*, 2001). In this structure, metallic rare-earth layers are stacked alternatively along the c direction with a covalently bonded B-C network consisting of nonregular

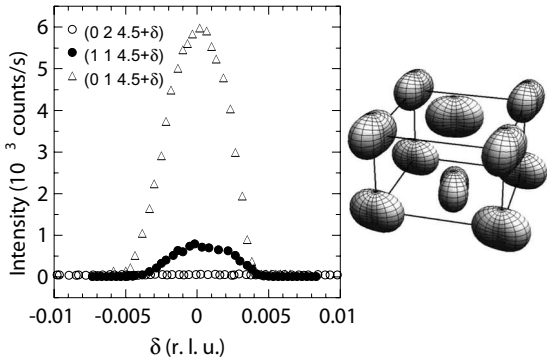

FIG. 14. Nonresonant x-ray diffraction intensity in DyB_2C_2, obtained from ℓ scans around three chosen (h k 9/2) superlattice reflections. Data were collected at $T=18$ K, below the AFQ ordering temperature $T_Q=24.7$ K but above the Néel temperature $T_N=15.3$ K. Data from Adachi *et al.*, 2002. Right panel: Schematic of the AFQ order in DyB_2C_2. For the ions Dy1, located at 000, the principal axis of the quadrupole moment forms an angle ϕ with the crystallographic axis **a**, whereas it is directed at angle $\pi/2-\phi$ from **a** in the case of the Dy2 ions at $\frac{1}{2}\frac{1}{2}0$. In the $z=1$ plane, the angle between the **a** direction and the quadrupole principal axis is $\pi/2+\phi$ for Dy3 at 001, and π-ϕ for Dy4 at $\frac{1}{2}\frac{1}{2}1$.

squares and octagons. Two parallel $(BC)_4$ rings sandwich each R^{3+} ion producing a CF of C_{4h} symmetry.

Much attention has been attracted by DyB_2C_2, where the Dy^{3+} ($4f^9$, $^5H_{15/2}$) CF ground state consists of two almost degenerate Kramers doublet, $|\pm 1/2\rangle$ and $|\pm 3/2\rangle$. AFQ ordering develops below $T_Q=24.7$ K (Yamauchi *et al.*, 1999), and the phase transition is accompanied by a structural distortion of the B-C network which reduces the symmetry to $P4_2/mnm$ (Tanaka *et al.*, 1999; Adachi *et al.*, 2002). Antiferromagnetic order is stabilized at a lower temperature, $T_N=15.3$ K (Yamauchi *et al.*, 1999). The magnetic structure is characterized by a (1, 0, 1/2) propagation vector and by four noncollinear magnetic sublattices with a net ferromagnetic moment (van Duijn *et al.*, 2000; Zaharko *et al.*, 2004). The Dy moments are perpendicular to the **c** axis; neighboring moments along **c** are mutually perpendicular, whereas neighboring moments along the [1 1 0] axis are canted away from [1 1 0] and almost oppositely aligned.

Evidence of AFQ ordering was given by RXS experiments at the Dy L_3 absorption edge through the appearance below T_Q of superlattice reflections at $\mathbf{q}_1=(0,0,1/2)$ and $\mathbf{q}_2=(1,0,1/2)$ (Tanaka *et al.*, 1999; Hirota *et al.*, 2000). Intensity enhancements have been observed at both the $E1$-$E1$ ($2p_{3/2}\rightarrow 5d$) and $E2$-$E2$ ($2p_{3/2}\rightarrow 4f$) thresholds (Tanaka, Inami, Lovesey, *et al.*, 2004; Matsumura *et al.*, 2005), the latter directly related to the spatial ordering of the orbitals.

The quadrupole motif compatible with the RXS results is shown in Fig. 14. The transition at T_Q is accompanied by a buckling of the B-C planes, reducing the point symmetry of the Dy site to C_{2h} (Tanaka *et al.*, 1999). Neighboring Dy along [0 0 1] have quadrupole components $\langle O_{xy}\rangle$ and $\langle O_{x^2-y^2}\rangle$ equal in magnitude and opposite in sign, whereas along [1 1 0] neighboring Dy have $\langle O_{xy}\rangle$ of one sign and $\langle O_{x^2-y^2}\rangle$ of opposite sign. A detailed analysis of the RXS structure factors has been given by Lovesey and Knight (2001), together with calculations of azimuth and polarization dependence of $E1$-$E1$ and $E2$-$E2$ superlattice-peak intensities. Most interestingly, (0 0 n/2) reflections at the $E2$-$E2$ resonance (7.780 keV) contain quadrupolar and hexadecapolar components transforming according to the representation Γ_1^+ of C_{2h}, but no Thomson contributions. The absence of a σ-σ signal at this energy has been interpreted as a consequence of the spatial order of rank-4 EMPs. Fitting the experimental data, a relation between the amplitude of the quadrupolar and hexadecapolar moments can be established that, in turn, sets stringent limits to the ground-state wave functions of the Dy $4f$ shell (Tanaka, Inami, Lovesey, *et al.*, 2004).

The above model describing the electric multipolar arrangement in DyB_2C_2 has been recently corroborated by soft-x-ray resonant diffraction measurements at the Dy $M_{4,5}$ edges (Mulders *et al.*, 2006). At this resonance, the $4f$ shell is probed directly through an $E1$-$E1$ $3d_{3/2,5/2}\rightarrow 4f$ virtual transition. In addition to the quadrupole and hexadecapole moments, the scattering amplitude also contains a term related to the rank-6 (hexacontatetrapole) moment, which becomes accessible if the intra-atomic quadrupole interaction splits the $3d$ core levels. Fitting the energy dependence of the (0 0 1/2) reflection, the magnitude of the hexadecapole and hexacontatetrapole moments is estimated at −20% and +30% of the quadrupole moment, respectively (Mulders *et al.*, 2006).

Interesting information has also been provided by nonresonant x-ray diffraction (Adachi *et al.*, 2002). The principal axes of the quadrupole moments are confined in the a-b plane by the lattice symmetry, and therefore $\langle O_{zx}\rangle=\langle O_{yz}\rangle=0$. For scattering vectors corresponding to Miller indices ($hk\ell$) such that ℓ is a half integer, the structure factors $F(hk\ell)=\Sigma_j f_j \exp(i\mathbf{Q}\cdot\mathbf{R}_j)$ become [see Eq. (77)]

$$F_{h+k=2n+1} \propto -15\alpha_J\langle j_2\rangle \frac{\cos(2\phi)}{h^2+k^2+(a\ell/c)^2} \times[(h^2-k^2)\langle O_{x^2-y^2}\rangle + 4hk\langle O_{xy}\rangle], \quad (87)$$

$$F_{h+k=2n} \propto -30\alpha_J\langle j_2\rangle \frac{\sin(2\phi)}{h^2+k^2+(a\ell/c)^2} \times[hk\langle O_{x^2-y^2}\rangle - (h^2-k^2)\langle O_{xy}\rangle]. \quad (88)$$

From Eqs. (87) and (88) it is evident that symmetry, magnitude, and orientation of the quadrupolar order parameter can be obtained from the intensity of an appropriately selected set of Bragg peaks. For instance, the zero intensity of the (0 2 9/2) superlattice reflection (Fig. 14) indicates that $\langle O_{xy}\rangle=0$. On the contrary, superlattice reflections with nonzero intensity are observed at (1 1 9/2) and (0 1 9/2), showing that the AFQ order involves the $\langle O_{x^2-y^2}\rangle$ component.

Interesting phenomena related to a strong interplay between magnetic-dipole and electric-quadrupole moments have been studied in TbB_2C_2, where an increase of the Néel temperature from T_N=21.7 to 35 K is observed upon application of a 10 T magnetic field along [1 1 0] (Kaneko *et al.*, 2003). In zero field, resonant soft-x-ray diffraction at the Tb $M_{4,5}$ edges and nonresonant x-ray diffraction at 30 keV reveal coexisting ferroquadrupolar and antiferromagnetic order below T_N (Mulders *et al.*, 2007). Application of a magnetic field **H** along [1 1 0] forces the magnetic-dipole moments to rotate toward the field direction. The electric quadrupoles, coupled to the magnetic dipoles, rotate accordingly and move gradually away from the parallel alignment as H increases. The corresponding enhancement of the ordering temperature signals a change of the quadrupole pair interaction, as expected for conduction-electron-mediated multipole coupling (Teitelbaum and Levy, 1976).

In most cases, the onset of quadrupolar order T_Q is above the Néel temperature T_N. HoB_2C_2 is an exception (Onodera *et al.*, 1999), as in this compound quadrupolar order (T_Q=4.5 K) develops inside the AF phase (T_N =5.9 K). μSR Knight shift measurements on a single crystal show clear deviation from a linear behavior in the K vs χ plot, reflecting an unusual temperature dependence of the contact hyperfine constant A_c in the paramagnetic phase (Lorenzi *et al.*, 2003). A_c is temperature independent, isotropic, and negative above about 100 K, whereas it becomes considerably larger, anisotropic, and positive below 50 K, where the Ho electric quadrupole moment aligns along the induced magnetic moment due to a spin-orbit interaction. This behavior signals the development of an anisotropic RKKY coupling due to the dependence of the exchange integrals on the relative orientation of the aspherical 4*f* charge distribution. The rich magnetic and quadrupolar phase diagram of HoB_2C_2 has been investigated by measurements of elastic constants in fields of up to 30 T applied along the [001] axis and in the basal plane (Yanagisawa *et al.*, 2005).

3. RT_4M_{12}

Filled skutterudites with the formula RT_4M_{12} (R =rare earth or actinide element, T=transition metal of the Fe group, M=metallic element of the pnictogen group) are a recently discovered family of *f*-electron compounds with cubic crystal structure. Much work has been done on these materials, partly because some of them are thought to be unconventional superconductors. The R-site symmetry is T_h, so that H_{CF} contains an extra term proportional to $\hat{O}_6^2-\hat{O}_6^6$ with respect to Eq. (19), its counterpart for the O_h point group; on the other hand, the number and degeneracy of CF levels for each J multiplet is the same for the two symmetry groups (Takegahara *et al.*, 2001).

It has been suggested that the peculiar properties of Pr-based skutterudites can be understood within a common model based on low-lying CF singlet-triplet states (Kiss and Fazekas, 2003a; Kohgi *et al.*, 2003). While the Γ_1 singlet, which is the ground state, does not carry any quadrupole moment by itself, the small energy gap with the excited triplet makes this a pseudoquartet system, with 15 active multipoles which have been tabulated by Shiina (2004).

The interplay of these multipoles determines the peculiar anisotropy of the phase diagram for $PrOs_4Sb_{12}$, where stable antiferroquadrupolar phases have been determined for certain directions of the magnetic field (Shiina and Aoki, 2004). It is interesting to note that the singlet-triplet level scheme has been treated in a pseudospin approach, which clarified a hidden symmetry in the Hamiltonian and its effect on possible order parameters. Neutron scattering experiments have revealed the field-induced ordered antiferromagnetic structure, leading to the conclusion that the antiferroquadrupolar phase is predominantly of O_{xy} character (Kaneko *et al.*, 2007). Quadrupolar fluctuations are suspected to play a role in the pairing mechanism of this unconventional superconductor (Koga *et al.*, 2006).

The same singlet-triplet level scheme accounts for the phase transition to an AFQ phase observed for $PrFe_4P_{12}$ at T_Q=6.5 K (Aoki *et al.*, 2002; Hao *et al.*, 2003), leading to the order of Γ_3 quadrupoles. However, another suggestion coming from the theoretical interpretation of recent NMR experiments (Sakai *et al.*, 2007) is that the order parameter is actually hexadecapolar. Antiferrohexadecapolar order has also been suggested (on the basis of a theoretical model based on the *j*-*j* coupling scheme) to explain the experimental results obtained for another closely related compound, $PrRu_4P_{12}$ (Takimoto, 2006). On the other hand, a scalar order parameter with Γ_{1g} symmetry has been suggested for both $PrFe_4P_{12}$ and $PrRu_4P_{12}$ (Kiss and Kuramoto, 2006, 2008).

$SmRu_4P_{12}$ displays a metal-insulator transition at T_{MI}=16.5 K (Matsuhira *et al.*, 2002). The magnetic entropy at the transition temperature, estimated from specific-heat measurements, is close to R ln 4, suggesting that the CF ground state is the Γ_6-Γ_7 quartet (which would correspond to Γ_8 in O_h symmetry, as for CeB_6 and NpO_2). An additional phase transition at T_N=15 K is associated with a barely detectable anomaly; when a magnetic field is applied, T_{MI} increases, T_N decreases and the latter anomaly becomes clearly visible (Yoshizawa *et al.*, 2005). While the similarity with the behavior of CeB_6 would suggest that the metal-insulator transition is associated with a quadrupolar ordering, this was later excluded by μSR measurements showing time-reversal symmetry breaking below T_{MI} (Hachitani *et al.*, 2006). The experimental detection (by specific-heat studies of the hyperfine-enhanced Sm nuclear contribution) of a small but nonzero magnetic moment ($0.29\mu_B$) leads to the conclusion that the primary order parameter is the Γ_4 octupole, and that the ordering of magnetic dipoles with the same symmetry follows as a secondary order parameter (Aoki *et al.*, 2007).

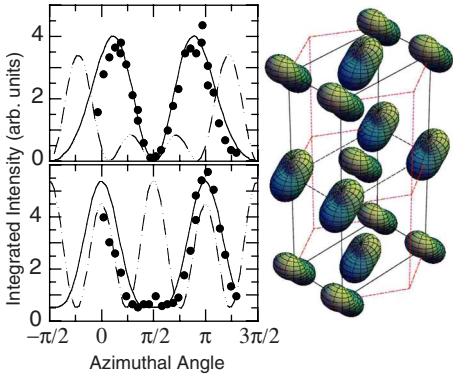

FIG. 15. (Color online) Azimuth dependence of (upper panel) the σ-π and (lower panel) the σ-σ scattering intensities of the (1 0 3) superlattice peak in UPd_3 at the U M_4 edge, at $T=7.1$ K. The experimental data are compared with calculations assuming ordering of the O_{zx} (solid line) and $O_{x^2-y^2}$ (dashed line) electric quadrupoles. The right panel is a representation of the O_{zx} AFQ structure. Data from Walker *et al.*, 2006.

4. UPd_3

UPd_3 crystallizes in the *dhcp* structure and has two different U^{4+} sites, one with hexagonal and the other with quasicubic point symmetry. It displays four distinct phase transitions below 8 K, which are attributed to switching between a series of different AFQ-ordered structures (McMorrow *et al.*, 2001). The localized nature of the 5*f* electrons in this compound was inferred by an inelastic neutron scattering experiment, which revealed narrow peaks due to excitations between CF levels (Buyers *et al.*, 1980). The strongest of these appears at about 15 meV and is attributed to the transition between the $M=0$ ground state and the $M=\pm1$ excited doublet of the hexagonal sites. This well-isolated nonmagnetic ground state does not allow these sites to play any active role in the transitions. The quadrupolar nature of the phase transitions was established by neutron scattering experiments where long-range lattice distortions were determined (Steigenberger *et al.*, 1992), and confirmed by ultrasonic attenuation and elastic constant measurements (Lingg *et al.*, 1999).

The suggestion that the order parameter below the 7.8 K transition was $O_{x^2-y^2}$ was first made from an analysis of polarized neutron diffraction measurements in a magnetic field (McEwen *et al.*, 1998, 2003). The results of the first resonant x-ray diffraction study of UPd_3 (McMorrow *et al.*, 2001) were consistent with this hypothesis. In their most recent papers, Walker *et al.* (2006) and McEwen *et al.* (2007) concluded that the primary order parameter is indeed O_{zx} (Fig. 15), but from symmetry considerations this induces an $O_{x^2-y^2}$ secondary order parameter. However, in the configuration of the polarized neutron experiment, only the $O_{x^2-y^2}$ component produced the antiferromagnetic moment that was detected, thus reconciling the previous hypotheses. This paper also reports the full crystal-field level scheme, deduced from recent inelastic neutron scattering data.

5. RPd_3S_4

The RPd_3S_4 family of compounds is particularly interesting for its strong quadrupolar pair interactions, which, coupled with the large degeneracy of their ground states resulting from the high-symmetry CF, can give rise to peculiar orbital effects (Abe *et al.*, 1999). These compounds crystallize in a bcc cubic lattice with space group $Pm\bar{3}n$ (Keszler and Ibers, 1983); the point symmetry of the R sites is T_h as for the skutterudites. $DyPd_3S_4$, for example, orders antiferroquadrupolarly below $T_Q=3.4$ K (2.7 K for a single crystal); below $T_{N1}\sim1$ K, two subsequent magnetic transitions follow (Kiss and Fazekas, 2003b). A temperature-dependent splitting of the ground-state quartet was evidenced by inelastic neutron scattering in the quadrupolar phase. Moreover, high-resolution neutron diffraction excluded the presence of any symmetry-lowering structural distortion at T_Q (which would be present for a ferroquadrupolar order), and revealed that the field-induced magnetic structure in the AFQ phase is similar to the spontaneous zero-field magnetic structure below T_{N1} (Keller *et al.*, 2004). AFQ ordering has also been suggested for other similar compounds with "reentrant" H-T phase diagrams, such as $PrPd_3S_4$ (Matsuoka *et al.*, 2007).

IV. *f*-ELECTRON DIOXIDES AS MODEL COMPOUNDS FOR MULTIPOLAR INTERACTIONS

As mentioned in the Introduction, actinide dioxides (AO_2) provide model systems where the delicate balance of various interactions can be thoroughly studied. In fact, due to their very simple crystallographic structure and insulating character, they are among the compounds described by the simplest Hamiltonians. The high (cubic) symmetry of the paramagnetic phase is ideal for maximizing the number of independent multipolar degrees of freedom (see Sec. II). In addition, the existence of a family of isostructural compounds allows us to build a reliable model for the single-ion wave functions working for all the different *f*-electron numbers involved. Fundamental questions concerning the nature of the 5*f* electrons and their degree of localization and covalency have been explored in numerous experimental investigations (Frazer *et al.*, 1965; Dolling and Cowley, 1966; Cowley and Dolling, 1968; Faber and Lander, 1976; Lander *et al.*, 1976; Schoenes, 1980; Veal and Lam, 1982; Fournier, 1985; Naegele and Ghijsen, 1985; Cox *et al.*, 1987). The importance of some dioxides (e.g., UO_2) as a nuclear fuel has made their high-temperature thermodynamic properties the subject of detailed analysis (Fink, 1982; Browning 1983; Clausen *et al.*, 1984; Buyers and Holden 1985; Gajek *et al.* 1988). The occurrence of a phase transition in UO_2 ($T_N=30.8$ K) and NpO_2 ($T_0=25$ K) was revealed in the early 1950s by large λ-like anomalies in the temperature dependence of the heat capacity (Jones *et al.*, 1952; Osborne and Westrum, 1953). Even if the behavior of the magnetic susceptibility resembles that of typical antiferromagnets (Arrott and Goldman, 1957; Ross and Lam, 1967), the actual static

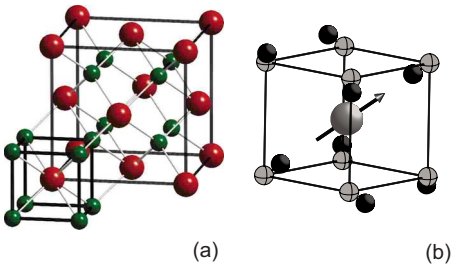

FIG. 16. (Color online) Crystallographic structure of actinide dioxides AO_2. (a) The cubic CaF_2-type structure with (large red circles) A^{4+} and (small green circles) O^{2-}. (b) 3-**k** internal distortion of the oxygen sublattice in the AF phase of UO_2. The oxygen displacement along the ⟨1 1 1⟩ directions is of 0.014 Å (not to scale in the figure).

and dynamical properties in the ordered phases are much more complex. Indeed, the interplay between CF, ME interactions, multipolar SE, and phonon-transmitted quadrupolar interactions gives rise to a number of effects that have attracted the attention of many physicists for the second half of the past century. However, only recently have the last pieces of the puzzle fallen into place.

Actinide dioxides are large-gap semiconductors crystallizing in the fcc fluorite structure [Fig. 16(a)], with $Fm\bar{3}m$ space group and room-temperature lattice parameter near 5.4 Å (a_U=5.47 Å, a_{Np}=5.44 Å, a_{Pu}=5.40 Å, a_{Am}=5.37 Å, a_{Cm}=5.36 Å, a_{Bk}=5.33 Å, and a_{Cf}=5.31 Å). The actinide ions occupy the 4*a* special positions with O_h point symmetry, whereas the oxygen ions at the 8*c* special positions ($\frac{1}{4}\frac{1}{4}\frac{1}{4}$, $\frac{3}{4}\frac{3}{4}\frac{3}{4}$) form a simple-cubic, internal sublattice with edge length $a/2$. The band structure comprises an occupied valence band mainly derived from oxygen 2*p* orbitals and an empty conduction band derived from actinide 6*d* and 7*s* orbitals (Naegele and Ghijsen, 1985; Prodan *et al.*, 2007), with the 5*f* states lying in the band gap. A metallic behavior due to direct *f*-*f* hopping is excluded, both because of the large *A*-*A* distance (Hill, 1970) and because of the lack of 5*f* contribution to the bonding (Brooks and Kelly, 1983b). Although there are no 5*f* bands in these oxides, a certain degree of mixing of 5*f* with oxygen *p* orbitals cannot be excluded (Brooks and Kelly, 1983b; Ellis, 1985; Naegele and Ghijsen, 1985; Gunnarson *et al.*, 1988), especially for the dioxides of Pu, Am, and Cm (Prodan *et al.*, 2007). Even if present, *f*-*p* mixing is believed to have no qualitative effects on the magnetic properties of PrO_2, UO_2, and NpO_2, where it is appropriate to use theoretical models based on a purely ionic picture. The occupation *n* of the 5*f* shell in the A^{4+} ion increases from 2 to 4, passing from U to Pu. In the case of PrO_2, the occupation of the 4*f* shell is 1. In the RS coupling scheme, this corresponds to $^2F_{5/2}$ (n=1), $^3H_4$ (n=2), $^4I_{9/2}$ (n=3), and $^5I_4$ (n=4) ground multiplets. Since the 5*f* states are well localized the CF potential plays a central role, so that knowledge of its size is necessary to understand both bulk and spectroscopic properties.

In the following sections, we illustrate in detail the properties of UO_2, NpO_2, and PrO_2, which are the most interesting dioxides from the point of view of multipolar interactions. Next, other dioxides will be discussed.

A. Uranium dioxide

The low-temperature behavior of UO_2 results from the interplay of SE interactions and ME coupling of electric quadrupoles to the lattice. As mentioned above, 5*f* electrons are well localized. The ground-state multiplet of the U^{4+} ions is $^3H_4$ within the *LS* coupling scheme, and it is only moderately (∼10%) modified by IC effects. The magnetic susceptibility is characterized by an effective Curie-Weiss paramagnetic moment $\mu_{eff}=3.2\mu_B$ and a paramagnetic temperature $\Theta_P=-220$ K. UO_2 exhibits a first-order phase transition at $T_N=30.8$ K to a transverse type-I AF state accompanied by a JT distortion of the oxygen sublattice. The ordered magnetic moment, determined by neutron diffraction, is $\mu_0=1.74(2)\mu_B$ (Frazer *et al.*, 1965; Willis and Taylor, 1976; Faber and Lander, 1976) Although the transition is discontinuous, short-range correlations are observed by critical neutron scattering above T_N (Buyers and Holden, 1985; Caciuffo *et al.*, 1999). By extrapolating the *T* dependence of the correlation length, a divergence is found for *T* close to 25 K, where a second-order phase transition would occur if the first-order phase transition did not prevent the staggered susceptibility from diverging. A volume discontinuity and discontinuities in the elastic constants were also found to occur at T_N (Brandt and Walker, 1967), showing that a coupling between magnetic and lattice degrees of freedom exists. The ordering was initially believed to be 1-**k** (Allen, 1968a, 1968b), accompanied by a homogeneous lattice distortion. Subsequent neutron diffraction experiments have actually found a lattice distortion (Faber *et al.*, 1975; Faber and Lander, 1976), but of a different kind. It consists of a frozen-in optical phonon with wave vector at the point *X* of the Brillouin zone (1-**k** distortion). Also, the magnetic structure was suggested to be 2-**k**, with moments along ⟨1 1 0⟩ directions. More recently, a 3-**k** structure has been proposed in order to explain the results of neutron scattering experiments under an external magnetic field (Burlet *et al.*, 1986). This structure preserves the cubic symmetry and is characterized by magnetic moments and oxygen displacements along the ⟨1 1 1⟩ directions (Fig. 9). Further evidence of a 3-**k** structure has been provided by NMR studies on samples enriched with ^{235}U and ^{17}O (Ikushima *et al.*, 2001), and later by Blackburn *et al.* (2005) in their study of the polarization of the magnetic excitations. The ^{235}U hyperfine interaction is consistent with an axially symmetric 5*f* wave function below T_N, and the ^{17}O spin-echo measurements of the electric field gradient gave evidence for lattice distortion, i.e., loss of cubic symmetry at the ^{17}O site, consistent with 3-**k** order. This distortion of the oxygen sublattice can be seen as the superposition of three

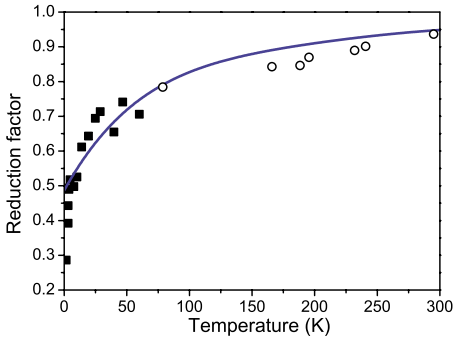

FIG. 17. (Color online) Temperature dependence of the reduction factor of the susceptibility of $U_{0.09}Th_{0.91}O_2$ (Slowinski and Elliott, 1952; Comly, 1968). The reduction factor is the ratio of the measured susceptibility to the Curie susceptibility expected from the Γ_5 CF ground state. The solid line is the result of a theoretical model based on the dynamical Jahn-Teller effect (Sasaki and Obata, 1970).

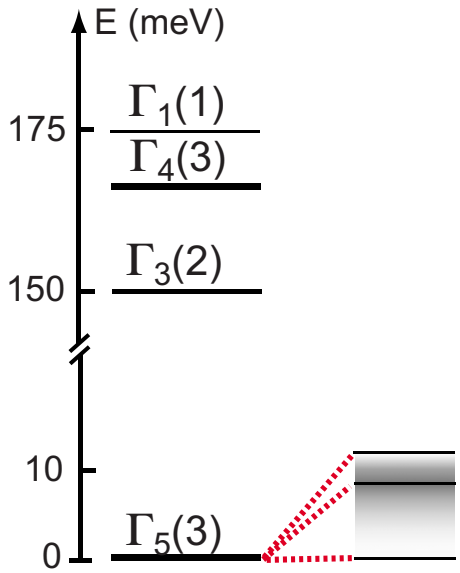

FIG. 18. (Color online) CF levels of UO_2 in the paramagnetic phase as deduced from inelastic neutron scattering (Amoretti *et al.*, 1989). The splitting of the Γ_5 ground triplet in the magnetically ordered phase is shown in the right-hand side. The shading illustrates the continuum of spin-wave excitations.

frozen optical phonon modes having the components of the star of X as wave vectors [Fig. 16(b)].

The value of the ordered moment of UO_2 [$1.74(2)\mu_B$] is strongly reduced with respect to $3.2\mu_B$, typical of the $J=4$ multiplet in RS coupling. This fact, together with the reduction of μ_{eff}, suggests that important CF effects are present in this compound. A nearest-neighbor point-charge estimation of the CF points to either a Γ_5-triplet or a Γ_1-singlet CF ground state. This suggested (Blume, 1966) a possible explanation for the first-order character of the transition based on the assumption of a ground Γ_1 singlet in the PM phase, with one component of the triplet becoming lower in energy for a sufficiently strong molecular field H_c. A self-consistent solution was found, with the magnetization falling discontinuously to zero when the self-consistent molecular field becomes smaller than H_c. This interpretation is suggestive and the approach has general interest and validity. However, it was later found that the CF ground state of the U ions cannot be a singlet and is actually a Γ_5 triplet. This was demonstrated by low-temperature measurements for U ions diluted in ThO_2, a diamagnetic isomorph of UO_2 (Comly, 1968), showing that the dependence of T_N on concentration and the observed Curie-type behavior of the susceptibility are inconsistent with Blume's model. Remarkably, the effective paramagnetic moment shows an anomalous T-dependent reduction so that at $T\rightarrow 0$ the susceptibility is less than 50% of that expected for the bare Γ_5 triplet (Fig. 17). This behavior was explained by a model (Sasaki and Obata, 1970) in which the coupling of the quadrupole degrees of freedom of the Γ_5 triplet with phonons produces a dynamical Jahn-Teller effect. Since it reduces the effective moment, a dynamical Jahn-Teller effect might also be responsible for the reduction of the saturation ordered moment from $2.0\mu_B$ (bare Γ_5 triplet in LS coupling) to $1.74\mu_B$ (Ippolito *et al.*, 2005). Such reduction had been initially attributed to strong J-mixing effects (Rahman and Runciman, 1966), or to the effect of the lattice distortion within the 1-**k** and 2-**k** models (within the 3-**k** model the distortion causes no reduction).

Excited CF states have been investigated by inelastic neutron scattering (Kern *et al.*, 1985). Two peaks at 155 and 172 meV were observed, in contrast to earlier predictions of one level at 169 meV with the next level at 624 meV (Rahman and Runciman, 1966). A higher-resolution experiment with extended energy range (Osborn *et al.*, 1988; Amoretti *et al.*, 1989) allowed a definitive determination of the CF by the analysis of the transition energies and intensities. The Γ_3, Γ_4, and Γ_1 CF states lie between 150 and 175 meV above the Γ_5 ground state (Fig. 18). No other excitations were observed up to approximately 700 meV. J-mixing effects are far less important than previously assumed. The so-determined CF of UO_2 has been shown in a recent theoretical study (Magnani, Santini, Amoretti, and Caciuffo, 2005; Magnani *et al.*, 2007) to be in line with that expected by scaling the CFs, of the other dioxides through Eq. (20), i.e., $A_4\sim -19$ meV$/a_0^4$ and $A_6\sim 0.65$ meV$/a_0^6$. Further support of this CF level scheme is provided by the specific heat which shows a Schottky contribution below 1000 K (Amoretti *et al.*, 1989). The high-energy inelastic neutron scattering spectra below T_N present considerably more structure than those above. It was shown that this is a consequence of the splitting of the CF levels by the combined effects of the molecular field and distortion of the oxygen ligand cage. The calculated energy spacings indicated that the 3-**k** model is by far more consistent with the observed splittings than the 2-**k** one. An interesting result of this experiment was the observation of splittings even at $T=35$ K, well into the paramagnetic phase, indicating that a dynamical Jahn-Teller effect persists above T_N.

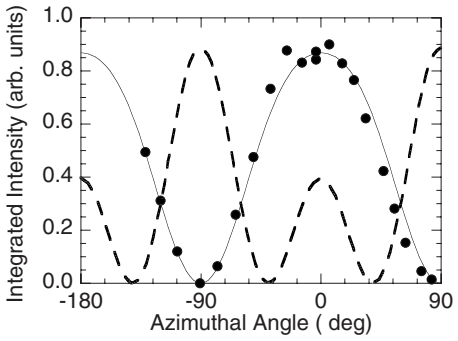

FIG. 19. Azimuth angle dependence of the (1 1 2) σ-σ intensity in UO_2 at 12 K. Data collected with incident energy E =3.728 keV (U_{M_4}). The solid (dashed) line shows the expected azimuth dependence for a 3-**k** transverse (longitudinal) structure of Γ_5 quadrupoles. From Wilkins *et al.*, 2006.

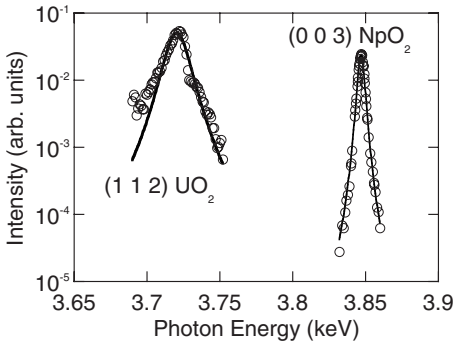

FIG. 20. The integrated intensity of the (1 1 2) reflection in UO_2 and of the (0 0 3) superlattice peak in NpO_2 as a function of the incident photon energy around the M_4 absorption edge of Np and U, respectively. Data were collected at T=12 K. The solid lines are fit to Lorentzian squared line shapes.

The 3-**k** magnetic order of UO_2 is accompanied by a 3-**k** order of quadrupoles, which corresponds to an axial distortion of the 5*f* charge density along the moment directions. Such ordering has been directly probed in a recent RXS experiment at the actinide $M_{4,5}$ absorption edges, at which photon energies the core 3*d* electrons are promoted to the partially occupied 5*f* valence states by a dipole ($E1$) transition (Wilkins *et al.*, 2006). Magnetic and quadrupolar structures have the same propagation vectors, and reflections arising from the quadrupoles coincide with those due to magnetic dipoles. A separation of the two contributions is possible through polarization analysis, provided that off-specular reflections are measured (see Sec. III.B.3). In this case, the signal from electric-quadrupolar scattering is partially σ-σ and therefore observable, whereas the σ-π channel is dominated by the magnetic contribution. Figure 19 shows the azimuth angle dependence of the intensity in the σ-σ polarization channel from the (1 1 2) reflection at 12 K. The origin of the azimuth angle corresponds to $[\bar{1}00]$ in the scattering plane. Data are compared with the predictions for an incoherent superposition of the two transverse symmetry-allowed quadrupole configurations, that is, $I \propto \cos^2\Psi(3-\cos^2\Psi)$ (Sec. III.B.3). The excellent agreement between model predictions and experimental data proves the transverse nature of the quadrupolar ordering in UO_2. The temperature dependence of the quadrupolar intensity closely follows the one measured for structural peaks arising from the oxygen displacements, as expected (Wilkins *et al.*, 2006).

Further information on the ordered ground state is provided by the energy profile of the integrated intensity of the superlattice reflections. Figure 20 shows data taken at the M_4 resonance in the σ-σ channel for the UO_2 (1 1 2) and NpO_2 (0 0 3) reflections (see the next section). In both cases, this quadrupole signal ($F^{(2)}$ tensor in $E1$-$E1$ scattering amplitude) is centered about 2 eV below the position of the dipole resonance, and it has an approximate Lorentzian squared shape with a narrow full width at half maximum of ~3 eV. These energy dependencies have been calculated on the basis of a localized electron model that takes into account the multiplet structure of the intermediate state. The results, reported by Nagao and Igarashi (2005), confirm the 3-**k** nature of the ordered structure and the symmetry of the quadrupole order parameter.

The low-energy magnetic dynamics of UO_2 below T_N are characterized by spin-wave (SW) excitations. Because of the technological importance of UO_2, a considerable effort to grow single crystals has been made, and even from the 1960s crystals as big as 100 g have existed. This has made the dynamics, both the phonons (Dolling *et al.*, 1965) and magnons, relatively easy to investigate in detail. Unfortunately, this is the only actinide oxide for which large single crystals exist. The first extensive inelastic neutron scattering experiments in the AF phase were performed by Cowley and Dolling (Dolling and Cowley, 1966; Cowley and Dolling, 1968). The measured SW dispersion provided evidence of sizable mixing between magnons and phonons, a further and spectacular manifestation of the importance of ME interactions in UO_2. Even more complex dispersion curves with additional magnetic modes were suggested on the basis of a subsequent experiment (Buyers and Holden, 1985). Inelastic neutron scattering experiments with standard (Caciuffo *et al.*, 1999) and spherical (Blackburn *et al.*, 2005; Caciuffo *et al.*, 2007) polarization analysis have been performed more recently. The main features of the SW spectrum (Fig. 21) are two optical branches and an acoustical one. The latter undergoes a clear-cut anticrossing with a TA phonon branch near (0, 0, 1.5).

From a theoretical point of view, the description of the phase transition and spin wave dispersion is not completely satisfactory. Some important aspects were understood by Allen (1968a, 1968b), but on the basis of an incorrect 1-**k** structure. Allen realized that the first-order character of the phase transition may be due to the spin-lattice interaction, which also was predicted to cause a distortion below T_N. As mentioned in Sec. II.E, the presence of a mixed third-order invariant which couples dipoles and quadrupoles leads to a quadrupolar secondary OP proportional to the square of the primary magnetic OP to leading order. For an OP direction cor-

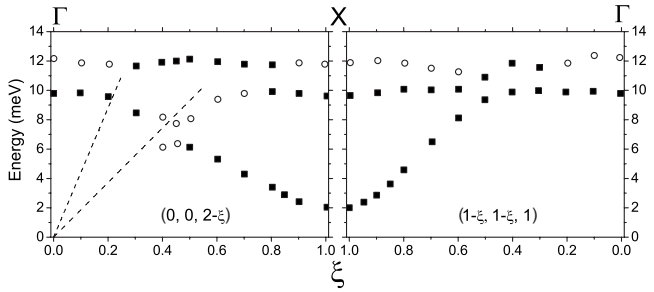

FIG. 21. The most intense spin-wave modes measured at 16.5 K along the principal crystallographic directions. The dashed lines correspond to acoustic phonon branches measured at 270 K. Inelastic neutron scattering data have been collected in the constant-Q mode, at the reciprocal-lattice points $(0,0,2-\xi)$ and $(1-\xi,1-\xi,1)$. Open symbols indicate significantly smaller intensity than the filled points. From Cacciuffo *et al.*, 1999.

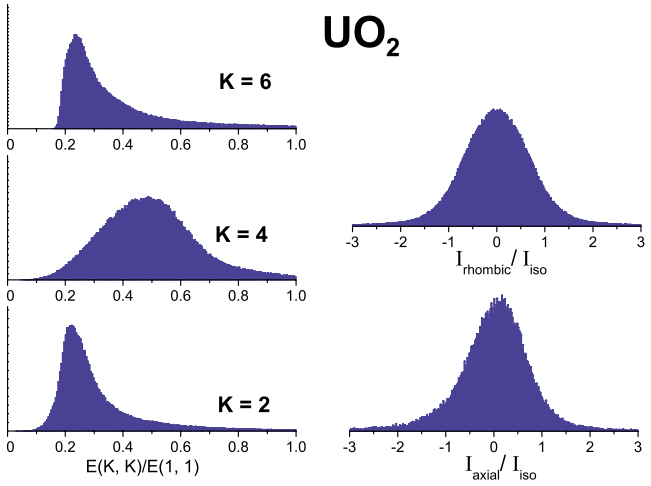

FIG. 22. (Color online) Multipolar coupling in a U^{4+} dimer. Left: Distribution of the ratio $E(K,K)/E(1,1)$, with $E(K_i,K_j)$ the ground-state energy of a dimer (C_{2v} bond) of U^{4+} ions coupled with the part of Eq. (35) associated with a specific pair of ranks K_i,K_j. The $t_{i,j}^{\Gamma_i\Gamma_j}$ parameters are varied on a cubic grid. Right: Distribution of the anisotropy of dipole-dipole interactions for NN U ions, i.e., the part of Eq. (35) with ($K_i=1$, $K_j=1$). The C_{2v} symmetry of the bond allows for three independent exchange constants. In the reference frame bringing the coupling to diagonal form, $H_{ij}=I_{xx}J_x(i)J_x(j)+I_{yy}J_y(i)J_y(j)+I_{zz}J_z(i)J_z(j)$. We have defined $I_{\rm iso}=(1/\sqrt{3})(I_{xx}+I_{yy}+I_{zz})$, $I_{\rm axial}=(1/\sqrt{6})(I_{xx}+I_{yy}-2I_{zz})$, and $I_{\rm rhombic}=(1/\sqrt{2})(I_{yy}-I_{xx})$. The histograms show that the two anisotropic components $I_{\rm axial}$ and $I_{\rm rhombic}$ are generally sizable. Note that in the 3-**k** phase the lattice distortion decreases the bond symmetry, so that additional anisotropic exchange parameters are switched on, even if these are most likely small.

responding to the 3-**k** ordering, the free-energy expansion has the form

$$\mathcal{F}=\mathcal{F}_0+a(T-T_c)\psi^2+a_4\psi^4+a_6\psi^6+b_2\eta^2+c_2\psi^2\eta+\cdots, \tag{89}$$

where $a,a_4,a_6,b_2>0$, ψ is the size of the magnetic primary OP (i.e., the modulus of the ordered moment, which is the same on the four sublattices), η is the size of the quadrupolar secondary OP [i.e., the charge distortion $\langle(3\hat{\boldsymbol{\mu}}\cdot\mathbf{J})^2-J(J+1)\rangle$, where $\hat{\boldsymbol{\mu}}$ is the moment direction], and T_c is the critical temperature for a second-order magnetic phase transition ($T_c\sim 25$ K for UO_2; see above). Minimization with respect to η gives

$$\eta=-c_2\psi^2/(2b_2), \tag{90}$$

which replaced in Eq. (89) yields an effective magnetic free energy,

$$\mathcal{F}_{\rm eff}=\mathcal{F}_0+a(T-T_c)\psi^2+\left(a_4-\frac{c_2^2}{4b_2}\right)\psi^4+a_6\psi^6+\cdots. \tag{91}$$

If $c_2^2/4b_2$ is large, the effective fourth-order coefficient may become negative (as in Blume's model) thus leading to a first-order phase transition at $T_1>T_c$ (Toledano and Toledano, 1987). Indeed, explicit MF calculations (Giannozzi and Erdös, 1987) show that large enough quadrupolar interactions lead to a discontinuous transition, even if full quantitative agreement with the experimental behavior was not achieved. For instance, exchange parameters consistent with SW energies lead to a transition temperature $T_1\sim 40$ K, and the size of the moment jump at T_1 is underestimated. It should be remarked that another possible explanation for the first-order character was proposed by Mukamel and Krinsky (1976a, 1976b), without considering quadrupoles. By means of the ϵ-expansion technique, it was shown that the Landau-Ginzburg-Wilson free-energy functional describing the magnetic OP of UO_2 (a six-component vector model) has no stable fixed points, a result that points to a first-order transition.

An important problem encountered in calculations is that the 1-**k** structure is found to be more stable than both the 2-**k** (Solt and Erdös, 1980) and 3-**k** (Giannozzi and Erdös, 1987) ones if quadrupolar interactions are assumed to originate entirely from a ME coupling (as in Sec. II.C.5). However, the model of SE described in Sec. II.C.3 shows that large two-ion EMP interactions of purely electronic origin are to be expected in UO_2. Figure 22 shows that the size of EMP couplings (in particular, $K=4$ hexadecapoles) is typically comparable with that of dipolar interactions. Thus, it is likely that the stabilization of the 3-**k** structure is the result of these SE couplings (Mironov *et al.*, 2003). It should be noted that within the well-isolated Γ_5 CF ground state of UO_2 many multipoles are proportional to one another (Sec. II.E). Nonvanishing odd-rank multipoles are proportional to the three dipoles, whereas nonvanishing even-rank multipoles are proportional to the five quadrupoles. For instance, interactions involving the five Γ_3 and Γ_5 hexadecapoles eventually map onto effective quadrupolar interactions, and interactions involving the six Γ_4 triakontadipoles eventually map onto effective dipolar interactions. Thus, even if multipolar magnetic interactions are sizable in UO_2, a purely nondipolar OP is pre-

vented by the poverty of the Γ_5 CF ground state. As we see in the next section, the situation drastically changes in NpO_2 because of its richer Γ_8 CF ground state.

The SW spectrum provides a further demonstration of the inadequacy of simple Heisenberg-type models for UO_2. Even if they fail to reproduce all observed modes, fit by dipolar models shows that anisotropic two-ion couplings must be present (Giannozzi and Erdös, 1987; Caciuffo *et al.*, 1999; Blackburn *et al.*, 2005). Such couplings originate from the same microscopic mechanism producing multipolar interactions, i.e., SE in the presence of orbital degeneracy. Indeed, the results of our calculations (shown in Fig. 22) demonstrate that the anisotropy of dipolar exchange is expected to be large in UO_2.

Qualitative features of the SW spectrum that do not fit dipolar models are, besides the ACs with phonons mentioned above, the presence of two clearly distinct high-energy branches and the additional excitations reported by Buyers and Holden (1985) in the energy range 9–12 meV. The latter were not put in evidence by Caciuffo *et al.* (1999) because of limited resolution, but their presence has been confirmed in recent measurements (Carretta *et al.*, 2009). These features can be understood within the theory proposed by Allen (1968a, 1968b), based on a 1-**k** magnetic structure. On the contrary, neither the two high-energy branches nor the additional modes can be accounted for on the basis of dipole models for the actual 3-**k** structure. If the magnetic structure is 3-**k**, the magnetic modes (without magnon-phonon interaction) along the Γ-X direction should belong to one acoustical branch and one nearly doubly degenerate optical branch, whose energies match at Γ and X, as expected given the $Pa\bar{3}$ symmetry of the 3-**k** structure.

We have explicitly checked this by means of SW calculations in which all symmetry-allowed exchange parameters in the ordered phase have been included. For example, for nearest-neighbor (NN) U ions, we have considered, in addition to the three parameters describing the anisotropic SE dipole-dipole coupling in $Fm\bar{3}m$ symmetry, the other (weak) additional couplings that might switch on in the distorted $Pa\bar{3}$ phase (where oxygen displacements decrease below C_{2v} the symmetry of the NN bond). Thus, not even the lowest-symmetry dipole-only model can explain the presence of the second optical branch found at 12 meV near Γ and X.

Most likely, the second branch corresponds to quadrupolar excitations, i.e., it represents quadrupolar waves that enter the inelastic neutron scattering cross section through mixed dipole-quadrupole dynamical susceptibilities. The latter are nonzero below T_N, and renormalize the dipole-dipole susceptibility (and the closely related cross section) if two-ion quadrupole-quadrupole couplings are present. However, the inelastic neutron scattering intensity of quadrupolar excitations calculated by assuming phonon-mediated couplings (Giannozzi and Erdös, 1987) did not fit experimental results, since the two quadrupolar branches have intensity much smaller than that of the spin ones (typically by a factor 10^{-2}). Figure 22 shows the importance of SE EMP couplings. Motivated by these results, we performed SW calculations where the form of these couplings is not constrained to that assumed by Giannozzi and Erdös (1987), but we adopted the most general symmetry-allowed expression. We found that there is a wide range of coupling parameters for which a quadrupolar branch with sizable intensity emerges at 12 meV near Γ and X in agreement with the data shown in Fig. 21 (Carretta *et al.*, 2009). Thus, it appears that the quadrupolar SE interactions are needed to understand both the stability of the 3-**k** structure and the associated spin dynamics.

As far as phonon ACs are concerned, these can be investigated by SW calculations based on a model in which vibrational degrees of freedom are explicitly included, as suggested by Dolling and Cowley (1966). The appropriate Hamiltonian is

$$H = \sum_{ij} \mathbf{S}_i \cdot \underline{\underline{\mathbf{J}}}_{ij} \cdot \mathbf{S}_j + H_{\mathrm{CF}}^{3\text{-}\mathbf{k}} + H_{\mathrm{ph}} + \sum_{i,\Gamma,\nu} O_{\Gamma\nu}^2(S_i) Q_{\Gamma\nu}(i), \tag{92}$$

where $\mathbf{S}$ is an $S=1$ pseudospin describing the ground CF triplet, $\underline{\underline{\mathbf{J}}}_{ij}$ are two-ion dipole-dipole couplings, $H_{\mathrm{CF}}^{3\text{-}\mathbf{k}}$ describes the effect of the static lattice distortion occurring below T_N, H_{ph} is the vibrational Hamiltonian (Dolling *et al.*, 1965), and the last term represents the ME coupling of the Γ_3 and Γ_5 quadrupoles (Table I) with modes (Q) of the cubic oxygen cage having the same symmetry. By expressing the latter in terms of lattice phonons and by performing a four-sublattice Holstein-Primakoff approximation, an effective boson Hamiltonian describing the coupled dynamics of spins and phonons is obtained (Carretta *et al.*, 2009). By calculating the inelastic neutron scattering cross section, we find that this model produces a rich spectrum, which accounts very well for the experimentally observed ACs.

To summarize, coupling of quadrupole to phonons plays an important role in both the static properties and low-T dynamics. For instance, below 200–300 K, a single-ion dynamical Jahn-Teller effect reduces the static susceptibility of UO_2 diluted in ThO_2 (Sasaki and Obata, 1970). Evidence of a dynamical counterpart of this high-T effect was found in the residual splitting of the CF states observed by Amoretti *et al.* (1989) and also in the presence of broad dispersive inelastic peaks that are detected between 3 and 10 meV (Amoretti *et al.*, 1999; Caciuffo *et al.*, 1999). Although weak, this signal was easily measurable even at 200 K, more than six times the Néel temperature, and probably reflects the mixing of spin and phonon wave functions which is at the basis of the dynamical Jahn-Teller effect (a similar effect occurs in PrO_2; see below). However, the situation is more complex than for the typical diluted dynamical John-Teller effect systems, and there are no well-established theoretical results with which to compare. The presence of two broad but distinct peaks suggests an image of a 1-**k** distortion in which the oxygen cages undergo the same shift as that assumed to occur statically

below T_N in the 2-**k** model (Faber *et al.*, 1975; Faber and Lander, 1976). Indeed, this distortion splits the ground Γ_5 triplet into three singlets (Amoretti *et al.*, 1989). Here, however, we are in the paramagnetic phase and the molecular field is zero, so that the distortion has to be a dynamical one. The excitations experimentally display dispersion, with their energy a minimum at the magnetic zone center. A possible interpretation of this effect is that the magnetic SE between the U ions introduces a wave-vector dependence of the peak position. The dispersion of these excitations has been calculated from the poles of the dynamical susceptibility in the random phase approximation (RPA), assuming the distortion to be static, and found to be consistent with observations (Amoretti *et al.*, 1999; Caciuffo *et al.*, 1999). The results of these calculations suggest a picture in which uncorrelated 1-**k** dynamical JT distortions occur above T_N along the three directions of the ⟨100⟩ star; at T_N a correlation builds up between their phases leading to the static 3-**k** distortion. New high-energy inelastic neutron scattering experiments above T_N would be interesting to examine the detailed form of the transitions from the ground triplet to the excited CF multiplets, taking advantage of the improved intensity and resolution available at spallation sources. The presence of sizable magnetovibrational effects in the paramagnetic phase is also most likely at the origin of the anomalously small variation of the entropy between $T=0$ and T_N (Osborne and Westrum, 1953), which is less than the expected $k_B \ln 3$ per U ion. In order to recover the missing entropy, temperatures of the order of 80 K are needed, which matches the energy scale of the observed high-T broad inelastic peaks.

B. Neptunium dioxide

NpO_2 is an apparently simple tetravalent oxide isostructural to UO_2. The anomalies at $T_0=25$ K in the heat capacity (Osborne and Westrum, 1953) and magnetic susceptibility (Ross and Lam, 1967; Erdös *et al.*, 1980; Friedt *et al.*, 1985) curves were initially interpreted as a consequence of magnetic ordering, as in UO_2. This was the most obvious assumption, as Np^{4+} ions with three electrons in the 5*f* shell are Kramers ions in which the CF ground state must be at least a magnetic doublet. Neutron diffraction experiments, however, failed to find any evidence of magnetic ordering (Cox and Frazer, 1967; Heaton *et al.*, 1967; Boeuf *et al.*, 1983). A search for a departure from cubic symmetry, or for internal JT distortions of the oxygen sublattice, was also made with a null result (Caciuffo *et al.*, 1987; Mannix *et al.*, 1999; Paixao *et al.*, 2002). Mössbauer spectroscopy failed to detect magnetic order as only a small and sample-dependent broadening of the ^{237}Np absorption line develops below T_0 (Dunlap *et al.*, 1968; Friedt *et al.*, 1985). Considering that Mössbauer spectroscopy is an extremely reliable and sensitive technique for probing magnetic moments on Np ions, no matter what the magnetic structure is, these results definitely ruled out conventional magnetic order: the analysis of Mössbauer

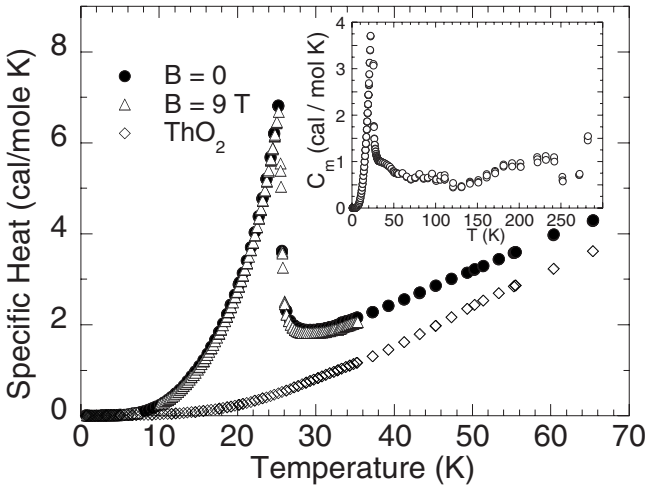

FIG. 23. Temperature dependence of the NpO_2 specific heat in zero magnetic field (circles) and in a magnetic field of 9 T (triangles). The specific heat of ThO_2 is shown by diamonds. Inset: The magnetic contribution to the NpO_2 specific heat obtained by taking the difference between the NpO_2 and the ThO_2 curves. Data from Magnani, Santini, Amoretti, Caciuffo, *et al.*, 2005.

spectra taken in a magnetic field is not in agreement with what is expected from an antiferromagnet (Friedt *et al.*, 1985); in addition, the small upper limit of the ordered moment ($\sim 0.01\mu_B$) which is found if the broadening is attributed to magnetic order is impossible to reconcile with the large value of T_0 and of the paramagnetic moment ($\sim 3\mu_B$) observed above T_0, and with the large size of the macroscopic anomalies.

Since a dipolar OP is to be excluded, the possibility of an EMP OP has been considered (Erdös *et al.*, 1980; Solt and Erdös, 1980; Friedt *et al.*, 1985; Amoretti *et al.*, 1992). For instance, Solt and Erdös (1980), in analogy to the UO_2 case, assumed a collective JT monoclinic distortion of the oxygen sublattice driven by quadrupolar interactions. As a consequence of this distortion, the Np^{4+} quadrupoles order in an antiferroquadrupolar configuration and the Γ_8 ground quartet would split into two Kramers doublets. However, as stated above, no evidence of this static distortion has been found. In addition, any primary time-even OP encounters two fundamental problems: the first one is that the magnetic susceptibility should diverge as $T\rightarrow 0$. Indeed, the Np ion is tetravalent, as confirmed by the isomer shift in Mössbauer spectra (Dunlap and Kalvius, 1985) and the magnetic form factor measured by neutron diffraction (Delapalme *et al.*, 1980). Thus, the ground state of Np ions in the low-T phase should be a Kramers doublet with an associated Curie-Weiss behavior as $T\rightarrow 0$. However, the measured susceptibility (Erdös *et al.*, 1980) saturates to a constant value (8.4×10^{-3} emu/mol at 5 K). The other problem with such an OP is that a second phase transition removing the Kramers degeneracy and the associated entropy should occur below T_0, but no evidence of a second transition exists (Fig. 23). It should also be possible to remove this residual entropy

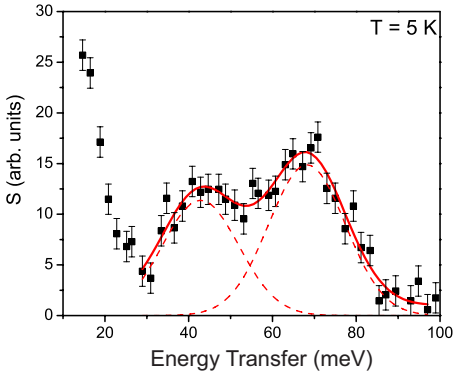

FIG. 24. (Color online) Magnetic inelastic neutron scattering cross section obtained for NpO_2 at $T=5$ K (Fournier *et al.*, 1991). The incident energy was 180 meV and the average scattering angle was $\phi=5°$. The solid line is a fit to the data of two Gaussian peaks (dashed lines) and a background.

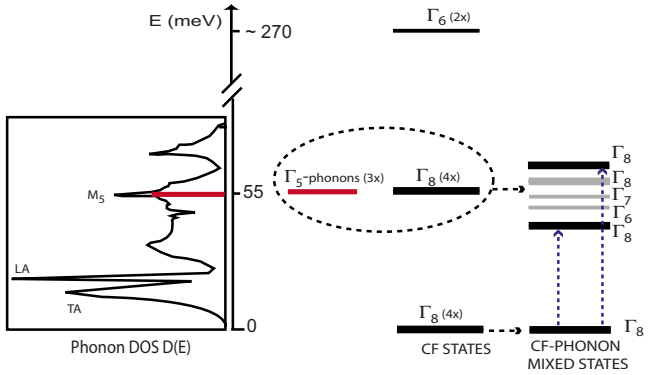

FIG. 25. (Color online) The energy spectrum of NpO_2 in the paramagnetic phase. Left: Phonon density of states of UO_2 (Dolling *et al.*, 1965), showing the presence of the M_5 optical bands near 55 meV. Center: Bare CF energy levels of NpO_2. Right: Structure of the mixed CF-phonon states resulting from the model of Eq. (93).

by applying a magnetic field, but measurements of the field dependence on the heat capacity (Fig. 23) show no evidence of such an effect (Magnani, Santini, Amoretti, Caciuffo, *et al.*, 2005; Di Matteo *et al.*, 2007). An even more fundamental problem with a time-even OP is the μSR results by Kopmann *et al.* (1998), which showed the sudden appearance of a precessing signal below T_0, corresponding to a local magnetic field at the muon site of about 500 G (Fig. 7). The presence of this field implies that time-reversal symmetry is broken below T_0 (Sec. III.A).

As in the case of UO_2, the determination of the CF potential is a crucial step for building a theoretical model. The free Np^{4+} ion with $5f^3$ configuration has $^4I_{9/2}$ ground state in the *LS* coupling scheme. In the paramagnetic phase, the tenfold degeneracy of this lowest manifold is lifted by the cubic CF potential (20) into a Γ_6 doublet and two quartets, $\Gamma_8^{(2)}$ and $\Gamma_8^{(1)}$. A series of experiments was performed to detect the CF transitions between these multiplets and to search for a possible splitting of the ground quartet below T_0 (Caciuffo *et al.*, 1991; Fournier *et al.*, 1991; Amoretti *et al.*, 1992). The situation is quite different from that of UO_2, where sharp CF states have been seen. In NpO_2, the CF excitation $\Gamma_8^{(2)} \rightarrow \Gamma_8^{(1)}$ between the ground and the first excited quartet results in a wide band with intensity in the region from 30 to 80 meV (Fig. 24). The second excitation $\Gamma_8^{(2)} \rightarrow \Gamma_6$ has too small a matrix element to be visible by inelastic neutron scattering, and in fact no other peaks were detected up to energy transfers of 350 meV.

The broadening of the $\Gamma_8^{(2)} \rightarrow \Gamma_8^{(1)}$ transition might be caused by several mechanisms. However, it is important to note that only in NpO_2, among the light actinide dioxides, does the most intense CF transition lie below the phonon cutoff of ~80 meV. In addition, a peak in the phonon density of states exists at ~55 meV (see Fig. 25), corresponding to the so-called M_5 optical modes (Dolling *et al.*, 1965), which are known to strongly couple with Γ_5 electric quadrupoles of the actinide ion. In fact, the lattice distortion induced by the quadrupole order of UO_2 corresponds to a freezing of the three M_5 modes. Since Γ_5 electric quadrupoles have a sizable matrix element between the two Γ_8 quartets (Fournier *et al.*, 1991), CF-phonon bound states may form as in the case of $CeAl_2$ (Thalmeier and Fulde, 1982; Thalmeier, 1984). The underlying physics is qualitatively captured by simple cluster models in which the active optical band is replaced by a triplet of Einstein-like local oscillators belonging to the Γ_5^+ irrep of O_h, i.e., having the same symmetry properties as the M_5 phonons at the Γ point. The corresponding Hamiltonian is (Fulde and Löwenhaupt, 1986; Santini and Amoretti, 2002)

$$H = H_{\mathrm{CF}} + \hbar\omega \sum_{\nu=1,3} (a_\nu^\dagger a_\nu + 1/2) + g \sum_{\nu=1,3} O^2_{\Gamma_5\nu}(J)(a_\nu^\dagger + a_\nu), \tag{93}$$

where the second term describes the three oscillators with $\hbar\omega \simeq 55$ meV, g is a ME coupling parameter, and $O^2_{\Gamma_5\nu}(J)$ are the Γ_5 quadrupole operators defined in Eq. (14). Figure 25 shows the resulting spectrum. Only two excited magnetovibrational Γ_8 quartets, separated by an energy increasing with g, provide a sizable contribution to the low-T inelastic neutron scattering cross section.

For the bare CF Hamiltonian, two possible choices for the cubic CF parameters were proposed ["weak" and "strong" CF solutions; if J mixing is neglected, the former corresponds to $x \sim -0.74$ and the latter to $x \sim -0.48$, Eq. (19)], both reproducing consistently the CF spectrum of UO_2 and NpO_2 (Amoretti *et al.*, 1992). The strong CF solution, corresponding to $A_4 \sim -19$ meV$/a_0^4$ and $A_6 \sim 0.65$ meV$/a_0^6$, scales more consistently across the whole dioxide series (Magnani, Santini, Amoretti, and Caciuffo, 2005).

Another important result of inelastic neutron scattering studies with polarization analysis is the proof that the ground Γ_8 quartet splits in the ordered phase below T_0 (Amoretti *et al.*, 1992). In fact, a single broad peak,

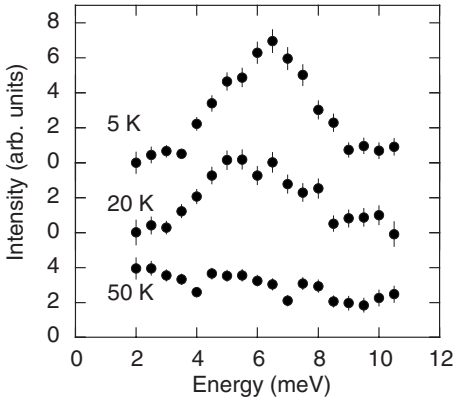

FIG. 26. Evolution of the inelastic neutron scattering intensity from NpO_2 as the temperature is increased through the phase transition point T_0=25 K. Data are collected with uniaxial polarization analysis in the spin-flip channel, with initial polarization parallel to the momentum transfer **Q**. With this configuration, the signal is entirely magnetic and indicates a splitting of the ground-state quartet below T_0. Data from Amoretti *et al.*, 1992.

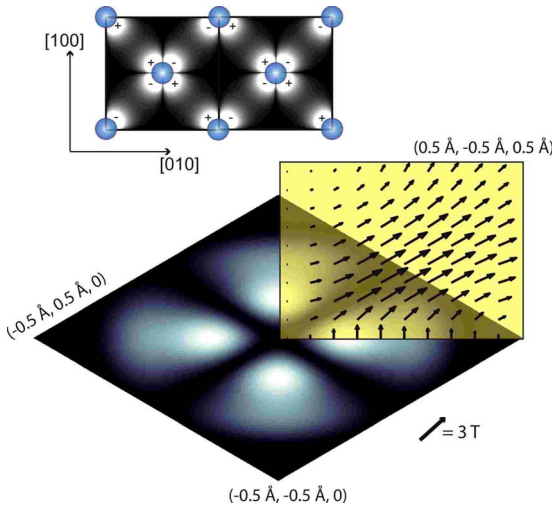

FIG. 27. (Color online) Intensity plot of the magnetic field produced by the Γ_2 OP of NpO_2 at T=0 (Santini and Amoretti, 2000), assuming uniform ordering within the (0 0 1) plane. The field is along [0 0 1] with the sign indicated. A zoom on a single ion is shown in the lower part. Arrows indicate the magnetic field within a (1 1 0) plane.

centered at 6.4 meV for T=5 K, was observed on a powder sample in the energy window between 3 and 11 meV (see Figs. 26 and 37). This was the first microscopic evidence on this phase transition, and was initially interpreted in terms of quadrupolar order. Since such an order would produce a splitting of the Γ_8 quartet into a pair of doublets, a single peak corresponding to this splitting should appear in the inelastic neutron scattering cross section below T_0. A calculation made by assuming an internal monoclinic distortion as proposed by Erdös *et al.* (1980) showed that the splitting of the ground Γ_8 quartet is of the correct order of magnitude, particularly in the case of the weak CF solution. Even if this model also leads to a nearly zero value of one of the three components of the magnetic moment, the two remaining components remain nonzero. So, the problem of the nondiverging susceptibility for $T\rightarrow 0$ remained open (see above) and it was not possible to provide a unified picture giving a convincing explanation of the nature of the phase transition.

A saturating susceptibility in the lack of dipole order points to a MMP OP (Santini *et al.*, 1999). Such an OP is also needed to understand the breaking of time-reversal symmetry evidenced by μSR experiments. Quadrupolar magnetic moments being excluded (Sec. II.A), magnetic octupole moments were considered as the most likely candidates (Santini and Amoretti, 2000, 2002). Only components of the magnetic octupole not belonging to the same representation as the dipole can be considered, otherwise the latter would be induced as secondary OPs. In O_h symmetry, this constraint selects four out of the seven octupolar components, belonging either to the three-dimensional Γ_5 representation or to the one-dimensional Γ_2 representation. The OP was initially assumed to be the Γ_2 octupole T_{xyz} (Table I).

The corresponding MF model has T_h symmetry and leads to a splitting of the Γ_8 CF ground state into a pair of doublets, as suggested by inelastic neutron scattering in the limited energy range up to ~11 meV. Within the weak CF solution (see above), the ground doublet has a nearly vanishing dipole moment, yielding a saturating susceptibility at low T, but the octupole moment generates an interstitial field consistently with μSR results (Fig. 27). In addition, the splitting into a pair of doublets appeared consistent with the small amount of entropy removed by the phase transition, even if subsequent measurements (Fig. 23) showed that the ground state has to be a singlet. Indeed, no residual entropy is left below T_0, so that the mechanism behind the missing entropy has probably the same ME origin as in UO_2. Another advantage of the Γ_2 model was the fact that an order of Γ_2 octupoles would not directly lead to charge ordering (neither quadrupolar nor of higher rank) and would not induce a distortion by a direct ME mechanism. On the other hand, an order of Γ_5 octupoles always induces an order of Γ_3 or Γ_5 quadrupoles, whose ME coupling to the lattice generally leads to a crystal distortion, with the unique exception of the complex 3-**k** arrangement.[6] The latter choice was shown to be correct when Paixao *et al.* (2002) provided direct evidence of AF order of the Np

[6]Magnetostriction might lead to a lattice distortion even with a Γ_2 OP, if the ordering is AF. The simple ferromagnetic ordering of Γ_2 octupoles lowers the space group to $Fm3$, with T_h point symmetry at the Np sites and no associated distortions of the lattice. For example, in the case of 1-**k**, type-I antiferro-octupolar order, the symmetry lowers to the tetragonal $P4_2/mnm$ group for which a uniform strain along the wave-vector direction is not forbidden by symmetry. However, this distortion should be driven by magnetostriction, i.e., a dependence of two-ion SE couplings on distance, and would presumably be smaller than the distortions typically associated with ME couplings (e.g., distortions in UO_2).

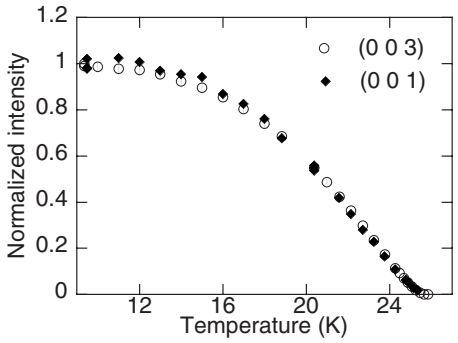

FIG. 28. Temperature dependence of the normalized intensity of the (0 0 1) and (0 0 3) superlattice reflections observed at the M_4 edge (3.845 keV) in NpO_2. Data from Mannix *et al.*, 1999.

quadrupoles by a series of RXS experiments at the actinide $M_{4,5}$ absorption edges. Resonant superlattice reflections with propagation vector (0, 0, 1), forbidden by symmetry at all order in $Fm\bar{3}m$, have been observed below T_0 (Mannix *et al.*, 1999). Their temperature dependence (Fig. 28) suggests the occurrence of a continuous (second-order) phase transition, in contrast to UO_2, where the transition is strongly first order. The large value of the β critical exponent (about 0.6) is consistent with the quadrupole OP being a secondary one.

No diffraction peaks corresponding to a deformation of the oxygen cube have been found in NpO_2, with an upper limit for the oxygen displacement of about 4×10^{-4} Å. Homogeneous internal distortions, corresponding to normal modes of the oxygen cage and producing only changes in the intensities of fluorite-structure peaks, are excluded by neutron diffraction (Caciuffo *et al.*, 1987). A search for a departure from cubic symmetry, an external distortion, was also made with null result by following the angular position and width of the (0 0 6) lattice reflection (Mannix *et al.*, 1999).

The results of azimuth scans around the (0, 0, 3) scattering vector are reported in Fig. 29 for both σ-π and σ-σ polarization. The intensity of the peak is measured

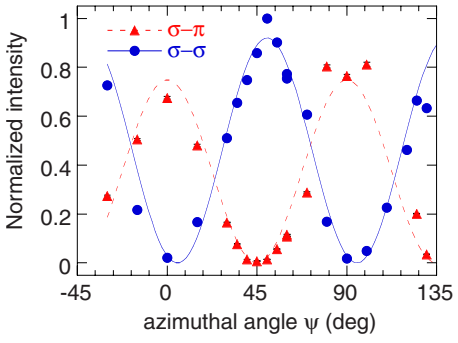

FIG. 29. (Color online) Azimuth angle dependence of the (0 0 3) intensity, at $T=12$ K, with π and σ final polarization and specular reflection geometry. Lines are calculations based on Eq. (76) for a longitudinal 3-**k** structure of Γ_5 quadrupoles. Data from Paixao *et al.*, 2002.

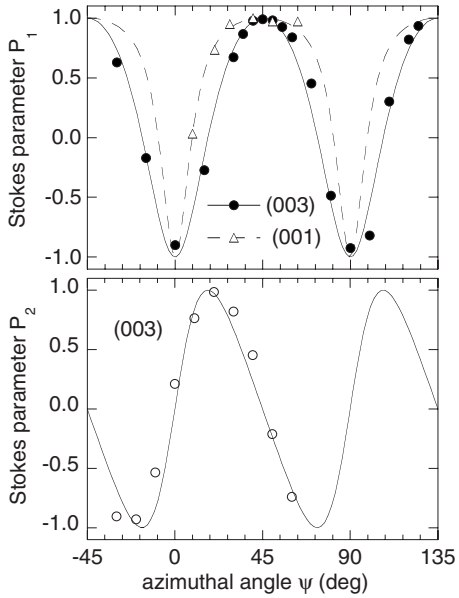

FIG. 30. Azimuth angle dependence of the Stokes parameters P_1 (upper panel) and P_2 (lower panel) of NpO_2 superlattice reflections measured at 10 K with $E=3.846$ keV. Lines are calculations for a longitudinal 3-**k** structure of Γ_5 quadrupoles. $P_1=(I_{\sigma\sigma}-I_{\sigma\pi})/(I_{\sigma\sigma}+I_{\sigma\pi})$; P_2 is defined by the intensities measured with the analyzer oriented at $\pm\pi/4$ with respect to the scattering plane, and is determined by the phase relation between the two polarization channels. From Paixao *et al.*, 2002.

while the sample is rotated around the scattering vector **Q**, kept constant at the chosen value. The origin of the azimuth angle Ψ is chosen so that at $\Psi=0$ the [1 0 0] axis is parallel to the incident beam. The presence of scattering intensity in both polarization channels, depending on Ψ, is in direct contradiction with the cross section of $E1$-$E1$ magnetic resonant scattering [i.e., the signal associated with the $F^{(1)}$ tensor in Eqs. (66) and (68)] and indicates the presence of electric quadrupole order [$F^{(2)}$ tensor in Eqs. (66) and (70)]. The absence of lattice distortions associated with the phase transition requires a 3-**k** quadrupolar structure. Moreover, as discussed in Sec. III.B.3, the 3-**k** order must be of the longitudinal type, since a signal is observed in the σ-σ channel for a specular reflection. This is confirmed by the azimuth angle dependence of the scattered intensity, which is in good agreement with the expected behavior for Γ_5 quadrupoles, that is, $I_{\sigma\sigma} \propto \sin^2 2\Psi$ and $I_{\sigma\pi} \propto \sin^2 \theta_B \cos^2 2\Psi$ for the σ-σ and σ-π channels, respectively.

The absence of a magnetic-dipole contribution to the σ-π intensity (that is, the absence of dipole magnetic order) is confirmed by the fact that only one scale factor is required to fit the experimental results for both polarization channels. This scale factor cancels in the definition of the Stokes parameters P_1 and P_2, and Fig. 30 shows excellent agreement between model predictions and experimental data for the (0 0 1) and (0 0 3) Bragg peaks (Paixao *et al.*, 2002).

The ordered structure is obtained by associating to each of the four Np sublattices an appropriate linear

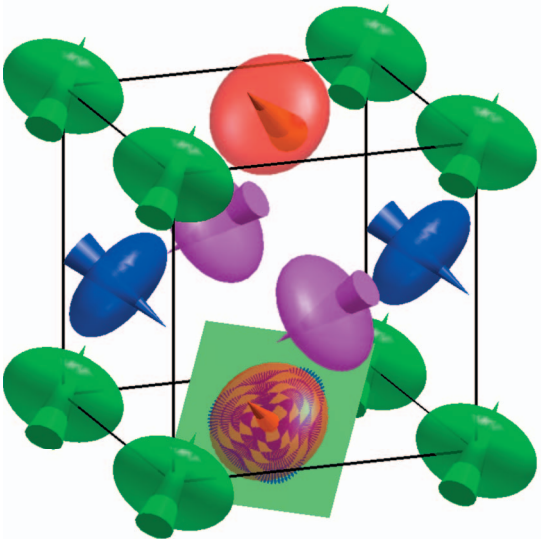

FIG. 31. (Color) Arrangement of the Γ_5 MMPs (cones) and induced Γ_5 quadrupoles (ellipsoids) in the four-sublattice 3-**k** ground state of NpO_2. The slice displays the direction of the local magnetic field around one of the Np ions. The cones are along the local D_{3d} axes, and the direction where they point illustrates the sign of the local multipole moment.

combination of the three quadrupole moments $\langle O_{ij}\rangle$ (R_1: $\langle O_{yz}\rangle+\langle O_{zx}\rangle+\langle O_{xy}\rangle$, R_2: $-\langle O_{yz}\rangle-\langle O_{zx}\rangle+\langle O_{xy}\rangle$ R_3: $-\langle O_{yz}\rangle+\langle O_{zx}\rangle-\langle O_{xy}\rangle$ R_4: $\langle O_{yz}\rangle-\langle O_{zx}\rangle-\langle O_{xy}\rangle$ (see Fig. 31). The quadrupole ordering reduces the local symmetry of Np^{4+} ions to $\bar{3}m$ (D_{3d}), while the space group is lowered to $Pn\bar{3}m$, the only maximal nonisomorphic subgroup of $Fm\bar{3}m$ that is nonsymmorphic and simple cubic. Np ions occupy the 4*b* sites, whereas oxygens are accommodated into two inequivalent Wyckoff positions, 2*a* and 6*d*, where all coordinates are fixed by symmetry. As a consequence, the electronic phase transition does not allow a shift of the oxygen ions. The symmetry of the ordered state remains cubic and, apart from a possible change of the lattice parameter (Mannix *et al.*, 1999), the transition is not accompanied by any distortion.

As stated above, the quadrupolar order alone cannot explain the saturating susceptibility and the breaking of invariance under time reversal. The quadrupolar order detected by RXS has to be a secondary OP, and selects Γ_5 MMPs as primary OP. For type-I ordering these ionic MMPs induce two possible small irreps of the wave-vector group, $\Gamma_4^{(+)}$ (one dimensional) or $\Gamma_5^{(+)}$ (two dimensional). The former describes a symmetry lowering to the cubic group $Pn\bar{3}m$ for 3-**k** ordering and induces the observed ordering of quadrupoles as secondary OP. Indeed, the Landau free energy of the $\Gamma_4^{(+)}$ MMP OP has the form given in Eq. (54) apart from the third-order contribution which violates time-reversal invariance and is therefore absent. Yet a mixed third-order term of the form $a_3\psi_{\mathbf{k}_1}\psi_{\mathbf{k}_2}\eta_{\mathbf{k}_3}$+(cyclic permutations) exists, where ψ are the three components of the primary OP and η are the three components of the secondary OP ($\psi_{\mathbf{k}_1}=\psi_{\mathbf{k}_2}=\psi_{\mathbf{k}_3}\equiv\psi$ for 3-**k** ordering). This leads to a secondary OP $\eta_{\mathbf{k}_1}=\eta_{\mathbf{k}_2}=\eta_{\mathbf{k}_3}\equiv\eta\propto\psi^2$, which corresponds to 3-**k** ordering of Γ_5 quadrupoles. Its critical exponent is therefore twice that of the primary OP, which is consistent with the observed large value of β.

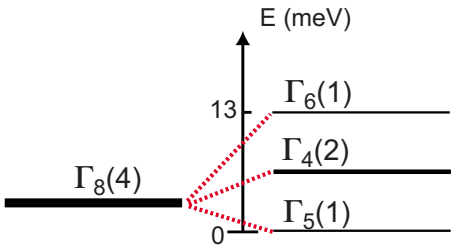

FIG. 32. (Color online) MF splitting of the ground Γ_8 quartet in the ordered phase resulting from Eq. (94) with the "strong" set of CF parameters and rank-5 MMPs. Numbers in parentheses are degeneracies.

The previous results fix the symmetry of the OP but not its specific form and the resulting structure of the low-energy wave functions and excitations in the ordered phase. In particular, in cubic symmetry there are four distinct, independent triplets of MMPs belonging to Γ_5, one of which may be constructed from rank-3 MMPs (octupoles), one from rank-5 MMPs (triakontadipoles), and two from rank-7 MMPs. As we show in the following, the existing information on NpO_2 provides strong evidence that rank-5 MMPs are the driving force of the phase transition (Santini *et al.*, 2006). In the 3-**k** ordered phase, there are four inequivalent sublattices (see Fig. 31). The simplest model for the ordering is one in which the CF Hamiltonian (20) is supplemented with the MF contribution (neglecting a *T*-dependent energy shift),

$$H_{\mathrm{MF}}(s)=H_{\mathrm{CF}}+\lambda T(s)\langle T(s)\rangle, \tag{94}$$

where $s=1,\ldots,4$ labels the four sublattices, λ is the MF constant, and $T(s)=\Sigma_{l=x,y,z}T_l n_l(s)$; $\mathbf{n}(s)$ represents one of the four inequivalent $\langle 111\rangle$ directions, and T_l ($l=1,2,3$) are the components of the Γ_5 MMP. In the ordered phase $\langle T(s)\rangle\neq 0$ and the point symmetry on Np ions lowers from O_h to D_{3d}, consistently with the properties of the $Pn\bar{3}m$ group. A local magnetization density appears around each Np ion, carrying no overall net ionic dipole moment. In addition, a distortion of the charge density, corresponding to the secondary quadrupolar OP $O\equiv\langle O(s)\rangle\propto\langle 3[\mathbf{n}(s)\cdot\boldsymbol{J}]^2-J(J+1)\rangle$, is induced (Fig. 31), with $O\propto\langle T(s)\rangle^2$ close to T_0.[7] The MF of Eq. (94) produces a splitting of the Γ_8 quartets into a Γ_4 doublet and a pair of time-reversal-related singlets Γ_5 and Γ_6 (Fig. 32). The Γ_5 and Γ_6 irreps of the D_{3d} double group are degenerate in

[7] $H_{\mathrm{MF}}(s)$ should be supplemented with the MF contribution from the secondary OP itself, $\lambda_Q O(s)\langle O(s)\rangle$, with λ_Q the MF constant for quadrupolar interactions. Even if the latter do not play a qualitative role, they may affect quantitative details such as the growth rate of the OPs or the excitation energies below T_0.

the presence of time-reversal invariance, but their degeneracy is removed when time reversal symmetry is broken.

In order to model the observed behavior, a choice for the T_l must be made. All rank-3 ($T_l^{(3)}$), rank-5 ($T_l^{(5)}$), and rank-7 ($T_l^{(7,a)}$, $T_l^{(7,b)}$) MMPs have nonzero average values below T_0, and all might provide distinct contributions to $H_{\mathrm{MF}}(s)$, including cross terms. Within the Γ_8-quartet CF ground state, these four triplets of observables are represented by matrices proportional to one another. Thus, if the Γ_8 quartet was completely isolated, the phase transition could be modeled with no need to distinguish these Γ_5 MMPs. However, the presence of excited CF levels at ~50 meV makes them inequivalent. The simplest possible choice for the OP is to identify T_l with the octupoles $T_l^{(3)}$. However, while this choice for T_l is as good as any other within a model including the ground CF quartet only, it does not work properly if all CF states are included. In fact, the CF ground quartet has tiny octupolar polarizability (see below), a fact that greatly enhances the role of excited CF states in the ordering process: for CF parameters with $x \simeq -0.48$ (strong CF solution), the order occurs through a strongly first-order phase transition. Even assuming parameters with $x \simeq -0.74$ (weak CF solution), which are unlikely for their lack of overall scaling properties (Magnani, Santini, Amoretti, and Caciuffo, 2005), does not solve the problem: a second-order transition occurs, but the Γ_4 doublet (Fig. 32) lies well below 3 meV, which is inconsistent with specific heat results (Magnani, Santini, Amoretti, Caciuffo, *et al.*, 2005). Moreover, the large mixing of the ground Γ_8-quartet wave functions with excited CF states below T_0 leads to a nonmonotonic T dependence of the secondary quadrupolar OP (Santini *et al.*, 2006), in disagreement with RXS results. Thus, the driving Γ_5 MMP cannot be an octupole. Such a result is not surprising in light of our calculations reported in Sec. II.C.3, which show that the strength of multipolar two-ion SE interactions is not correlated in an obvious way with the multipole rank, so that the contributions of rank-5 and rank-7 Γ_5 MMP in the MF Hamiltonian are not in general smaller than that of octupoles (rank 3). In particular, Fig. 2 shows that in NpO_2 the leading multipolar interactions are between rank-5 MMPs. The importance of multipolar interactions involving Γ_5 MMPs in NpO_2 has also been demonstrated by Kubo and Hotta (2005b) on the basis of a *j-j* model restricted to the Γ_8 single-particle states (Sec. II.D).

Besides being expected to be the largest, rank-5 MMPs are also favored by the CF. In fact, in addition to the strength of two-ion couplings [determining λ in Eq. (94)], a key factor in selecting which of the Γ_5 MMPs plays a driving role is the CF potential, because this dominant interaction strongly affects the size of the corresponding multipolar moments at low T. This effect can be quantified by comparing the effective multipolar paramagnetic moment μ_{CF} associated with the ground Γ_8 quartet with the corresponding free-ion moment μ_0. In fact, for a given value of λ, the MF transition temperature $T_0 \propto \mu_{\mathrm{CF}}^2$ (neglecting the contribution of excited CF states to the multipolar polarizability). Figure 33 shows the ratio $r = \mu_{\mathrm{CF}}^2/\mu_0^2$ as a function of the CF parameter x. This quantity measures how much the multipolar susceptibility of the Γ_8 quartet is reduced ($r<1$) or increased ($r>1$) by the CF, and it is the factor by which the ordering temperature is changed in passing from the full degenerate $J=9/2$ multiplet to the Γ_8 CF ground state. The figure shows that the octupolar moment is greatly reduced by the CF, and nearly completely quenched for $x \simeq -0.48$. On the contrary, the rank-5 moment is increased by the CF and peaks at $x=-0.5$, whereas the dipole moment is reduced for all values of x. The two rank-7 moments are heavily reduced too (Santini *et al.*, 2006). Thus, for $x \simeq -0.48$ the rank-5 MMP is the most likely driving OP, and the MF model Eq. (94) with T_l identified with $T_l^{(5)}$ is the most reasonable approximation. Indeed, if $T_l^{(5)}$ are used as OP, the role of excited CF states is much smaller and the resulting growth of the quadrupolar OP is monotonic as in experiments.

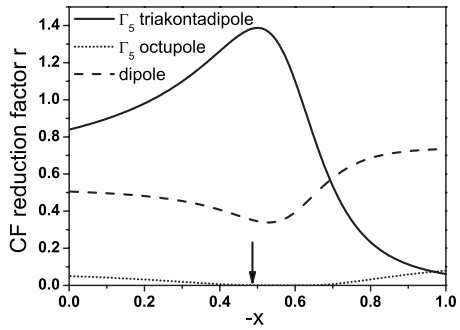

FIG. 33. CF reduction factor for the Γ_8 ground quartet, $r = \mu_{\mathrm{CF}}^2/\mu_0^2$, as a function of the CF parameter x ($W<0$). The arrow indicates the most likely value of x. We have neglected J mixing here since the associated small correction to the Γ_8 wave functions does not affect the conclusions. Then, these wave functions depend on the x CF parameter only. From Santini *et al.*, 2006.

The ordering of triakontadipoles produces around each Np ion a magnetic field $\mathbf{H}(\mathbf{r})$ with a peculiar $\mathbf{r}$ dependence, reflecting the local D_{3d} symmetry of the OP. For instance, Figs. 34 and 31 show the field produced by the ordered rank-5 MMPs of one Np ion in two representative planes. The field has been calculated with Eq. (83) and is of the order of a few tesla at distances between 0.5 and 1 Å. As expected from the quenching of the rank-3 MMPs discussed above (Fig. 33), the octupolar contribution to the interstitial field is much smaller; see Fig. 35. The field $\mathbf{H}(\mathbf{r})$ is the one inducing the precession signal seen in μSR (Fig. 7). Yet the spatial structure of the field cannot be extracted from μSR. Conversely, as discussed in Sec. III.D, single-crystal neutron diffraction has the potential to directly probe this structure. Indeed, $\mathbf{H}(\mathbf{r})$ is probably large enough to be detectable by polarized neutron diffraction. Unfortunately, the available single crystals are less than 1 mm^3 and are too small for this experiment.

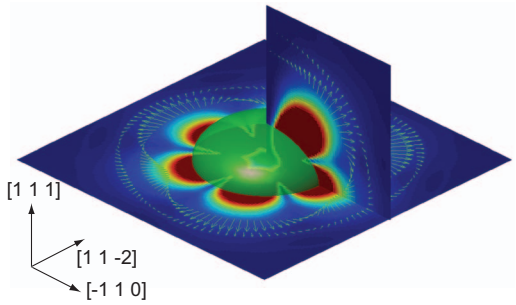

FIG. 34. (Color) Intensity plot illustrating the magnetic field produced by the rank-5 component of the OP of NpO_2 at $T=0$ in two representative planes. The darkest area corresponds to a field intensity larger than 5 T. The Np ion at the center belongs to the sublattice characterized by a MMP moment having [1 1 1] as C_3 axis and its charge distribution has a quadrupole moment (illustrated by the central ellipsoid). Arrows show the field calculated at distances of 1 and 1.2 Å from the Np nucleus. The maximum intensity of the field at 1 Å is close to 1.2 T.

Additional indirect evidence for the existence of a longitudinal 3-**k** multipole order in NpO_2 has been given by NMR measurements on ^{17}O enriched samples (Tokunaga *et al.*, 2005a; Tokunaga, Aoki, Homma, *et al.*, 2006). In the paramagnetic phase, the spectrum consists of only one line, narrow and symmetric. Below T_0, the splitting of the resonance confirms the presence of two inequivalent oxygen sites. In the ordered phase, the field-sweep spectrum collected at a resonance frequency of 59.2 MHz on a powder sample is the sum of two powder-pattern line shapes (Tokunaga *et al.*, 2005a). The one at higher field is isotropic and corresponds to an oxygen site $O^{(1)}$ with cubic symmetry; the other is composed of a main peak and a shoulder, and stems from an oxygen site $O^{(3)}$ with tetragonal symmetry. This observation is consistent with the symmetry lowering from $Fm\bar{3}m$ to $Pn\bar{3}m$ suggested by RXS experiments ($O^{(1)}$ and $O^{(3)}$ are located on the 2*a* and 6*d* sites of $Pn\bar{3}m$, respectively). Indeed, the inequivalent oxygen sites do not appear in the transverse 3-**k** ordered structure of UO_2, with $Pa\bar{3}$ space group (Ikushima *et al.*, 2001). The HF interaction observed below T_0 has opposite sign for the $O^{(1)}$ and $O^{(3)}$ sites, and for both oxygen sites is proportional to the magnitude of the applied magnetic field. Its origin is related to the presence of field-induced dipole and multipole magnetic moments on the Np sites, in presence of an underlying 3-**k** AF-type order of the electric quadrupoles (Sakai *et al.*, 2003, 2005; Tokunaga *et al.*, 2005a). In this case, in agreement with the experimental results, the classical dipolar field produced on oxygen sites by the AF moments on Np sites is along the applied field for the $O^{(1)}$, and along the symmetry axes for the $O^{(3)}$ sites.

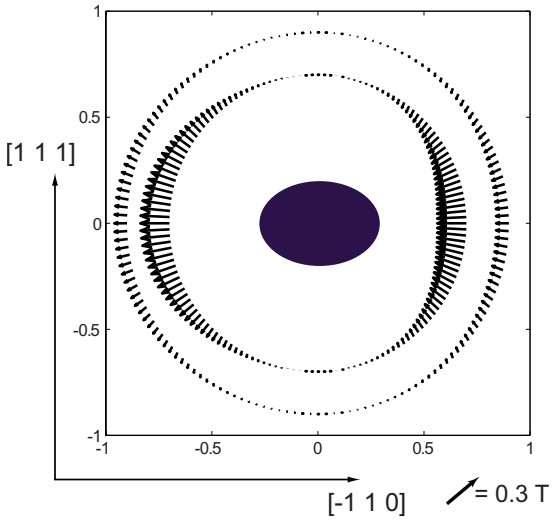

FIG. 35. (Color online) Arrows indicate the magnetic field produced by the rank-3 component of the OP of NpO_2 at $T=0$. As in Fig. 34, the Np ion at the center belongs to the sublattice characterized by a MMP moment having [1 1 1] as C_3 axis and the field has been calculated at distances of 0.7 and 0.9 Å from the Np nucleus. The field direction in the plane perpendicular to [1 1 1] closely resembles that of Fig. 34 and is not shown.

Field-angle-resolved ^{17}O-NMR results on a single crystal of NpO_2 allow one to address the multiple hyperfine field components individually, and provide a further confirmation of the electric AFQ order through the observation of an oscillatory spin-echo behavior (Tokunaga, Aoki, Homma, *et al.*, 2006). Fast-Fourier-transform spectra have been measured below T_0 in a field of 10.7 T for a different direction of the magnetic field **H**, which was rotated in the $(1\bar{1}0)$ plane. For a generic orientation of **H**, the spectra show three peaks. One appears at an angle-independent frequency and is associated with the $O^{(1)}$ site, the two others shift in frequency as **H** is rotated and are superposed with $\mathbf{H}\|[111]$. These peaks are associated with the $O^{(3)}$ sites, which having local symmetry axes along the edges of the unit cell become inequivalent in a magnetic field [$O^{(3)}_{x,y,z}$, with $O^{(3)}_x$ and $O^{(3)}_y$ always equivalent with **H** in the $(1\bar{1}0)$ plane]. The angular dependence of the NMR line shift, $\Delta f=f_{\rm res}-f_0$, for the three peaks is shown in Fig. 36. It can be reproduced assuming the proposed longitudinal 3-**k** Γ_5 MMP primary OP, from field-induced magnetic-dipole and octupole moments arising from the secondary AFQ order. Direct contributions from Np MMPs in zero field are not accessible, as they vanish by symmetry at the oxygen sites (Sakai *et al.*, 2005).

Electric quadrupole order effects can be observed by measuring the integrated spin-echo intensity $M(\tau)$ as a function of the time τ between the excitation pulse and the refocusing pulse. At the cubic site $O^{(1)}$, $M(\tau)$ shows a Gaussian decay whereas it has an oscillatory behavior at the $O^{(3)}$ sites. The primary oscillation frequency ν_m for the latter case is obtained from the corresponding fast-Fourier-transform spectrum, which has a distinct peak at ν_m and satellites at higher harmonic frequencies $2\nu_m$, $3\nu_m$, and $4\nu_m$ (Tokunaga, Aoki, Homma, *et al.*, 2007). These behaviors are rationalized in terms of an axially

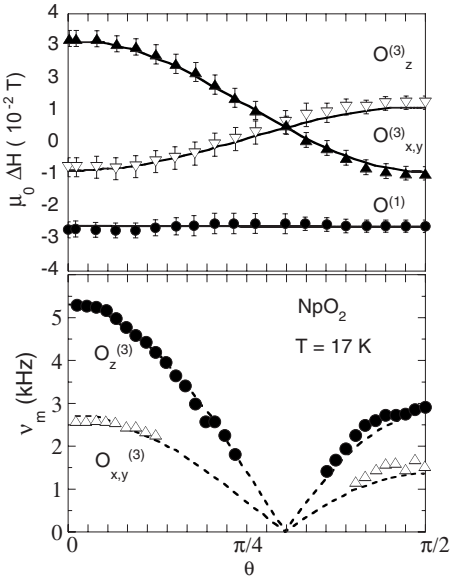

FIG. 36. Results of NMR experiments on NpO_2. (Upper panel) Angular dependence of the ^{17}O-NMR line splitting $\mu_0\Delta H=(f_{\rm res}-f_0)/\gamma$ in the ordered phase of NpO_2; $f_{\rm res}$ is the center of gravity of one of the three observed peaks, $f_0=\mu_0\gamma H$, and $\gamma=5.7719$ MHz/T. The applied field **H** rotates in the $(1\bar{1}0)$ plane, and θ is the angle between **H** and the [0 0 1] direction. Data have been recorded with $\mu_0 H=10.17$ T, with the sample kept at 17 K. Solid lines are splitting calculated from hyperfine fields derived from field-induced magnetic dipoles and octupoles. (Lower panel) Principal oscillation frequency of the spin-echo decay at the $O^{(3)}_\alpha$ sites of NpO_2 as a function of θ. The dashed lines are calculated assuming the principal axis of the EFG tensor along [1 0 0], [0 1 0], and [0 0 1] for $\alpha=x$, y, and z, respectively. Data from Tokunaga, Aoki, Homma, *et al.*, 2006.

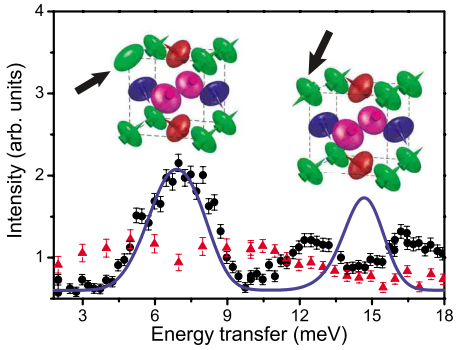

FIG. 37. (Color online) Measured powder spin-flip inelastic neutron scattering spectrum for $Q=1.9$ Å^{-1} (black circles, $T=5$ K; triangles, $T=35$ K) (Magnani *et al.*, 2008). Line: Calculation convoluted with the 1.5 meV Gaussian resolution function. The left-hand peak involves excited states where typically one Np ion (indicated by an arrow) has its quadrupole reverted and vanishing Γ_5 MMP moment (i.e., the Γ_4 MF excited state in Fig. 32). The other peak(s) involves excited states where typically one Np ion has its Γ_5 MMP moment reverted.

symmetric EFG dominated by electronic contributions, producing an HF interaction that vanishes at the $O^{(1)}$ site and is nonzero at the $O^{(3)}$ sites. The angular dependence of ν_m follows the simple relation $\nu_m=\nu_Q(3\cos^2\theta'-1)/2$, where θ' is the angle between the principal axis of the EFG tensor and the magnetic field and ν_Q is the electric quadrupole frequency proportional to the square root of the AFQ order parameter. As shown in Fig. 36, excellent agreement is obtained assuming the principal axes for the three $O^{(3)}_{x,y,z}$ sites along the edges of the cubic cell, as predicted by Sakai *et al.* (2005).

Even if neutron diffraction would provide the most direct evidence of the proposed primary MMP order, at present large enough single crystals are not available. Alternatively, information on the nature of the primary OP can be extracted from the dynamics in the ordered phase. As mentioned above, an ordering of Γ_5 MMPs implies a splitting of the Γ_8 quartets into a Γ_4 doublet and a pair of time-reversal-related singlets Γ_5 and Γ_6 (Fig. 32), which are degenerate in the presence of time-reversal invariance, whereas their degeneracy is removed when time reversal symmetry is broken. Therefore, if only the Γ_5 quadrupolar order detected by RXS and NMR took place, the Γ_8 quartets would split in a pair of Kramers doublets, whereas if a hidden order of Γ_5 MMPs is behind the observed quadrupolar order, the Γ_8 quartets should split in three levels. Whether and how this actually occurs can be checked by inelastic neutron scattering. In fact, it is easy to show by group theory that $\Gamma_5\to\Gamma_4$, $\Gamma_6\to\Gamma_4$, and $\Gamma_5\to\Gamma_6$ are all allowed dipole transitions. Therefore, in the case of pure quadrupole order a single MF magnetic transition exists, which physically corresponds to changing the charge-density character from oblate to prolate along ⟨111⟩. In the case of Γ_5 MMP order there are two MF magnetic transitions at low T. These physically correspond to concurrent changes of the local magnetization and charge densities (Fig. 37). Since a single peak at about 6.4 meV had been identified by inelastic neutron scattering on powder samples (Amoretti *et al.*, 1992) in the energy window between 3 and 11 meV, if a second peak exists it has to be located outside this energy range. Low-T specific-heat measurements (Fig. 23) are inconsistent with the presence of excited MF levels at low energy, indicating that the second inelastic neutron scattering peak, if any, must be sought above 11 meV.

Dynamical susceptibilities in the ordered phase have been calculated by including fluctuations around the four-sublattice MF configuration within the RPA approach, and using Eq. (94) (with $T_l\equiv T_l^{(5)}$) as a single-ion Hamiltonian (Santini *et al.*, 2006). In the simplest conceivable model, the joint dynamics of magnetic dipoles (J_1,J_2,J_3) and Γ_5 MMPs (T_1,T_2,T_3), corresponding to $24=(3\times2)\times(4$ sublattices) degrees of freedom per cell, are obtained in $(\mathbf{k},E)$ Fourier space by solving a 24×24 RPA system.

If only NN dipole-dipole and triakontadipole-triakontadipole interactions are assumed, and describing each of them by a single constant (instead of 3), the model contains two free parameters only. The first parameter is fixed by the Curie-Weiss shift in the inverse

static magnetic susceptibility in the paramagnetic phase, and the second parameter is determined by fitting the position of the lowest-E peak in the powder inelastic neutron scattering cross section (Figs. 26 and 37). The **Q** dependence of low-E excitations is obtained by calculating the poles of the absorptive part of the dynamical magnetic susceptibility, which is directly probed by measuring the inelastic neutron scattering cross section. The two allowed MF transitions from the ground state yield dispersive branches, whose details depend on the specific assumptions on two-ion couplings made in the calculations. The resulting spherically averaged (powder) inelastic neutron scattering cross section (Fig. 37) displays two broad peaks.

In order to demonstrate the presence of further magnetic inelastic neutron scattering signal above the previously explored energy window (3–11 meV), we have performed a new powder experiment on the triple-axis polarized neutron spectrometer IN20 at the Institut Laue Langevin (Magnani *et al.*, 2008). Some results for the magnetic (spin-flip) scattering are shown in Fig. 37: in addition to the already measured peak at about 7 meV, there is indeed a further structured signal in the range 11–18 meV disappearing above T_0. The observed powder high-E signal is structured in two peaks whose overall intensity compares well with the calculated one. The presence of two peaks instead of a single one shows that further terms must be added to the simple MF-RPA model described above. In fact, many more two-ion EMP and MMP couplings (including cross-terms coupling different ranks) than assumed in the calculation are expected to contribute to the dynamic susceptibility. A weak and broad magnetic signal observed above T_0 recalls the one detected in UO_2, and also in this case can explain why the amount of entropy removed by the phase transition is smaller than expected.

C. Praseodymium dioxide

Although praseodymium in metallic systems is usually trivalent, with two $4f$ electrons, it has been known for many years that the tetravalent Pr^{4+} (as well as Ce^{4+} and Tb^{4+}) can also exist, especially in the oxide form (Eyring, 1979; Kang, 2008). The high-T crystallographic structure of PrO_2 is identical to that of the previously discussed actinide dioxides, indeed it crystallizes in the fluorite structure with the cubic lattice parameter equal to 5.39 Å. The ground-state multiplet of the Pr^{4+} ion is a $^2F_{5/2}$ sextet, which is split in a ground Γ_8 quartet and an excited Γ_7 doublet by the cubic CF. Hence, as in NpO_2, the CF ground state carries many multipolar degrees of freedom. ME interactions play a key role in determining the low-T properties of PrO_2 because of the large quadrupolar and hexadecapolar susceptibilities [proportional to the square of the rank-2 and rank-4 Stevens factors (Abragam and Bleaney, 1970)] of its f^1 electronic configuration.

Single-crystal neutron diffraction experiments revealed that oxygen ions are displaced from their cubic equilibrium position below a phase transition occurring at $T_D = 120$ K (Gardiner, Boothroyd, Pattison, *et al.*, 2004); see Fig. 38(a). This internal distortion is very large at low T and the displacements of oxygen ions are five times larger than those occurring in UO_2, consistent with the high value of T_D. This distortion has been attributed to a cooperative static JT effect and leads to a doubling of the unit cell along one of the cubic axes with the Pr lattice left unchanged. Magnetic ordering does not accompany this transition, but the populations of structural domains can be influenced by an external magnetic field (Gardiner, Boothroyd, McKelvy, *et al.*, 2004). The actual structure in the JT distorted phase has been determined by a synchrotron x-ray diffraction study (Webster *et al.*, 2007), showing that below T_D oxygen ions display a chiral structure [Fig. 38(a)] in which neighboring oxygen chains have opposite chiralities. This distortion involves only an internal displacement of oxygen atoms leaving the Pr lattice undisturbed (there is no splitting in the fluorite-structure peaks). The lowering of the local symmetry experienced by Pr ions leads to a splitting of the Γ_8 quartet into a pair of doublets, as confirmed by specific-heat (Gardiner, Boothroyd, Pattison, *et al.*, 2004) and inelastic neutron scattering measurements (Webster *et al.*, 2007).

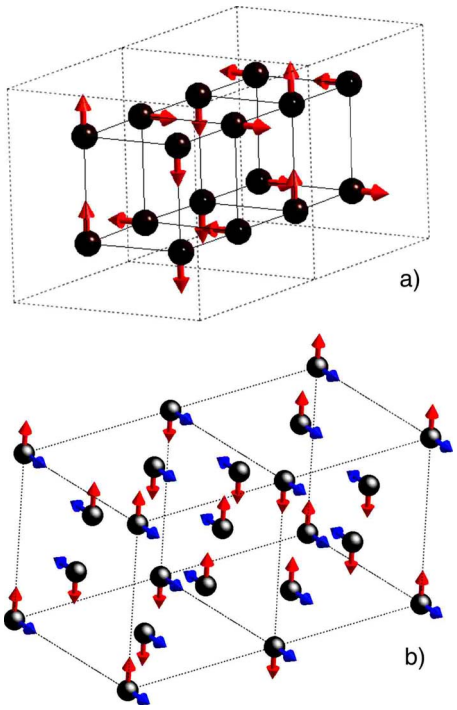

FIG. 38. (Color online) Crystallographic and magnetic structure of PrO_2. (a) Schematic representation of the distortion of the oxygen sublattice in the ordered phase of PrO_2 (Webster *et al.*, 2007). Arrows indicate the direction of the displacements. Pr ions at the vertices and at the face centers of the dashed cube are not shown. (b) Schematic representation of the magnetic dipolar order in PrO_2 (Gardiner, Boothroyd, Pattison, *et al.*, 2004). The magnetic moment at each site is represented by its components along the cubic cell axes.

The system displays a second-order transition to an AF phase at $T_N \simeq 13.5$ K (Kern *et al.*, 1984). The magnetic order is characterized by a pattern of moments described by two components (Gardiner, Boothroyd, Pattison, *et al.*, 2004): the first one, with $\mathbf{k}_1=(1,0,0)$ and $\mu_1=0.65\mu_B$, corresponds to a transverse type-I AF arrangement as in UO_2, but here most likely 1-**k** instead of 3-**k**. The secondary component, with $\mathbf{k}_2=(1,1/2,0)$ and $\mu_2=0.35\mu_B$, doubles the unit cell along one crystal direction and reflects the presence of the underlying JT distorted lattice [Fig. 38(b)]. The saturation value of the Pr moment is about $0.75\mu_B$, about half that expected for the Γ_8 ground state. A possible explanation of this quenching is the mixing produced by the dynamic JT interaction between phonons and electronic states (Boothroyd *et al.*, 2001; Bevilacqua *et al.*, 2004; Jensen, 2007); see below. The critical exponent for the magnetic phase transition $\beta=0.28$ has been extracted from the T dependence of the magnetic diffraction peaks. Below T_N, the populations of both the structural and magnetic domains can be influenced by the application of a magnetic field (Gardiner, Boothroyd, McKelvy, *et al.*, 2004).

An important step toward the understanding of PrO_2 is the determination of the CF level scheme of Pr ions. The gap between the Γ_8 ground quartet and the excited Γ_7 doublet was first measured on a polycrystalline sample by Kern *et al.* (1984) and found to be 130 meV. Subsequent higher-resolution and higher-E powder inelastic neutron scattering experiments at 10 K (Boothroyd *et al.*, 2001) revealed several other magnetic features besides the already observed peak at 130 meV: a broad peak centered at ~30 meV and extending from about 10 to 80 meV, a peak at 3 meV, and a shoulder of the 130 meV peak centered at ~160 meV. Finally, the ${}^2F_{5/2} \rightarrow {}^2F_{7/2}$ intermultiplet transitions were studied, together with the temperature dependence of the intramultiplet excitations, by Webster *et al.* (2007).

The broad band of scattering above 10 meV is seen both below and above T_D. While the scattering above 35 meV is relatively independent of T, the region below 35 meV is strongly T dependent (Fig. 39), with a maximum decreasing from ~28 meV at 7 K to ~20 meV at 100 K. The scattering then becomes quasielastic close to T_D. This provides strong evidence that the broad band contains a component reflecting the transition between the two doublets into which the Γ_8 quartet splits below T_D. In fact, the energy of this transition goes to zero as the quadrupolar OP vanishes (Webster *et al.*, 2007).

Jensen (2007) recently constructed a MF model for PrO_2 including both static and dynamic JT effects due to the ME coupling with Γ_5 local distortion modes. The main parameters of the model, i.e., the spin-orbit coupling parameter, the CF parameters, and the dynamical Jahn-Teller effect interaction parameters, have been derived by fitting the single-ion level scheme determined by inelastic neutron scattering and the value of T_D. The CF parameters are consistent with the values obtained by scaling those of actinide dioxides (Magnani, Santini, Amoretti, and Caciuffo, 2005): the bare CF gap between

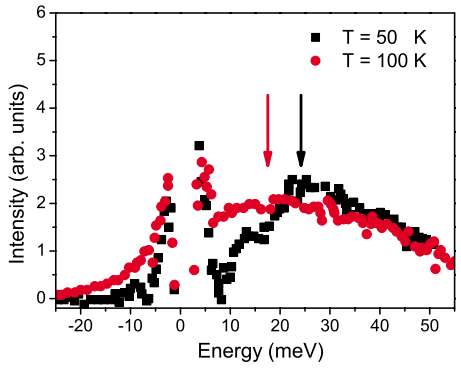

FIG. 39. (Color online) PrO_2 inelastic neutron scattering spectra with CeO_2 background subtracted, showing the variation of the broad band of vibronic scattering with temperature. The centers of the transition determined from the fits at the two temperatures are indicated by arrows. Data from Webster *et al.*, 2007.

the Γ_8 quartet and the Γ_7 doublet is close to 100 meV, slightly larger than the gap of about 82 meV expected from scaling. The ME interaction increases this gap to the observed value of 130 meV and is also responsible for the T-independent component in the broad band of excitations observed by inelastic neutron scattering. The analysis of the experimental data shows that the ME coupling to hexadecapolar degrees of freedom is of the same importance as those to the quadrupolar ones.

The symmetry of the magnetically ordered state has been discussed on the basis of an isotropic Heisenberg spin Hamiltonian (Jensen, 2007). The model correctly predicts a number of the properties of the AF phase, but does not reproduce correctly the behavior in an applied field. In order to fit the observed ratio between the two components of the AF moment, unrealistic exchange parameters have to be used. In addition, the calculated total size of the moment is about 40% larger than observed. The size of the moment is reduced with respect to the bare CF value by the mixing of phonon and CF states (the same dynamical Jahn-Teller effect mechanism reducing the susceptibility of UO_2, Fig. 17), but this reduction is not sufficient to reproduce the small observed value of the ordered moment. Finally, the low-energy powder inelastic neutron scattering spectrum shows at 10 K a peak centered at about 2.7 meV and associated with the spin waves in the AF phase (Boothroyd *et al.*, 2001). This energy should be close to the MF splitting of the ground-state doublet, which the model predicts to be about 1.8 meV at 10 K, one-third too small. This is unexpected since the calculated moment, and therefore also the corresponding exchange field, are 40% larger than observed.

The problems encountered in reproducing the properties of the AF phase of PrO_2 on the basis of a Heisenberg model point to the existence of sizable two-ion SE interactions involving multipoles (Jensen, 2007). Indeed, as shown in Fig. 2, such interactions are expected to be even larger than the dipolar ones. These couplings do not affect the paramagnetic properties, but would play

an important role in the AF-ordered phase. In fact, even if the low symmetry of the JT-distorted phase prevents a purely multipolar OP (Sec. II.E), the interactions driving the phase transition may well be of multipolar type. The resulting properties of the AF phase are different from those obtained by a Heisenberg model. For instance, the value of the ordered moment may be significantly smaller.

D. Other dioxides

1. Heavier actinide dioxides

Plutonium dioxide (PuO_2) has a $J=4$ lowest-energy manifold, just as UO_2, which is split by the CF into a Γ_1 singlet, a Γ_3 doublet, and two triplets (Γ_4 and Γ_5). Given that the magnetic susceptibility is temperature independent below 1000 K (Raphael and Lallement, 1968), the CF ground state is expected to be the nonmagnetic Γ_1 singlet. This is in agreement with the fact that only one peak, corresponding to the $\Gamma_1 \rightarrow \Gamma_4$ transition, is observed in the inelastic neutron scattering spectra (Kern *et al.*, 1999), since magnetic-dipole matrix elements for other transitions involving the Γ_1 singlet are zero. This peak is centered near 120 meV, and this energy gap is well reproduced by density-functional-theory (Colarieti-Tosti *et al.*, 2002) and CF calculations (Magnani, Santini, Amoretti, and Caciuffo, 2005). Observation of a high-energy peak in the inelastic neutron scattering cross section is a clear indication of the localized nature of the $5f$ states, so that the above CF model is expected to be appropriate, and excludes a scenario involving nonlocalized degrees of freedom.

Since the ground state is a singlet, any magnetic or multipolar degree of freedom is frozen in when k_BT is well below the crystal-field gap. Indeed, no phase transition occurs in PuO_2, and its magnetic susceptibility is finite down to $T=0$ (Raphael and Lallement, 1968). There are some problems with the magnetic response of PuO_2. First, the value of the susceptibility is only 50% of what one would expect from the Van Vleck coupling of Γ_1 with Γ_4, when a Russell-Saunders coupling scheme is used. To fit the susceptibility by a single-ion CF model, the Γ_4 level should be at 280 meV and not at 120 meV as observed. On the other hand, susceptibility measurements on PuO_2 diluted in ThO_2 (Candela *et al.*, 1959) are compatible with a gap of about 145 meV. A second problem is that the peak observed at 120 meV by neutron scattering is broad, with a width of about 11 meV. Most likely, the explanation of these apparent anomalies is provided by the presence of AF magnetic SE interactions between Pu ions, which make the Γ_1-Γ_4 transition dispersive. The wave-vector dependence gives rise to a broad peak in the powder spherical average. Moreover, these same AF interactions decrease the static susceptibility by the usual Curie-Weiss mechanism. This scenario accounts well for the different value of the susceptibility measured in PuO_2 diluted in ThO_2, since the dilution suppresses interactions between Pu ions. On the other hand, the temperature independence of the magnetic susceptibility up to 1000 K cannot be accounted for by the models proposed so far. Indeed, whatever its specific modeling, the observed energy scale of 120 meV implies that macroscopic observables display a sizable T dependence above about 600 K, when the first excited state begins to become thermally populated. Several ideas have been put forward, from a failure of the weak CF approach (Kern *et al.*, 1990) to a possible role of covalency between $5f$-Pu and $2p$-O orbitals (Kern *et al.*, 1999; Prodan *et al.*, 2007); however, a truly flat susceptibility cannot be obtained (Colarieti-Tosti *et al.*, 2002).

Americium dioxide (AmO_2) displays a $5f^5$ configuration, hence a $J=5/2$ ground multiplet which is split in a Γ_7 doublet and a Γ_8 quartet by the cubic CF. A phase transition at 8.5 K has been detected by magnetic susceptibility measurements (Karraker, 1975), but no evidence of magnetic order has been found, neither by Mössbauer (Kalvius *et al.*, 1969) nor by neutron diffraction (Boeuf *et al.*, 1979). The similarity between this behavior and that of NpO_2 has been pointed out, suggesting the possibility that quadrupolar or multipolar order takes place (Edelstein and Lander, 2006); however, EPR experiments on Am^{4+} in ThO_2 hint to a Γ_7 Kramers doublet as ground state (Abraham *et al.*, 1971), which does not allow any type of phase transition apart from those that involve dipolar order. Susceptibility data for pure AmO_2, although not conclusive, also point to a Γ_7 ground state (Karraker, 1975), and recent CF calculations confirm this picture (Magnani, Santini, Amoretti, and Caciuffo, 2005). In addition to this, the model reported in Sec. II.C.3 shows that the SE Hamiltonian is expected to be almost purely dipolar for the electronic configuration of Am^{4+}. Further experiments on AmO_2, e.g., a repetition of susceptibility measurements below 10 K with modern equipment and measurements of specific heat, are envisaged in order to clarify the situation, as nothing new has been reported in the last 30 years (Edelstein and Lander, 2006).

Curium dioxide (CmO_2) should contain Cm^{4+} ions in a $5f^6$ configuration, having a $J=0$ nonmagnetic singlet as ground state. However, magnetic susceptibility experiments yield an effective magnetic moment of $3.36\mu_B$/ion (Morss *et al.*, 1989). The stoichiometry of the sample was carefully checked for the absence of trivalent curium impurities, so it appears that this magnetic behavior is intrinsic to the CmO_2 compound. One possible explanation is that this is due to an anomalous ground state produced by free-ion interactions; in fact, while compounds containing the isoconfigurational Am^{3+} ion generally show the expected temperature-independent susceptibility, it is quite common for Cm^{4+} compounds not to follow this rule (Soderholm, 1987). On the other hand, recent atomic structure calculations do not support this picture (Gaigalas *et al.*, 2009). Another possibility is that this behavior might be due to the $5f-2p$ orbital degeneracy which would induce unexpected orbital mixing for the intermediate members of the AO_2 series, resulting in a crossover from localized to delocalized

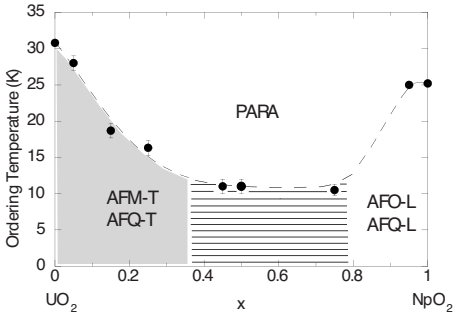

FIG. 40. Phase diagram of $U_{1-x}Np_xO_2$ solid solutions, showing the evolution of the low-T phase from a transversal type-I magnetic-quadrupolar state to a longitudinal type-I octupolar-quadrupolar state. For intermediate values of x, incommensurate short-range magnetic ordering has been detected.

f-electron character with increasing Z and a shift toward +3 valence (Prodan *et al.*, 2007).

2. $U_{1-x}Np_xO_2$ solid solutions

Dioxides form solid solutions with each other and the resulting compounds retain the CaF_2 lattice structure, with the different actinide species randomly distributed over the anion sublattice. These solutions, as well as those composed of a given actinide dioxide and the homologous nonmagnetic thorium dioxide, are interesting by themselves and may also be used to extract information on microscopic interactions in the pure dioxides. For instance, the removal of U-U interactions in $U_{1-x}Th_xO_2$ solutions enabled the single-ion dynamical Jahn-Teller effect to be evidenced in a clean way, and the associated ME coupling parameters to be assessed (Fig. 17). On the other hand, $U_{1-x}Np_xO_2$ solutions are interesting to investigate the nature of two-ion interactions and for the possible exotic states that they may display. The magnetic behavior of these compounds has been investigated by powder neutron diffraction, Mössbauer spectroscopy, and magnetic susceptibility measurements (Tabuteau, Jové, Pagès, *et al.*, 1984; Tabuteau, Pagès, Boeuf, *et al.*, 1984; Boeuf *et al.*, 1987). The ^{237}Np Mössbauer isomer shift indicates that Np ions are tetravalent, with $5f^3$, $^4I_{9/2}$ electronic configuration, independent of temperature and composition. Magnetic order has been detected in the composition range $x<0.75$, with T_N decreasing with increasing x: $T_N\sim31$ K for $x=0$, $T_N\sim17$ K for $x=0.25$, and $T_N\sim11$ K for $x=0.75$ (Fig. 40). This shows that substitution of Np for U reduces the importance of dipolar exchange interactions, which eventually become irrelevant in the multipolar-ordered state occurring for $x\gtrsim0.8$. For $x\lesssim0.4$, the magnetic structure is transverse AF type I, as in UO_2, whereas for larger Np content the magnetic order is short range and incommensurate. RXS experiments on a $U_{0.75}Np_{0.25}O_2$ crystal (Wilkins *et al.*, 2004) have shown the presence of AF-ordered magnetic moments and electric quadrupoles on both U and Np sites below $T_N\simeq19$ K. The different energy of the $M_{4,5}$ edges of U and Np allows one, in fact, to probe independently the two types of cations. A theoretical analysis of the azimuth and energy dependencies has been reported (Nagao and Igarashi, 2006), and confirmed the interpretation given by Wilkins *et al.* (2004).

The presence of several active degrees of freedom on U and Np ions and the richness of the associated interactions makes it difficult to identify a unique model providing an overall unified description of $U_{1-x}Np_xO_2$ compounds, whose properties result from the subtle interplay between the intrinsic complexity of these materials and the effect of disorder. The behavior of the transition temperature across the solid solution, with a minimum for intermediate compositions, can be understood by observing that the primary OP is different in the two pure compounds. Hence, on both limits, the minority component acts as a dilution agent for the dominant two-ion interaction.

Some qualitative observations can be formulated from a virtual-crystal-approximation perspective, i.e., focusing on average properties and neglecting effects specifically associated with the disorder in the sample. For $x\to1$, U ions are particularly effective on the multipolar-ordered state since they act as dilution centers for the primary OP of NpO_2, being the corresponding ionic MMP quenched on these ions. On the contrary, the secondary quadrupolar OP does not experience dilution since the corresponding ionic moment is not quenched on U. On the opposite side, $x\to0$, Np ions dilute neither the magnetic primary OP of UO_2 nor the secondary quadrupolar OP, but do of course modify the behavior of pure UO_2 by their different single-ion response and two-ion interactions. In particular, the decrease of T_N with increasing x shows that the presence of Np ions destabilizes the magnetically ordered state. Most likely, this is due to U-Np dipolar interactions being weaker than the corresponding U-U interactions, and also due to the fact that the dipole moment of the CF ground state of Np ions is slightly smaller than that of U ions. Since adding Np makes the transition second order, and considering that the first-order character in pure UO_2 is believed to be associated with interactions between Γ_5 quadrupoles, it is likely that these quadrupolar two-ion interactions are smaller for U-Np pairs than for U-U pairs. U-Np MMP interactions are absent since MMPs inequivalent to dipoles are quenched in U. Thus, for small values of x the phase transition of $U_{1-x}Np_xO_2$ is mainly driven by U-U dipolar interactions. U quadrupoles (and the associated lattice distortion) follow U dipoles as secondary OPs, but their contribution to the free energy is too small to affect the phase transition qualitatively (i.e., to change the value of T_N and the order of the transition). Np ions appear to play quite a passive role. The leading rank-5 MMP interaction of NpO_2 has no significant effects for small x since it involves the minority Np-Np pairs but not U-Np and U-U pairs. As U ions order, Np ions feel the growing U dipoles and quadrupoles through U-Np interactions, and themselves acquire ordered dipoles and quadrupoles. This picture is consistent with the RXS experiments for $x=0.25$ (Wilkins *et al.*,

2004), which show that below T_N Np moments develop more slowly than U moments. In fact, since the U-Np dipolar interaction by which Np ions feel the U dipolar order is (relatively) weak, thermal fluctuations on Np ions are quenched by the phase transition more slowly than on U ions.

Even if calculations based on the virtual crystal approximation provide a qualitatively satisfactory theoretical framework for $U_{0.75}Np_{0.25}O_2$, the entropy removed by the phase transition is anomalously small, just as in pure UO_2 and NpO_2, and cannot be correctly reproduced by a simple model. In addition, in all magnetically ordered solid solutions the saturation ordered moment of Np ions is of the order of $0.5\mu_B$, much less than expected if the same 3-**k** structure as in pure UO_2 is assumed. This problem would remain even if theoretical approaches different from the virtual crystal approximation were used, being associated with the structure of the single-ion CF states of Np. These carry a moment along [1 1 1] much larger than $0.5\mu_B$, no matter whether the CF is varied or whether quadrupole interactions are included. In fact, since the dipole and quadrupole order parameters appearing in the 3-**k** structure commute, the bare CF value of the moment is not reduced by quadrupolar interactions. This would not be true if the structure was not 3-**k**. In particular, the 2-**k** structure looks like a promising candidate since the associated quadrupole order strongly reduces the bare Np moment to a value close to $0.5\mu_B$ (Amoretti *et al.*, 1992).

The properties of solid solutions with long-range magnetic order have not yet been completely understood, and neither are the short-range ordered intermediate-x compounds, where the effect of disorder is maximal and so is the competition between the different OPs of the pure compounds. It will be interesting in the future to grow samples with $0.75<x<0.95$, to understand where and how the MMP order of NpO_2 is eventually destabilized by U doping.

V. SUMMARY AND CONCLUSIONS

The present article focuses on the role of multipolar interactions in *f*-electron systems. We have followed the theory in some detail to show the variety of potential effects that can be encountered, and given a detailed review of experiments, with particular focus on the dioxides of praseodymium, uranium, and neptunium. For several reasons, these compounds offer unique opportunities to explore in depth the mechanisms of multipolar interactions: the appropriate Hamiltonian is not too complicated, because of the insulating character and the simplicity of the crystallographic structure; the number of independent multipolar degrees of freedom supported by their ground state is large, due to the cubic symmetry of the paramagnetic phase; the single-ion wave functions are well established, on the basis of the analysis of reliable spectroscopic data available for the series; finally, in the case of the actinide dioxides, the symmetry of the multipolar order parameters is known from experiments probing them directly.

A particularly interesting situation is realized in NpO_2, because the nature of the ground state allows observing the effects of higher-rank MMP order in the absence of magnetic dipole moments. This makes NpO_2 an archetype of the SE two-ion MMP interaction model. On the other hand, the low-temperature physics of UO_2 provides a textbook example of phenomena connected to the ME coupling of electric quadrupoles to the lattice. U-Np mixed oxides, in addition, give the possibility of studying the complex interplay between magnetic and electric multipolar two-ion interactions.

Of course, in nature there are always many interactions that compete or concur in determining the ground state of a given system. Multipolar interactions are one of the possible panoply, and whether or not they dominate will depend on their strength relative to other interactions. For the localized systems such as the actinide dioxides and UPd_3, as discussed in this review, multipolar interactions may be very important, whereas for itinerant *f*-electron materials such as UPd_2Al_3 (a heavy-fermion superconductor at low temperature) multipolar interactions have not usually been found significant. In surveying the general properties of materials, some guidelines emerge as to the systems that are potentially dominated by multipolar interactions. (i) *f*-electron systems are likely to be more affected than those with *d* electrons because of the larger orbital interactions in the former. The quenching of the orbital degrees of freedom often occurring in *d* systems results in the ground-state properties being dominated by the spin degrees of freedom. (ii) If the point symmetry at the *f*-ion site is too low, the presence of multipolar interactions may be obscured by the effect of the CF, which reduces the number of inequivalent multipole degrees of freedom and quenches many of them. (iii) In metallic *f*-electron systems, the often sizable mixing between the conduction states (normally predominantly of *d* nature) and the *f*-electron orbitals may tend to induce Kondo fluctuations or even delocalization and a dual nature of *f*-electrons (Thalmeier and Zwicknagl, 2005). Indeed, there have been many attempts to describe this type of *f*-electron physics in terms of band states; see, for example, Toropova *et al.* (2007) for a recent critique. Whereas multipolar interactions may still be important, they may not dominate the physics of the ground state.

In the light actinides (U, Np, and Pu) and their compounds, the number of electrons in the 5*f* shell n is often controversial, and in the band-theory approach there is no reason for an integral value of n. An example of this is the recent works on the ground state of the element plutonium (Lashley *et al.*, 2005; Shim *et al.*, 2007). Some idea of the number of *f* electrons can be obtained from magnetic and Mössbauer measurements (Edelstein and Lander, 2006), but it is only recently that the development of sum rules at the *M* and *N* absorption edges (van der Laan *et al.*, 2004; Moore, van der Laan, Haire, *et al.*, 2007; Moore, van der Laan, Wall, *et al.*, 2007; Moore and

van der Laan, 2009) have given us a general method in the case of metallic systems. If the number of 5*f* electrons is not fixed, the approach outlined in the present review is difficult to follow.

From the experimental perspective, the early work of Morin and Schmitt (1990) showed that with careful elastic constant and susceptibility measurements, the symmetry of the quadrupolar ground states could be deduced. Such methods work, of course, only if there is a finite coupling to strains that result in reductions of the overall lattice symmetry. This is almost always the case for uniform ordering of multipoles, but may not be if the alignment is staggered. In the latter case, one is faced with the complex problem of finding the so-called "hidden order," a considerable challenge given the vast emptiness of reciprocal space and the unknown nature of the multipole. Of course, the presence of a phase transition is best established by specific heat, but that is only the beginning. NpO_2 is perhaps the best example so far of this mystery, and one that lasted for half a century after the specific-heat experiments showed the presence of a phase transition at 25 K. Neutron scattering will not observe even-order multipoles, and the technique of choice is resonant x-ray scattering, although in this case single crystals are imperative, even if small. Finally, precise information about the ground state and the multipolar interactions can be extracted from NMR and inelastic neutron scattering. In both cases, a considerable amount of theory input is needed in the extraction of the relevant parameters. With both inelastic neutron scattering and NMR, polycrystalline materials may be used. More information is always gained using single crystals, although for inelastic neutron scattering they have to be reasonably large, which is often a severe constraint. In the NMR case, only certain isotopes can be used, adding a restriction also to this technique.

We anticipate more examples of multipole ordering to be found as well as further development of the experimental techniques of RXS, NMR, and inelastic neutron scattering. Although the physical properties of PrO_2, UO_2, and NpO_2 now seem to be reasonably well understood, there are still interesting questions about PuO_2, AmO_2, and CmO_2.

ACKNOWLEDGMENTS

The authors are greatly obliged to Sergio Di Matteo, Keith A. McEwen, Kevin T. Moore, Ryousuke Shiina, and Russ E. Walstedt, for critical reviews of the manuscript.

REFERENCES

Abe, K., J. Kitagawa, N. Takeda, and M. Ishikawa, 1999, Phys. Rev. Lett. **83**, 5366.
Abragam, A., and B. Bleaney, 1970, *Electron Paramagnetic Resonance of Transition Ions* (Clarendon, Oxford).
Abraham, M. M., L. A. Boatner, C. B. Finch, and R. W. Reynolds, 1971, Phys. Rev. B **3**, 2864.
Adachi, H., H. Kawata, M. Mizumaki, T. Akao, M. Sato, N. Ikeda, Y. Tanaka, and H. Miwa, 2002, Phys. Rev. Lett. **89**, 206401.
Akatsu, M., T. Goto, Y. Nemoto, O. Suzuky, S. Nakamura, and S. Kunii, 2003, J. Phys. Soc. Jpn. **72**, 205.
Aléonard, R., and P. Morin, 1979, Phys. Rev. B **19**, 3868.
Allen, S. J., 1968a, Phys. Rev. **166**, 530.
Allen, S. J., 1968b, Phys. Rev. **167**, 492.
Amara, M., S. E. Luca, and R. M. Galéra, 2001, J. Phys.: Condens. Matter **13**, 9621.
Amara, M., and P. Morin, 1998, J. Phys.: Condens. Matter **10**, 9875.
Amoretti, G., A. Blaise, R. Caciuffo, D. Di Cola, J. M. Fournier, M. T. Hutchings, G. H. Lander, R. Osborn, A. Severing, and A. D. Taylor, 1992, J. Phys.: Condens. Matter **4**, 3459.
Amoretti, G., A. Blaise, R. Caciuffo, J. M. Fournier, M. T. Hutchings, R. Osborn, and A. D. Taylor, 1989, Phys. Rev. B **40**, 1856.
Amoretti, G., R. Caciuffo, P. Santini, G. H. Lander, J. Kulda, and P. de V. Du Plessis, 1999, J. Appl. Phys. **85**, 4524.
Anderson, P. W., 1959, Phys. Rev. **115**, 2.
Anderson, P. W., 1963, in *Magnetism Vol. 1*, edited by G. T. Rado and H. Suhl (Academic, New York).
Aoki, Y., T. Namiki, T. D. Matsuda, K. Abe, H. Sugawara, and H. Sato, 2002, Phys. Rev. B **65**, 064446.
Aoki, Y., S. Sanada, D. Kikuchi, H. Sugawara, and H. Sato, 2007, J. Phys. Soc. Jpn. **76**, 113703.
Arrott, A., and J. E. Goldman, 1957, Phys. Rev. **108**, 948.
Baker, J. M., 1971, Rep. Prog. Phys. **34**, 109.
Bevilacqua, G., D. Ippolito, and L. Martinelli, 2004, Phys. Rev. B **69**, 155208.
Birgeneau, R. J., M. T. Hutchings, J. M. Baker, and J. D. Riley, 1969, J. Appl. Phys. **40**, 1070.
Blackburn, E., R. Caciuffo, N. Magnani, P. Santini, P. J. Brown, M. Enderle, and G. H. Lander, 2005, Phys. Rev. B **72**, 184411.
Blum, K., 1996, *Density Matrix Theory and Applications* (Plenum, New York).
Blume, M., 1966, Phys. Rev. **141**, 517.
Blume, M., 1985, J. Appl. Phys. **57**, 3615.
Blume, M., 1994, in *Resonant Anomalous X-ray Scattering*, edited by G. Materlik, J. Sparks, and K. Fisher (Elsevier, Amsterdam), p. 495.
Blume, M., and D. Gibbs, 1988, Phys. Rev. B **37**, 1779.
Boeuf, A., R. Caciuffo, J. Fournier, L. Manes, J. Rebizant, J. Spirlet, and A. Wright, 1983, Phys. Status Solidi B **79**, K1.
Boeuf, A., R. Caciuffo, M. Pagès, J. Rebizant, F. Rustichelli, and A. Tabuteau, 1987, Europhys. Lett. **3**, 221.
Boeuf, A., F. Rustichelli, J. M. Fournier, J. F. Gueugnon, L. Manes, and J. Rebizant, 1979, J. Phys. (Paris), Lett. **40**, L335.
Boothroyd, A. T., C. H. Gardiner, S. J. S. Lister, P. Santini, B. D. Rainford, L. D. Noailles, D. B. Currie, R. S. Eccleston, and R. I. Bewley, 2001, Phys. Rev. Lett. **86**, 2082.
Bradley, C., and A. Cracknell, 1972, *Mathematical Theory of Symmetry in Solids: Representation Theory for Point Groups and Space Groups* (Oxford University Press, Oxford).
Brandt, O. G., and C. T. Walker, 1967, Phys. Rev. Lett. **18**, 11.
Broholm, C., J. K. Kjems, W. J. L. Buyers, P. Matthews, T. T. M. Palstra, A. A. Menovsky, and J. A. Mydosh, 1987, Phys. Rev. Lett. **58**, 1467.
Broholm, C., H. Lin, P. T. Matthews, T. E. Mason, W. J. L. Buyers, M. F. Collins, A. A. Menovsky, J. A. Mydosh, and J. K. Kjems, 1991, Phys. Rev. B **43**, 12809.
Brooks, M. S. S., and P. J. Kelly, 1983a, Phys. Rev. Lett. **51**,

1708.
Brooks, M. S. S., and P. J. Kelly, 1983b, Solid State Commun. **45**, 689.
Brown, P. J., J. B. Forsyth, and R. Mason, 1980, Philos. Trans. R. Soc. London, Ser. B **290**, 481.
Browning, P., G. J. Hyland, and J. Ralph, 1983, High Temp. - High Press. **15**, 169.
Burlet, P., J. Rossat-Mignod, S. Quezel, O. Vogt, J. C. Spirlet, and J. Rebizant, 1986, J. Less-Common Met. **121**, 121.
Buyers, W. J. L., and T. M. Holden, 1985, in *Handbook on the Physics and Chemistry of the Actinides, Vol. 2*, edited by A. J. Freeman and G. H. Lander (Elsevier, Amsterdam), p. 239.
Buyers, W. J. L., A. F. Murray, T. M. Holden, E. C. Svensson, P. de V. du Plessis, G. H. Lander, and O. Vogt, 1980, Physica B & C **102**, 291.
Caciuffo, R., G. Amoretti, J. M. Fournier, A. Blaise, R. Osborn, A. D. Taylor, J. Larroque, and M. T. Hutchings, 1991, Solid State Commun. **79**, 197.
Caciuffo, R., G. Amoretti, P. Santini, G. H. Lander, J. Kulda, and P. d. V. Du Plessis, 1999, Phys. Rev. B **59**, 13892.
Caciuffo, R., G. H. Lander, J. C. Spirlet, J. M. Fournier, and W. F. Kuhs, 1987, Solid State Commun. **64**, 149.
Caciuffo, R., N. Magnani, P. Santini, S. Carretta, G. Amoretti, E. Blackburn, M. Enderle, P. J. Brown, and G. H. Lander, 2007, J. Magn. Magn. Mater. **310**, 1698.
Caciuffo, R., J. A. Paixao, C. Detlefs, M. J. Longfield, P. Santini, N. Bernhoeft, J. Rebizant, and G. H. Lander, 2003, J. Phys.: Condens. Matter **15**, S2287.
Caciuffo, R., L. Paolasini, A. Sollier, P. Ghigna, E. Pavarini, J. van den Brink, and M. Altarelli, 2002, Phys. Rev. B **65**, 174425.
Candela, G. A., C. A. J. Hutchison, and W. B. Lewis, 1959, J. Chem. Phys. **30**, 246.
Carra, P., A. Jerez, and I. Marri, 2003, Phys. Rev. B **67**, 045111.
Carra, P., and B. T. Thole, 1994, Rev. Mod. Phys. **66**, 1509.
Carra, P., B. T. Thole, M. Altarelli, and X. Wang, 1993, Phys. Rev. Lett. **70**, 694.
Carretta, S., G. Amoretti, R. Caciuffo, A. Hiess, G. H. Lander, N. Magnani, L. P. Regnault, and P. Santini, 2009, unpublished.
Castleton, C. W. M., and M. Altarelli, 2000, Phys. Rev. B **62**, 1033.
Chandra, P., P. Coleman, J. A. Mydosh, and V. Tripathi, 2002, Nature (London) **417**, 831.
Clausen, K., W. Hayes, J. E. Macdonald, R. Osborn, and M. T. Hutchings, 1984, Phys. Rev. Lett. **52**, 1238.
Colarieti-Tosti, M., O. Eriksson, L. Nordström, J. Wills, and M. S. S. Brooks, 2002, Phys. Rev. B **65**, 195102.
Coldea, R., S. M. Hayden, G. Aeppli, T. G. Perring, C. D. Frost, T. E. Mason, S. W. Cheong, and Z. Fisk, 2001, Phys. Rev. Lett. **86**, 5377.
Collins, S. P., S. W. Lovesey, and E. Balcar, 2007, J. Phys.: Condens. Matter **19**, 213201.
Comly, J. B., 1968, J. Appl. Phys. **39**, 716.
Cooper N. G., 2000, Ed., *Los Alamos Science, Vol. 26*, *Challenges in Plutonium Science* (Los Alamos National Laboratory), URL http://www.fas.org/sgp/othergov/doe/lanl/pubs/number26.htm.
Copland, G. M., and P. M. Levy, 1970, Phys. Rev. B **1**, 3043.
Coqblin, B., and J. R. Schrieffer, 1969, Phys. Rev. **185**, 847.
Cowley, R. A., and G. Dolling, 1968, Phys. Rev. **167**, 464.
Cox, D. E., and B. C. Frazer, 1967, J. Phys. Chem. Solids **28**, 1649.
Cox, D. L., 1987, Phys. Rev. Lett. **59**, 1240.
Cox, D. L., and A. Zawadowski, 1998, Adv. Phys. **47**, 599.
Cox, L. E., W. P. Ellis, R. D. Cowan, J. W. Allen, S. J. Oh, I. Lindau, B. B. Pate, and A. J. Arko, 1987, Phys. Rev. B **35**, 5761.
Cyrot, M., and C. Lyon-Caen, 1975, J. Phys. (Paris) **36**, 253.
Delapalme, A., M. Forte, J. M. Fournier, J. Rebizant, and J. C. Spirlet, 1980, Physica B & C **102**, 171.
Di Matteo, S., Y. Joly, A. Bombardi, L. Paolasini, F. de Bergevin, and C. R. Natoli, 2003, Phys. Rev. Lett. **91**, 257402.
Di Matteo, S., Y. Joly, and C. R. Natoli, 2005, Phys. Rev. B **72**, 144406.
Di Matteo, S., N. Magnani, F. Wastin, J. Rebizant, and R. Caciuffo, 2007, J. Alloys Compd. **444-445**, 278.
Di Matteo, S., and C. R. Natoli, 2002, J. Synchrotron Radiat. **9**, 9.
Dmitrienko, V. E., 1983, Acta Crystallogr., Sect. A: Found. Crystallogr. **39**, 29.
Dmitrienko, V. E., and E. N. Ovchinnikova, 2001, Acta Crystallogr., Sect. A: Found. Crystallogr. **57**, 642.
Dolling, G., and R. A. Cowley, 1966, Phys. Rev. Lett. **16**, 683.
Dolling, G., R. A. Cowley, and A. D. B. Woods, 1965, Can. J. Phys. **43**, 1397.
Dubovik, V. M., and V. V. Tugushev, 1990, Phys. Rep. **187**, 145.
Dunlap, B. D., and G. M. Kalvius, 1985, in *Handbook on the Physics and Chemistry of the Actinides, Vol. 2*, edited by A. J. Freeman and G. H. Lander (North-Holland, Amsterdam).
Dunlap, B. D., G. M. Kalvius, D. J. Lam, and B. Brodsky, 1968, J. Phys. Chem. Solids **29**, 1365.
Edelstein, N. M., and G. H. Lander, 2006, in *The Chemistry of the Actinide and Transactinide Elements, Vol. 4, 3rd ed.*, edited by L. R. Morss, N. M. Edelstein, J. Fuger and J. J. Katz (Springer, Dordrecht, The Netherlands), pp. 2225–2306.
Effantin, J. M., J. Rossat-Mignod, P. Burlet, H. Bartholin, S. Kunii, and T. Kasuya, 1985, J. Magn. Magn. Mater. **47-48**, 145.
Elliott, R. J., and M. F. Thorpe, 1968, J. Appl. Phys. **39**, 802.
Ellis, D. E., 1985, in *Handbook on the Physics and Chemistry of the Actinides, Vol. 2*, edited by A. J. Freeman and G. H. Lander (North-Holland, Amsterdam).
Erdös, P., G. Solt, Z. Zołnierek, A. Blaise, and J. M. Fournier, 1980, Physica B & C **102**, 164.
Erkelens, W. A. C., L. P. Regnault, P. Burlet, J. Rossat-Mignod, S. Kunii, and T. Kasuya, 1987, J. Magn. Magn. Mater. **63-64**, 61.
Evarestov, R., and V. Smirnov, 1997, *Site Symmetry in Crystals: Theory and Applications* (Springer-Verlag, Berlin).
Eyring, L., 1979, in *Handbook on the Physics and Chemistry of Rare Earths, Vol. 3*, edited by K. A. Gschneidner and L. Eyring (Elsevier, Amsterdam), p. 171.
Faber, J., and G. H. Lander, 1976, Phys. Rev. B **14**, 1151.
Faber, J., G. H. Lander, and B. R. Cooper, 1975, Phys. Rev. Lett. **35**, 1770.
Fazekas, P., 2003, *Lecture Notes on Electron Correlation and Magnetism* (World Scientific, Singapore).
Fazekas, P., A. Kiss, and K. Radnoczi, 2005, Prog. Theor. Phys. Suppl. **160**, 114.
Felcher, G. P., G. H. Lander, T. Arai, S. K. Sinha, and F. H. Spedding, 1976, Phys. Rev. B **13**, 3034.
Fert, A., and P. M. Levy, 1977, Phys. Rev. B **16**, 5052.
Fink, J. K., 1982, Int. J. Thermophys. **3**, 165.
Fischer, P., K. Iwasa, K. Kuwahara, M. Kohgi, T. Hansen, and S. Kunii, 2005, Phys. Rev. B **72**, 014414.
Fournier, J. M., 1985, in *Structure and Bonding Vol. 59/60* (Springer-Verlag, Berlin), p. 127.

Fournier, J. M., A. Blaise, G. Amoretti, R. Caciuffo, J. Larroque, M. T. Hutchings, R. Osborn, and A. D. Taylor, 1991, Phys. Rev. B **43**, 1142.
Frazer, B. C., G. Shirane, D. E. Cox, and C. E. Olsen, 1965, Phys. Rev. **140**, A1448.
Friedt, J. M., F. J. Litterst, and J. Rebizant, 1985, Phys. Rev. B **32**, 257.
Fulde, P., and M. Löwenhaupt, 1986, Adv. Phys. **34**, 589.
Furuno, T., N. Sato, S. Kunii, T. Kasuya, and W. Sasaki, 1985, J. Phys. Soc. Jpn. **54**, 1899.
Gaigalas, G., E. Gaidamauskas, Z. Rudzikas, N. Magnani, and R. Caciuffo, 2009, Phys. Rev. A **79**, 022511.
Gajek, Z., M. P. Lahalle, J. C. Krupa, and J. Mulak, 1988, J. Less-Common Met. **139**, 351.
Gardiner, C. H., A. T. Boothroyd, M. J. McKelvy, G. J. McIntyre, and K. Prokes, 2004, Phys. Rev. B **70**, 024416.
Gardiner, C. H., A. T. Boothroyd, P. Pattison, M. J. McKelvy, G. J. McIntyre, and S. J. S. Lister, 2004, Phys. Rev. B **70**, 024415.
Gehring, G. A., and K. A. Gehring, 1975, Rep. Prog. Phys. **38**, 1.
Giannozzi, P., and P. Erdös, 1987, J. Magn. Magn. Mater. **67**, 75.
Givord, F., J. X. Boucherle, P. Burlet, B. Gillon, and S. Kunii, 2003, J. Phys.: Condens. Matter **15**, 3095.
Goodrich, R. G., D. P. Young, D. Hall, L. Balicas, Z. Fisk, N. Harrison, J. Betts, A. Migliori, F. M. Woodward, and J. W. Lynn, 2004, Phys. Rev. B **69**, 054415.
Gunnarson, O., D. D. Sarma, F. U. Hillebrecht, and K. Schönhammer, 1988, J. Appl. Phys. **63**, 3676.
Hachitani, K., H. Fukazawa, Y. Kohori, I. Watanabe, C. Sekine, and I. Shirotani, 2006, Phys. Rev. B **73**, 052408.
Hall, D., Z. Fisk, and R. G. Goodrich, 2000, Phys. Rev. B **62**, 84.
Hannon, J. P., G. T. Trammell, M. Blume, and D. Gibbs, 1988, Phys. Rev. Lett. **61**, 1245.
Hanzawa, K., 2000a, J. Phys. Soc. Jpn. **69**, 510.
Hanzawa, K., 2000b, J. Phys. Soc. Jpn. **69**, 2121.
Hanzawa, K., 2007, J. Phys.: Condens. Matter **19**, 072202.
Hanzawa, K., and T. Kasuya, 1984, J. Phys. Soc. Jpn. **53**, 1809.
Hao, L., K. Iwasa, M. Nakajima, D. Kawana, K. Kuwahara, M. Kohgi, H. Sugawara, T. D. Matsuda, Y. Aoki, and H. Sato, 2003, Acta Phys. Pol. B **34**, 1113.
Heaton, L., M. H. Mueller, and J. M. Williams, 1967, J. Phys. Chem. Solids **28**, 1651.
Herring, C., 1966, in *Magnetism Vol. 2B*, edited by G. T. Rado and H. Suhl (Academic, New York).
Hiess, A., F. Bourdarot, S. Coad, P. J. Brown, P. Burlet, G. H. Lander, M. S. S. Brooks, D. Kaczorowski, A. Czopnik, and R. Troc, 2001, Europhys. Lett. **55**, 267.
Hill, H. H., 1970, J. Nucl. Mater. **17**, 2.
Hill, J. P., and D. F. McMorrow, 1996, Acta Crystallogr., Sect. A: Found. Crystallogr. **52**, 236.
Hiroi, M., S. Kobayashi, M. Sera, N. Kobayashi, and S. Kunii, 1997, J. Phys. Soc. Jpn. **66**, 1762.
Hiroi, M., M. Sera, N. Kobayashi, and S. Kunii, 1997, Phys. Rev. B **55**, 8339.
Hirota, K., N. Oumi, T. Matsumura, H. Nakao, Y. Wakabayashi, Y. Murakami, and Y. Endoh, 2000, Phys. Rev. Lett. **84**, 2706.
Hirst, L. L., 1978, Adv. Phys. **27**, 231.
Hotta, T., 2006, Rep. Prog. Phys. **69**, 2061.
Hotta, T., and H. Harima, 2006, J. Phys. Soc. Jpn. **75**, 124711.
Hotta, T., and K. Ueda, 2003, Phys. Rev. B **67**, 104518.
Hutchings, M. T., 1964, in *Solid State Physics*, edited by F. Seitz and D. Turnbull (Academic, New York), Vol. 16, p. 227.
Igarashi, J.-I., and M. Takahashi, 2001, Phys. Rev. B **63**, 184430.
Ikushima, K., S. Tsutsui, Y. Haga, H. Yasuoka, R. E. Walstedt, N. M. Masaki, A. Nakamura, S. Nasu, and Y. Ōnuki, 2001, Phys. Rev. B **63**, 104404.
Ippolito, D., L. Martinelli, and G. Bevilacqua, 2005, Phys. Rev. B **71**, 064419.
Jensen, J., 2007, Phys. Rev. B **76**, 144428.
Joly, Y., S. Di Matteo, and C. R. Natoli, 2004, Phys. Rev. B **69**, 224401.
Jones, W. M., J. Gordon, and E. A. Long, 1952, J. Chem. Phys. **20**, 695.
Kalvius, G. M., S. L. Ruby, B. D. Dunlap, G. K. Shenoy, D. Cohen, and M. B. Brodsky, 1969, Phys. Lett. **29B**, 489.
Kaneko, K., N. Metoki, R. Shiina, T. D. Matsuda, M. Kohgi, K. Kuwahara, and N. Bernhoeft, 2007, Phys. Rev. B **75**, 094408.
Kaneko, K., H. Onodera, H. Yamauchi, T. Sakon, M. Motokawa, and Y. Yamaguchi, 2003, Phys. Rev. B **68**, 012401.
Kang, Z. C., 2008, in *Handbook on the Physics and Chemistry of Rare Earths*, edited by K. A. Gschneidner, J. C. G. Bünzli, and V. K. Pecharsky (Elsevier, Amsterdam), Vol. 38, p. 1.
Karraker, D. G., 1975, J. Chem. Phys. **63**, 3174.
Katanin, A. A., and A. P. Kampf, 2002, Phys. Rev. B **66**, 100403(R).
Keating, D. T., 1969, Phys. Rev. **178**, 732.
Keller, L., V. Pomjakushin, K. Conder, and A. Schenck, 2004, Phys. Rev. B **70**, 060407.
Kern, S., C.-K. Loong, J. Faber, and G. H. Lander, 1984, Solid State Commun. **49**, 295.
Kern, S., C. K. Loong, G. L. Goodman, B. Cort, and G. H. Lander, 1990, J. Phys.: Condens. Matter **2**, 1933.
Kern, S., C.-K. Loong, and G. H. Lander, 1985, Phys. Rev. B **32**, 3051.
Kern, S., R. A. Robinson, H. Nakotte, G. H. Lander, B. Cort, P. Watson, and F. A. Vigil, 1999, Phys. Rev. B **59**, 104.
Keszler, D. A., and J. A. Ibers, 1983, Inorg. Chem. **22**, 3366.
Khomskii, D., and G. Sawatzky, 1997, Solid State Commun. **102**, 87.
Kishimoto, S., A. Kondo, M.-S. Kim, H. Tou, M. Sera, and F. Iga, 2005, J. Phys. Soc. Jpn. **74**, 2913.
Kiss, A., and P. Fazekas, 2003a, Phys. Rev. B **68**, 174425.
Kiss, A., and P. Fazekas, 2003b, J. Phys.: Condens. Matter **15**, S2109.
Kiss, A., and P. Fazekas, 2005, Phys. Rev. B **71**, 054415.
Kiss, A., and Y. Kuramoto, 2006, J. Phys. Soc. Jpn. **75**, 103704.
Kiss, A., and Y. Kuramoto, 2008, J. Phys. Soc. Jpn. **77**, 034602.
Koga, M., M. Matsumoto, and H. Shiba, 2006, J. Phys. Soc. Jpn. **75**, 014709.
Kohgi, M., K. Iwasa, M. Nakajima, N. Metoki, S. Araki, N. Bernhoeft, J.-M. Mignot, A. Gukasov, H. Sato, Y. Aoki, and H. Sugawara, 2003, J. Phys. Soc. Jpn. **72**, 1002.
Kondo, A., H. Tou, M. Sera, and F. Iga, 2007, J. Phys. Soc. Jpn. **76**, 013701.
Kopmann, W., F. J. Litterst, H.-H. Klauss, M. Hillberg, W. Wagener, G. M. Kalvius, E. Schreier, F. J. Burghart, J. Rebizant, and G. H. Lander, 1998, J. Alloys Compd. **271-273**, 463.
Kosaka, M., H. Onodera, K. Ohoyama, M. Ohashi, Y. Yamaguchi, S. Nakamura, T. Goto, H. Kobayashi, and S. Ikeda, 1998, Phys. Rev. B **58**, 6339.
Kotegawa, H., M. Yogi, Y. Imamura, Y. Kawasaki, G.-Q.

Zheng, Y. Kitaoka, S. Ohsaki, H. Sugawara, Y. Aoki, and H. Sato, 2003, Phys. Rev. Lett. **90**, 027001.
Kubo, K., and T. Hotta, 2005a, Phys. Rev. B **72**, 132411.
Kubo, K., and T. Hotta, 2005b, Phys. Rev. B **71**, 140404.
Kubo, K., and T. Hotta, 2005c, Phys. Rev. B **72**, 144401.
Kubo, H., and Y. Kuramoto, 2003, J. Phys. Soc. Jpn. **72**, 1859.
Kugel, K. I., and D. I. Khomskii, 1982, Sov. Phys. Usp. **25**, 231.
Kusunose, H., and Y. Kuramoto, 2001, J. Phys. Soc. Jpn. **70**, 1751.
Kusunose, H., and Y. Kuramoto, 2005, J. Phys. Soc. Jpn. **74**, 3139.
Kuwahara, K., K. Iwasa, M. Kohgi, N. Aso, M. Sera, and F. Iga, 2007, J. Phys. Soc. Jpn. **76**, 093702.
Lander, G. H., J. Faber, A. J. Freeman, and J. P. Desclaux, 1976, Phys. Rev. B **13**, 1177.
Lashley, J. C., A. Lawson, R. J. McQueeney, and G. H. Lander, 2005, Phys. Rev. B **72**, 054416.
Lea, K. R., M. J. M. Leask, and W. P. Wolf, 1962, J. Phys. Chem. Solids **23**, 1381.
Levy, P. M., 1964, Phys. Rev. **135**, A155.
Levy, P. M., P. Morin, and D. Schmitt, 1979, Phys. Rev. Lett. **42**, 1417.
Lingg, N., D. Maurer, V. Müller, and K. A. McEwen, 1999, Phys. Rev. B **60**, R8430.
Link, P., A. Gukasov, J.-M. Mignot, T. Matsumura, and T. Suzuki, 1998, Phys. Rev. Lett. **80**, 4779.
Liviotti, E., S. Caretta, and G. Amoretti, 2002, J. Chem. Phys. **117**, 3361.
Lorenzi, F. D., F. N. Gygax, A. Schenck, A. Tobo, and H. Onodera, 2003, Physica B **326**, 581.
Lovesey, S. W., 1987, *Theory of Neutron Scattering from Condensed Matter* (Oxford University Press, Oxford).
Lovesey, S. W., 1996, J. Phys.: Condens. Matter **8**, 11009.
Lovesey, S. W., 2002, J. Phys.: Condens. Matter **14**, 4415.
Lovesey, S. W., and E. Balcar, 1996, J. Phys.: Condens. Matter **8**, 10983.
Lovesey, S. W., E. Balcar, C. Detlefs, G. van der Laan, D. S. Sivia, and U. Staub, 2003, J. Phys.: Condens. Matter **15**, 4511.
Lovesey, S. W., E. Balcar, K. S. Knight, and J. F. Rodríguez, 2005, Phys. Rep. **411**, 233.
Lovesey, S. W., and S. P. Collins, 1996, *X-ray Scattering and Absorption by Magnetic Materials* (Clarendon, Oxford).
Lovesey, S. W., and K. S. Knight, 2001, Phys. Rev. B **64**, 094401.
Luo, J., G. T. Trammell, and J. P. Hannon, 1993, Phys. Rev. Lett. **71**, 287.
Magishi, K., M. Kawakami, T. Saito, K. Koyama, K. Mizuno, and S. Kunii, 2002, Z. Naturforsch., A: Phys. Sci. **57**, 441.
Magnani, N., G. Amoretti, S. Carretta, P. Santini, and R. Caciuffo, 2007, J. Phys. Chem. Solids **68**, 2020.
Magnani, N., S. Carretta, R. Caciuffo, P. Santini, G. Amoretti, A. Hiess, J. Rebizant, and G. H. Lander, 2008, Phys. Rev. B **78**, 104425.
Magnani, N., P. Santini, G. Amoretti, and R. Caciuffo, 2005, Phys. Rev. B **71**, 054405.
Magnani, N., P. Santini, G. Amoretti, R. Caciuffo, P. Javorský, F. Wastin, J. Rebizant, and G. H. Lander, 2005, Physica B **359-361**, 1087.
Mannix, D., G. H. Lander, J. Rebizant, R. Caciuffo, N. Bernhoeft, E. Lidstrom, and C. Vettier, 1999, Phys. Rev. B **60**, 15187.
Mannix, D., Y. Tanaka, D. Carbone, N. Bernhoeft, and S. Kunii, 2005, Phys. Rev. Lett. **95**, 117206.
Marri, I., and P. Carra, 2004, Phys. Rev. B **69**, 113101.
Matsuhira, K., Y. Hinatsu, C. Sekine, T. Togashi, H. Maki, I. Shirotani, H. Kitazawa, T. Takamasu, and G. Kido, 2002, J. Phys. Soc. Jpn. **71** (Suppl.), 237.
Matsumura, T., D. Okuyama, N. Oumi, K. Hirota, H. Nakao, Y. Murakami, and Y. Wakabayashi, 2005, Phys. Rev. B **71**, 012405.
Matsuoka, E., D. Usui, H. Tanida, S. Nakamura, T. Nojima, and H. Onodera, 2007, J. Phys. Soc. Jpn. **76**, 073707.
Mattis, D. C., 2006, *The Theory of Magnetism Made Simple* (World Scientific, Singapore).
McEwen, K. A., J.-G. Park, A. J. Gipson, and G. A. Gehring, 2003, J. Phys.: Condens. Matter **15**, S1923.
McEwen, K. A., U. Steigenberger, K. N. Clausen, J. Kulda, J.-G. Park, and M. B. Walker, 1998, J. Magn. Magn. Mater. **177-181**, 37.
McEwen, K. A., H. C. Walker, M. D. Le, D. F. McMorrow, E. Colineau, F. Wastin, S. B. Wilkins, J.-G. Park, R. I. Bewley, and D. Fort, 2007, J. Magn. Magn. Mater. **310**, 718.
McMorrow, D. F., K. A. McEwen, U. Steigenberger, H. M. Rønnow, and F. Yakhou, 2001, Phys. Rev. Lett. **87**, 057201.
Mironov, V. S., L. F. Chibotaru, and A. Ceulemans, 2003, Adv. Quantum Chem. **44**, 599.
Moore, K. T., and G. van der Laan, 2009, Rev. Mod. Phys. **81**, 235.
Moore, K. T., G. van der Laan, R. G. Haire, M. A. Wall, A. J. Schwartz, and P. Soderlind, 2007, Phys. Rev. Lett. **98**, 236402.
Moore, K. T., G. van der Laan, M. A. Wall, A. J. Schwartz, and R. G. Haire, 2007, Phys. Rev. B **76**, 073105.
Morie, T., T. Sakakibara, T. Tayama, and S. Kunii, 2004, J. Phys. Soc. Jpn. **73**, 2381.
Morin, P., and J. Rouchy, 1993, Phys. Rev. B **48**, 256.
Morin, P., J. Rouchy, and D. Schmitt, 1988, Phys. Rev. B **37**, 5401.
Morin, P., and D. Schmitt, 1990, in *Ferromagnetic Materials*, edited by K. H. J. Buschow and E. P. Wohlfarth (Elsevier, Amsterdam), Vol. 5, pp. 1–132.
Morin, P., D. Schmitt, and E. du Tremolet de Lacheisserie, 1980, Phys. Rev. B **21**, 1742.
Morss, L. R., J. W. Richardson, C. W. Williams, G. H. Lander, A. C. Lawson, N. M. Edelstein, and G. V. Shalimoff, 1989, J. Less-Common Met. **156**, 273.
Mukamel, D., and S. Krinsky, 1976a, Phys. Rev. B **13**, 5065.
Mukamel, D., and S. Krinsky, 1976b, Phys. Rev. B **13**, 5078.
Mulders, A. M., U. Staub, V. Scagnoli, S. W. Lovesey, E. Balcar, T. Nakamura, A. Kikkawa, G. van der Laan, and J. M. Tonnerre, 2006, J. Phys.: Condens. Matter **18**, 11195.
Mulders, A. M., U. Staub, V. Scagnoli, Y. Tanaka, A. Kikkawa, K. Katsumata, and J. M. Tonnerre, 2007, Phys. Rev. B **75**, 184438.
Murakami, Y., J. P. Hill, D. Gibbs, M. Blume, I. Koyama, M. Tanaka, H. Kawata, T. Arima, Y. Tokura, K. Hirota, and Y. Endoh, 1998, Phys. Rev. Lett. **81**, 582.
Murakami, Y., H. Kawada, H. Kawata, M. Tanaka, T. Arima, Y. Moritomo, and Y. Tokura, 1998, Phys. Rev. Lett. **80**, 1932.
Naegele, J. R., and J. Ghijsen, 1985, *Structure and Bonding Vol. 59/60* (Springer-Verlag, Berlin), p. 197.
Nagao, T., and J.-I. Igarashi, 2005, Phys. Rev. B **72**, 174421.
Nagao, T., and J.-I. Igarashi, 2006, Phys. Rev. B **74**, 104404.
Nakamura, T., U. Staub, Y. Narumi, K. Katsumata, and F. Juranyi, 2003, Europhys. Lett. **62**, 251.
Nakao, H., K. I. Magishi, Y. Wakabayashi, Y. Murakami, K. Koyama, K. Hirote, Y. Endoh, and S. Kunii, 2001, J. Phys.

Soc. Jpn. **70**, 1857.
Nathans, R., C. G. Shull, G. Shirane, and A., Andresen, 1959, J. Phys. Chem. Solids **10**, 138.
Newman, D. J., and B. Ng, 2000, *Crystal Field Handbook* (Cambridge University Press, Cambridge).
Nikolaev, A. V., and K. H. Michel, 2003, Phys. Rev. B **68**, 054112.
Ohkawa, F. J., and H. Shimizu, 1999, J. Phys.: Condens. Matter **11**, L519.
Ohoyama, K., K. Kaneko, K. Indoh, H. Yamauchi, A. Tobo, H. Onodera, and Y. Yamaguchi, 2001, J. Phys. Soc. Jpn. **70**, 3291.
Onimaru, T., T. Sakakibara, N. Aso, H. Yoshizawa, H. S. Suzuki, and T. Takeuchi, 2005, Phys. Rev. Lett. **94**, 197201.
Onodera, H., H. Yamauchi, and Y. Yamaguchi, 1999, J. Phys. Soc. Jpn. **68**, 2526.
Osborn, R., A. D. Taylor, Z. A. Bowden, M. A. Hackett, W. Hayes, M. T. Hutchings, G. Amoretti, R. Caciuffo, A. Blaise, and J. M. Fournier, 1988, J. Phys. C **21**, L931.
Osborne, D. W., and E. F. Westrum, 1953, J. Chem. Phys. **21**, 1884.
Ovchinnikova, E. N., and V. E. Dmitrienko, 2000, Acta Crystallogr., Sect. A: Found. Crystallogr. **56**, 2.
Paixao, J. A., C. Detlefs, M. J. Longfield, R. Caciuffo, P. Santini, N. Bernhoeft, J. Rebizant, and G. H. Lander, 2002, Phys. Rev. Lett. **89**, 187202.
Palstra, T. T. M., A. A. Menovsky, J. van den Berg, A. J. Dirkmaat, P. H. Kes, G. J. Nieuwenhuys, and J. A. Mydosh, 1985, Phys. Rev. Lett. **55**, 2727.
Paolasini, L., R. Caciuffo, A. Sollier, P. Ghigna, and M. Altarelli, 2002, Phys. Rev. Lett. **88**, 106403.
Paolasini, L., C. Detlefs, C. Mazzoli, S. B. Wilkins, P. P. Deen, A. Bombardi, N. Kernavanois, F. de Bergevin, F. Yakhou, J. P. Valade, I. Breslavetz, A. Fondacaro, G. Pepellin, and P. Benard, 2007, J. Synchrotron Radiat. **14**, 301.
Paolasini, L., C. Vettier, F. de Bergevin, F. Yakhou, D. Mannix, A. Stunault, W. Neubeck, M. Altarelli, M. Fabrizio, P. A. Metcalf, and J. M. Honig, 1999, Phys. Rev. Lett. **82**, 4719.
Park, J. G., D. T. Adroja, K. A. McEwen, M. Kohgi, K. Iwasa, and Y. S. Kwon, 2005, Physica B **359-361**, 868.
Prodan, I. D., G. E. Scuseria, and R. L. Martin, 2007, Phys. Rev. B **76**, 033101.
Rahman, H. U., and W. A. Runciman, 1966, J. Phys. Chem. Solids **27**, 1833.
Raphael, G., and R. Lallement, 1968, Solid State Commun. **6**, 383.
Regnault, L. P., W. A. C. Erkelens, J. Rossat-Mignod, C. Vettier, S. Kunii, and T. Kasuya, 1988, J. Magn. Magn. Mater. **76-77**, 413.
Ross, J. W., and D. J. Lam, 1967, J. Appl. Phys. **38**, 1451.
Rossat-Mignod, J., 1987, in *Methods of Experimental Physics, Vol. 23 C*, edited by K. Skold and D. L. Price (Academic, Orlando), pp. 69–157.
Rudowicz, C., and C. Y. Chung, 2004, J. Phys.: Condens. Matter **16**, 5825.
Sakai, O., J. Kikuchi, R. Shiina, H. Sato, H. Sugawara, M. Takigawa, and H. Shiba, 2007, J. Phys. Soc. Jpn. **76**, 024710.
Sakai, O., R. Shiina, and H. Shiba, 2003, J. Phys. Soc. Jpn. **72**, 1534.
Sakai, O., R. Shiina, and H. Shiba, 2005, J. Phys. Soc. Jpn. **74**, 457.
Sakai, O., R. Shiina, H. Shiba, and P. Thalmeier, 1997, J. Phys. Soc. Jpn. **66**, 3005.
Sakai, O., R. Shiina, H. Shiba, and P. Thalmeier, 1999, J. Phys. Soc. Jpn. **68**, 1364.
Sakakibara, T., T. Tayama, T. Onimaru, D. Aoki, Y. Ōnuki, H. Sugawara, Y. Aoki, and H. Sato, 2003, J. Phys.: Condens. Matter **15**, S2055.
Sakurai, J. J., 1993, *Modern Quantum Mechanics* (Addison-Wesley, Reading, MA).
Santini, P., 1998, Phys. Rev. B **57**, 5191.
Santini, P., and G. Amoretti, 1994, Phys. Rev. Lett. **73**, 1027.
Santini, P., and G. Amoretti, 2000, Phys. Rev. Lett. **85**, 2188.
Santini, P., and G. Amoretti, 2002, J. Phys. Soc. Jpn. **71** (Suppl.), 11.
Santini, P., G. Amoretti, R. Caciuffo, F. Bourdarot, and B. Fåk, 2000, Phys. Rev. Lett. **85**, 654.
Santini, P., S. Carretta, N. Magnani, G. Amoretti, and R. Caciuffo, 2006, Phys. Rev. Lett. **97**, 207203.
Santini, P., R. Lemanski, and P. Erdös, 1999, Adv. Phys. **48**, 537.
Sasaki, K., and Y. Obata, 1970, J. Phys. Soc. Jpn. **28**, 1157.
Schenck, A., F. Gygax, and S. Kunii, 2002, Phys. Rev. Lett. **89**, 037201.
Schenck, A., F. N. Gygax, and Y. Ōnuki, 2003, Phys. Rev. B **68**, 104422.
Schenck, A., F. N. Gygax, G. Solt, O. Zaharko, and S. Kunii, 2004, Phys. Rev. Lett. **93**, 257601.
Schenck, A., and G. Solt, 2004, J. Phys.: Condens. Matter **16**, S4639.
Schoenes, J., 1980, Phys. Rep. **63**, 301.
Schrieffer, J. R., and P. A. Wolff, 1966, Phys. Rev. **149**, 491.
Schwieger, S., and W. Nolting, 2002, Phys. Rev. B **65**, 205210.
Sera, M., H. Ichikawa, T. Yokoo, J. Nishi, K. Kakurai, and S. Kunii, 2001, Phys. Rev. Lett. **86**, 1578.
Sera, M., and S. Kobayashi, 1999, J. Phys. Soc. Jpn. **68**, 1664.
Shiba, H., O. Sakai, and R. Shiina, 1999, J. Phys. Soc. Jpn. **68**, 1988.
Shiina, R., 2004, J. Phys. Soc. Jpn. **73**, 2257.
Shiina, R., and Y. Aoki, 2004, J. Phys. Soc. Jpn. **73**, 541.
Shiina, R., O. Sakai, and H. Shiba, 2007, J. Phys. Soc. Jpn. **76**, 094702.
Shiina, R., O. Sakai, H. Shiba, and P. Thalmeier, 1998, J. Phys. Soc. Jpn. **67**, 941.
Shiina, R., H. Shiba, and P. Thalmeier, 1997, J. Phys. Soc. Jpn. **66**, 1741.
Shiina, R., H. Shiba, P. Thalmeier, A. Takahashi, and O. Sakai, 2003, J. Phys. Soc. Jpn. **72**, 1216.
Shim, J. H., K. Haule, and G. Kotliar, 2007, Nature (London) **446**, 513.
Slater, J. C., and G. F. Koster, 1954, Phys. Rev. **94**, 1498.
Slowinski, E., and N. Elliott, 1952, Acta Crystallogr. **5**, 768.
Smith, D., and J. H. M. Thornley, 1966, Proc. Phys. Soc. London **89**, 779.
Soderholm, L., 1987, J. Less-Common Met. **133**, 77.
Solt, G., and P. Erdös, 1980, Phys. Rev. B **22**, 4718.
Squires, G. L., 1978, *Introduction to the Theory of Thermal Neutron Scattering* (Cambridge University Press, Cambridge).
Staub, U., A. M. Mulders, O. Zaharko, S. Janssen, T. Nakamura, and S. W. Lovesey, 2005, Phys. Rev. Lett. **94**, 036408.
Staub, U., Y. Tanaka, K. Katsumata, A. Kikkawa, Y. Kuramoto, and Y. Ōnuki, 2006, J. Phys.: Condens. Matter **18**, 11007.
Steigenberger, U., K. A. McEwen, J. L. Martinez, and D. Fort, 1992, J. Magn. Magn. Mater. **108**, 163.
Stevens, K. W. H., 1952, Proc. Phys. Soc., London, Sect. A **65**, 209.

Stewart, G. R., 1984, Rev. Mod. Phys. **56**, 755.
Stewart, G. R., 2001, Rev. Mod. Phys. **73**, 797.
Stirling, W. G., and K. A. McEwen, 1987, in *Methods of Experimental Physics, Vol. 23 C*, edited by K. Skold and D. L. Price (Academic, Orlando), pp. 159–235.
Sugihara, K., 1959, J. Phys. Soc. Jpn. **14**, 1231.
Suzuki, O., T. Goto, S. Nakamura, T. Matsumura, and S. Kunii, 1998, J. Phys. Soc. Jpn. **67**, 4243.
Suzuki, O., S. Nakamura, M. Akatsu, Y. Nemoto, T. Goto, and S. Kunii, 2005, J. Phys. Soc. Jpn. **74**, 735.
Tabuteau, A., J. Jové, M. Pagès, C. de Novion, and J. Gal, 1984, Solid State Commun. **50**, 357.
Tabuteau, A., M. Pagès, A. Boeuf, J. Rebizant, L. Manes, R. Caciuffo, and F. Rustichelli, 1984, J. Phys. (Paris), Lett. **45**, 373.
Takahashi, A., and H. Shiba, 2000, J. Phys. Soc. Jpn. **69**, 3328.
Takahashi, M., 1977, J. Phys. C **10**, 1289.
Takegahara, K., H. Harima, and A. Yanase, 2001, J. Phys. Soc. Jpn. **70**, 1190.
Takigawa, M., H. Yasuoka, T. Tanaka, and Y. Ishizawa, 1983, J. Phys. Soc. Jpn. **52**, 728.
Takimoto, T., 2006, J. Phys. Soc. Jpn. **75**, 034714.
Tanaka, Y., T. Inami, S. W. Lovesey, K. S. Knight, F. Yakhou, D. Mannix, J. Kokubun, M. Kanazawa, K. Ishida, S. Nanao, T. Nakamura, H. Yamauchi, H. Onodera, K. Ohoyama, and Y. Yamaguchi, 2004, Phys. Rev. B **69**, 024417.
Tanaka, Y., T. Inami, T. Nakamura, H. Yamauchi, H. Onodera, K. Ohoyama, and Y. Yamaguchi, 1999, J. Phys.: Condens. Matter **11**, L505.
Tanaka, Y., M. Sera, K. Katsumata, S. W. Lovesey, Y. Tabata, S. Shimomura, A. Kikkawa, F. Iga, and S. Kishimoto, 2006, J. Phys. Soc. Jpn. **75**, 073702.
Tanaka, Y., U. Staub, K. Katsumata, S. W. Lovesey, J. E. Lorenzo, Y. Narumi, V. Scagnoli, S. Shimomura, Y. Tabata, Y. Ōnuki, Y. Kuramoto, A. Kikkawa, T. Ishikawa, and H. Kitamura, 2004, Europhys. Lett. **68**, 671.
Tayama, T., T. Sakakibara, K. Tenya, H. Amitsuka, and S. Kunii, 1997, J. Phys. Soc. Jpn. **66**, 2268.
Teitelbaum, H. H., and P. M. Levy, 1976, Phys. Rev. B **14**, 3058.
Templeton, D. H., and L. K. Templeton, 1982, Acta Crystallogr., Sect. A: Cryst. Phys., Diffr., Theor. Gen. Crystallogr. **38**, 62.
Templeton, D. H., and L. K. Templeton, 1985, Acta Crystallogr., Sect. A: Found. Crystallogr. **41**, 133.
Thalmeier, P., 1984, J. Phys. C **17**, 4153.
Thalmeier, P., and P. Fulde, 1982, Phys. Rev. Lett. **49**, 1588.
Thalmeier, P., H. Shiba, R. Shiina, and O. Sakai, 1998, J. Phys. Soc. Jpn. **67**, 2363.
Thalmeier, P., and G. Zwicknagl, 2005, in *Handbook on the Physics and Chemistry of Rare Earths*, edited by K. A. Gschneidner, J. C. G. Bünzli, and V. K. Pecharsky (Elsevier, Amsterdam), Vol. 34, p. 135.
Tokunaga, Y., D. Aoki, Y. Homma, S. Kambe, H. Sakai, S. Ikeda, T. Fujimoto, R. E. Walstedt, H. Yasuoka, Y. Shiokawa, E. Yamamoto, and A. Nakamura, 2007, J. Magn. Magn. Mater. **310**, 735.
Tokunaga, Y., D. Aoki, Y. Homma, S. Kambe, H. Sakai, S. Ikeda, T. Fujimoto, R. E. Walstedt, H. Yasuoka, E. Yamamoto, A. Nakamura, and Y. Shiokawa, 2006, Phys. Rev. Lett. **97**, 257601.
Tokunaga, Y., Y. Homma, S. Kambe, D. Aoki, H. Sakai, E. Yamamoto, A. Nakamura, Y. Shiokawa, R. E. Walstedt, and H. Yasuoka, 2005a, Phys. Rev. Lett. **94**, 137209.
Tokunaga, Y., Y. Homma, S. Kambe, D. Aoki, H. Sakai, E. Yamamoto, A. Nakamura, Y. Shiokawa, R. E. Walstedt, and H. Yasuoka, 2005b, Physica B **359-361**, 1096.
Tokunaga, Y., Y. Homma, S. Kambe, D. Aoki, H. Sakai, E. Yamamoto, A. Nakamura, Y. Shiokawa, R. E. Walstedt, and H. Yasuoka, 2006, Physica B **378-380**, 929.
Tokunaga, Y., H. Sakai, T. Fujimoto, S. Kambe, R. E. Walstedt, K. Ikushima, H. Yasuoka, D. Aoki, Y. Homma, Y. Haga, T. D. Matsuda, S. Ikeda, E. Yamamoto, A. Nakamura, Y. Shiokawa, K. Nakajima, Y. Arai, and Y. Ōnuki, 2007, J. Alloys Compd. **444-445**, 241.
Tokunaga, Y., R. E. Walstedt, Y. Homma, D. Aoki, S. Kambe, H. Sakai, T, Fujimoto, S. Ikeda, E. Yamamoto, A. Nakamura, Y. Shiokawa, and H. Yasuoka, 2007, J. Phys. Chem. Solids **68**, 2016.
Toledano, J., and P. Toledano, 1987, *The Landau Theory of Phase Transitions* (World Scientific, Singapore).
Toropova, A., C. A. Marianetti, K. Haule, and G. Kotliar, 2007, Phys. Rev. B **76**, 155126.
van den Brink, J., and D. Khomskii, 2001, Phys. Rev. B **63**, 140416.
van Duijn, J., J. P. Attfield, and K. Suzuki, 2000, Phys. Rev. B **62**, 6410.
van der Laan, G., K. T. Moore, J. G. Tobin, B. W. Chung, M. A. Wall, and A. J. Schwartz, 2004, Phys. Rev. Lett. **93**, 097401.
Veal, B. W., and D. J. Lam, 1982, *Gmelin Handbook of Inorganic Chemistry, System Nr. 55, Uranium Suppl., Vol. A5* (Springer-Verlag, Berlin) p. 176.
Walker, H. C., K. A. McEwen, D. F. McMorrow, S. B. Wilkins, F. Wastin, E. Colineau, and D. Fort, 2006, Phys. Rev. Lett. **97**, 137203.
Walstedt, R. E., S. Kambe, Y. Tokunaga, and H. Sakai, 2007, J. Phys. Soc. Jpn. **76**, 072001.
Webster, C. H., L. M. Helme, A. T. Boothroyd, D. F. McMorrow, S. B. Wilkins, C. Detlefs, B. Detlefs, R. I. Bewley, and M. J. McKelvy, 2007, Phys. Rev. B **76**, 134419.
Wiebe, C. R., J. A. Jank, G. J. MacDougall, G. M. Luke, J. D. Garrett, H. D. Zhou, Y.-J. Jo, L. Balicas, Y. Qiu, J. R. D. Copley, Z. Yamani, and W. J. L. Buyers, 2007, Nat. Phys. **3**, 96.
Wilkins, S. B., R. Caciuffo, C. Detlefs, J. Rebizant, E. Colineau, F. Wastin, and G. H. Lander, 2006, Phys. Rev. B **73**, 060406.
Wilkins, S. B., P. D. Hatton, M. D. Roper, D. Prabhakaran, and A. T. Boothroyd, 2003, Phys. Rev. Lett. **90**, 187201.
Wilkins, S. B., J. A. Paixao, R. Caciuffo, P. Javorský, F. Wastin, J. Rebizant, C. Detlefs, N. Bernhoeft, P. Santini, and G. H. Lander, 2004, Phys. Rev. B **70**, 214402.
Wilkins, S. B., P. D. Spencer, P. D. Hatton, S. P. Collins, M. D. Roper, D. Prabhakaran, and A. T. Boothroyd, 2003, Phys. Rev. Lett. **91**, 167205.
Wilkins, S. B., N. Stojic, T. A. W. Beale, N. Binggeli, C. W. M. Castleton, P. Bencok, D. Prabhakaran, A. T. Boothroyd, P. D. Hatton, and M. Altarelli, 2005, Phys. Rev. B **71**, 245102.
Willis, B. T. M., and R. I. Taylor, 1965, Phys. Lett. **17**, 188.
Wolf, W. P., and R. J. Birgeneau, 1968, Phys. Rev. **166**, 376.
Wulff, M., G. H. Lander, B. Lebech, and A. Delapalme, 1989, Phys. Rev. B **39**, 4719.
Wulff, M., G. H. Lander, J. Rebizant, J. C. Spirlet, B. Lebech, C. Broholm, and P. J. Brown, 1988, Phys. Rev. B **37**, 5577.
Yamauchi, H., H. Onodera, K. Ohoyama, T. Onimaru, M. Kosaka, M. Ohashi, and Y. Yamaguchi, 1999, J. Phys. Soc. Jpn. **68**, 2057.

Yanagisawa, T., T. Goto, Y. Nemoto, R. Watanuki, K. Suzuki, O. Suzuki, and G. Kido, 2005, Phys. Rev. B **71**, 104416.
Yatskar, A., W. P. Beyermann, R. Movshovich, and P. C. Canfield, 1996, Phys. Rev. Lett. **77**, 3637.
Yoshizawa, M., Y. Nakanishi, M. Oikawa, C. Sekine, I. Shirotani, S. R. Saha, H. Sugawara, and H. Sato, 2005, J. Phys. Soc. Jpn. **74**, 2141.
Zaharko, O., P. Fisher, A. Schenck, S. Kunii, P. J. Brown, F. Tasset, and T. Hansen, 2003, Phys. Rev. B **68**, 214401.
Zaharko, O., W. Sikora, F. Bialas, U. Staub, and T. Nakamura, 2004, Phys. Rev. B **69**, 224417.